Cardiac magnetic resonance in catheter ablation of atrial arrhythmias characterisation of substrate and guidance of therapy

Harrison, James Lloyd

Awarding institution:
King's College London

Cardiac magnetic resonance in catheter ablation of atrial arrhythmias: characterisation of substrate and guidance of therapy

James L Harrison

A dissertation submitted for the degree of

Doctor of Philosophy

Division of Imaging Sciences and Biomedical Engineering
School of Medicine
King's College London
University of London

For Oliver

Abstract

Cardiac magnetic resonance (CMR) imaging has been recently used to provide non-invasive tissue characterisation before and after catheter ablation of atrial arrhythmias and to guide real-time electrophysiology procedures within the CMR environment. This thesis develops and validates new CMR techniques for use at the interface between cardiac imaging and interventional electrophysiology using both pre-clinical animal and clinical human studies. There are three main objectives:

1) Whilst the use of CMR to characterise acute and chronic ventricular myocardial injury only became clinically accepted and in widespread use following comprehensive pathological validation, there has been no fundamental validation work on the CMR assessment of the atrium. *This thesis provides the first comprehensive histological validation of CMR and electroanatomical mapping (EAM) of acute and chronic ablation injury in a new animal model of atrial ablation.*

2) Previous studies have suggested a qualitative and quantitative relationship between atrial CMR findings and endocardial voltage. However, there is conflicting evidence regarding the reproducibility and diagnostic accuracy of atrial CMR as a surrogate for electrical disease. *This thesis compares atrial CMR findings with endocardial voltage mapping in patients undergoing repeat catheter ablation for left atrial (LA) arrhythmias and assesses the ability of atrial CMR to predict gaps in ablation lesions.*

3) The final objective of the thesis is to assess the feasibility of a real-time magnetic resonance-guided electrophysiology (MR-EP) system in an animal model of atrial ablation. MR-EP offers several potential advantages over x-ray fluoroscopy and conventional EAM systems. It provides rapid, high resolution, 3D visualisation of

the true anatomy and endocardial surface of the cardiac chambers with unrivalled soft tissue contrast, the potential to visualise ablation lesions and acute complications with high spatial resolution, and raises the possibility of eliminating patient and physician exposure to ionising radiation. *This thesis demonstrates, for the first time, the feasibility of using an actively-tracked radiofrequency (RF) ablation catheter within a fully MR-compatible EP system as a prelude to a planned human study.*

Table of contents

Table of figures

Abbreviations

AF – atrial fibrillation

AT – atrial tachycardia

b-SSFP – balanced steady-state free precession

CI – confidence interval

(C)MR – (cardiac) magnetic resonance

CNR – contrast to noise ratio

CS – coronary sinus

EAM – electroanatomical mapping

IR – inversion recovery

IVC – inferior vena cava

LA – left atrium/atrial

LGE – late gadolinium enhancement

LV – left ventricle/ventricular

MIP – maximum intensity projection

MR-EP – magnetic resonance-guided electrophysiology

PV – pulmonary vein

PVI – pulmonary vein isolation

RA – right atrium/atrial

RF – radiofrequency

SD – standard deviation

SI – signal intensity/intensities

SNR – signal to noise ratio

SVC – superior vena cava

T2W – T2-weighted

TE – echo time

TFE – turbo field echo

TI – inversion time

TOE – transoesophageal echocardiography

TR – repetition time

TSE – turbo spin echo

Thesis outline

The aim of this thesis is to evaluate the role of CMR in the characterisation of atrial ablation injury in a controlled animal model, applying these findings to a clinical study of patients undergoing repeat catheter ablation for atrial arrhythmias, and to develop an integrative approach between CMR and interventional cardiac electrophysiology. The thesis is organised as follows:

SECTION ONE: BACKGROUND AND LITERATURE REVIEW

Chapter 1 introduces the mechanism, classification and current treatment of atrial arrhythmias.

Chapter 2 discusses the methodology of atrial CMR, including its use before and after catheter ablation for atrial fibrillation (AF) and its role in defining atrial anatomy, volume and function.

Chapter 3 provides a short introduction to the physical principles of atrial CMR, including a description of MR signal generation and encoding, and the main pulse sequences used in atrial CMR.

Chapter 4 describes how the principles from Chapters 1, 2 and 3 can be applied to real-time MR-EP.

SECTION TWO: METHODS AND EXPERIMENTAL DATA

Chapter 5 presents the methods used for Chapters 6, 7 and 8.

Chapter 6 provides a comprehensive histological validation of CMR and EAM of acute and chronic ablation injury in a new animal model of atrial ablation.

Chapter 7 compares atrial CMR findings with endocardial voltage mapping in patients undergoing repeat catheter ablation for LA arrhythmias and assesses the ability of atrial CMR to predict gaps in ablation lesions.

Chapter 8 demonstrates the feasibility of using an actively-tracked RF ablation catheter within a fully MR-compatible EP system as a prelude to a planned human study.

Chapter 9 concludes the thesis by discussing the original contributions, implications, limitations and future directions of this work.

SECTION ONE:

BACKGROUND AND

LITERATURE REVIEW

1 Atrial arrhythmias

1.1 Introduction

The aim of this thesis is to develop and validate CMR techniques, which have the potential to improve catheter ablation therapy for atrial arrhythmias (atrial tachycardia (AT), atrial flutter and AF). This chapter provides an overview of the current classification and treatment of atrial arrhythmias.

1.2 Atrial tachycardia

Atrial tachycardia was originally classified exclusively based on the ECG appearances as an arrhythmia of atrial origin with a ventricular rate below 240-250 beats per minute, a regular P wave activity and an isoelectric baseline between P waves, except in atrial flutter.[1] However, with an improved understanding of arrhythmia mechanism through the development of sophisticated interventional techniques, it became clear that this classification correlated poorly with the underlying tachycardia mechanism and substrate, and so a mechanistic classification was necessary. A consensus statement from a Joint Expert Group from the Working Group of Arrhythmias of the European Society of Cardiology and the North American Society of Pacing and Electrophysiology classified AT as either focal or macroreentrant, which is now widely adopted.[2] Focal ATs are characterised by a single site (focus) of origin with centrifugal spread of electrical activation from this point. The underlying mechanism may be abnormal automaticity, triggered activity or microreentry. Macroreentrant ATs involve a large (typically greater than 2 cm) circuit within the atrium around a central obstacle, which may be anatomical (e.g. pulmonary veins (PVs), mitral or tricuspid

annulus, surgical or spontaneous scar) or an area of functional block (e.g. crista terminalis). They have no point of origin, are characterised by a site of 'early-meets-late' activation and include typical or reverse typical (cavotricuspid isthmus-dependent) atrial flutter and atypical right atrial (RA) and LA flutters. Since this classification, a third mechanistic category, localised reentry, has been described, involving reentrant circuits less than 2 cm in size and most commonly seen following extensive substrate modification during catheter ablation for persistent AF.[3]

1.2.1 Focal AT

Focal ATs are responsible for approximately 10% of all supraventricular tachycardias[4] and occur most commonly in the absence of structural heart disease,[5] but can be associated with low voltage atrial tissue.[6] Typically, the ECG shows discrete P-waves with an intervening isoelectric baseline, but this can be obscured by a rapid ventricular response rate. Focal ATs often demonstrate a gradual increase in rate at onset ("warm-up") and a gradual decrease in rate at offset ("cool-down"), unlike macroreentrant ATs, which tend to have sudden initiation and termination. The sites of focal ATs are not randomly distributed, with a predilection for the RA, particularly certain anatomical structures, including the crista terminals, tricuspid annulus, coronary sinus (CS) os, superior vena cava (SVC) and RA appendage. As a result, algorithms based on the ECG P-wave morphology have been described to localise the focus prior to catheter ablation, with a positive and negative P-wave in lead V1 suggesting an LA and RA focus respectively.[7, 8]

First-line therapy is pharmacological, using cardioselective beta-blockers or non-dihydropyridine calcium channel blockers for rate control or Class Ic (e.g.

flecainide or propafenone) or Class III (e.g. sotalol or amiodarone) antiarrhythmics. However, all of these have relatively poor efficacy and are associated with significant side effects. As a result, the past two decades have seen a significant increase in the use of catheter ablation to treat focal ATs, and this is now considered first-line therapy for those with recurrent or incessant tachycardia of tachycardia-induced cardiomyopathy.[9]

Catheter ablation for focal AT requires the presence of sustained tachycardia or frequent ectopy in order to find the site of earliest atrial activation. This is often aided by a 3D EAM system to produce a colour-coded isochronal activation map, with the characteristic pattern of a central point of activation with radial propagation. Ablation, most commonly RF energy, is applied to the focus with an acute success rate of 85-90%.[10] Complications and recurrence are rare[11] and patients presenting with tachycardia-induced cardiomyopathy generally show good recovery of left ventricular (LV) function following successful ablation.[12]

1.2.2 Macroreentrant AT

1.2.2.1 Typical atrial flutter

Typical (cavotricuspid isthmus-dependent) atrial flutter was the first macroreentrant AT treated with catheter ablation, based on an understanding of the arrhythmia mechanism.[13] The reentrant circuit is well defined, with an anterior boundary of the tricuspid annulus and a posterior boundary of the crista terminalis (a functional barrier to transverse conduction in the RA due to tissue anisotropy) and the Eustachian ridge.[14] Septal activation of the RA is from inferior to superior, whilst activation of the lateral wall of the RA is in the opposite direction. Activation around the tricuspid annulus is in an anticlockwise direction in most cases (resulting in the classical sawtooth ECG pattern in the inferior leads),

but is clockwise (reverse typical) in 10% of patients.[15] The cavotricuspid isthmus, a body of fibrous tissue in the lower RA between the inferior vena cava (IVC) and the tricuspid valve, is an integral part of the circuit and is the preferred target for catheter ablation as it is narrow and provides a safe and stable catheter position for the delivery of a linear ablation lesion.

Typical atrial flutter may occur in the absence of structural heart disease ("lone") or with concomitant ischaemic heart disease, valvular heart disease, cardiomyopathy or any cause of increased RA pressure. Its prevalence increases with age and is more common in males than females.[16] It may present in many different ways: paroxysmal or persistent palpitations, syncope (particularly if there is 1:1 atrial to ventricular conduction), silently (as an incidental finding), transient ischaemic attack or cerebrovascular accident, a tachycardia-induced cardiomyopathy or pre-syncope/syncope due to sinus node disease as part of the bradycardia-tachycardia syndrome. Furthermore, patients with typical atrial flutter are predisposed to the later development of AF (in over 30% of cases[17]) and guidelines suggest that thromboprophylaxis in patients with atrial flutter should follow the same guidance as for AF.[18]

Catheter ablation targeting the critical (cavotricuspid) isthmus was first shown to terminate the tachycardia and prevent reinduction in the early 1990s[13, 19] and is now considered first-line therapy for typical atrial flutter due to the high efficacy, low complication rates and the relative ineffectiveness of pharmacotherapy. A randomised controlled trial of antiarrhythmic medication versus first-line RF ablation in 61 patients showed that after a mean follow-up of 21 ± 11 months, 36% of patients receiving drugs were in sinus rhythm, whilst 80% of patients who

underwent ablation were in sinus rhythm ($p<0.01$).[20] Furthermore, there were more hospitalisations in the group receiving drugs.

In early studies, the endpoint of ablation was tachycardia termination and an inability to reinduce tachycardia. However, this resulted in frequent recurrence of atrial flutter[13] and contemporary practice uses the endpoint of bidirectional conduction block across the cavotricuspid isthmus. This is demonstrated using differential pacing techniques and is associated with a less than 5% flutter recurrence rate.[21] An additional endpoint is the presence of double potentials with an interpotential interval of greater than 110 ms.[22]

In a survey of multiple centres, the results for 7,071 patients who had undergone catheter ablation for typical atrial flutter were pooled.[21] A repeat ablation procedure was performed in 4% of patients, and the long-term success rate was 97%. The overall incidence of serious complications was 0.4%, with the most common complication being atrioventricular block in 0.2% of patients. In a meta-analysis of 1,323 patients, single and multiple procedure success rates were 92% and 97% respectively and repeat ablation was necessary in 8% of patients.[23]

1.2.2.2 Atypical atrial flutter

This term encompasses all macroreentrant ATs except cavotricuspid-isthmus dependent atrial flutter. They can occur in patients with no previous atrial surgery with circuits around areas of spontaneous LA or RA fibrosis. In these patients, the circuit may involve the lateral RA wall, lower loop reentry around the IVC or single or dual LA circuits (around the PVs and/or mitral annulus) associated with LA enlargement (e.g. heart failure, mitral regurgitation). With LA enlargement, fibrosis may develop, providing an obstacle that permits and stabilises reentry. One study reported eight patients with macroreentrant AT related to a zone of spontaneous

scar in the posterolateral RA,[24] whilst another described *de novo* LA macroreentrant tachycardias associated with areas of reduced or absent voltage, particularly on the posterior LA wall.[25]

More commonly, atypical AT occur in patients with previous atrial surgery or ablation, around surgical scars, suture lines or prosthetic patches following surgical correction of congenital heart disease (lesional AT) or around scar formed by surgical or catheter ablation for AF. Whilst uncommon following PV isolation for paroxysmal AF, left ATs are increasingly seen (in up to 50% of cases[26]) following extensive LA ablation for persistent AF, involving the formation of linear ablation lesions and targeting of complex fractionated atrial electrograms (substrate modification). Gaps in these linear ablation lesions permit macroreentry, most commonly around the LA roof, the mitral annulus or PVs. The circuits can be complex, not infrequently involving dual loops, whereby ablation of one unmasks the other. The P wave characteristics of atypical atrial flutters are highly variable and rarely provide clues as to the location or circuit. Drug therapy is rarely effective and catheter ablation is indicated with recurrent or poorly tolerated symptoms.

Catheter ablation of atypical macroreentrant AT is often complex and most commonly involves the use of 3D EAM, which permits the integration of complex anatomy with endocardial voltage to identify areas of scar, activation mapping to determine the direction of propagation and entrainment values to define sites that are within or outside of the circuit. As with all macroreentrant tachycardias, there is no site of origin, but there is a site of 'early-meets-late' activation and it is normally possible to map a large percentage of the tachycardia cycle length (unlike focal tachycardias, in which only a small percentage of the tachycardia cycle length

can be mapped, the rest coinciding with the isoelectric interval). Mapping may demonstrate lines of functional block, which can act as a substrate for macroreentry, with double potentials resulting from activation either side of the line. Ablation success requires identification of an anatomical or functional isthmus critical to the macroreentrant circuit, which can be interrupted with a linear or focal ablation lesion. As a result of the complex circuits involved, success rates are more modest compared with ablation of typical atrial flutter. Success is variable, with better results in patients with simpler previous surgery or catheter ablation than those who have had more complex congenital heart disease repairs.

1.2.2.3 Localised reentry

Also known as "small circuit reentry", this has been increasingly recognised in the past few years, and is most commonly seen following extensive substrate modification during catheter ablation for persistent AF.[3, 27, 28] The circuits are smaller than macroreentry, typically 1-2 cm in size. In a study of 128 patients with previous catheter ablation for AF, there were a total of 246 ATs.[3] Approximately half of these were macroreentrant, whilst of the non-macroreentrant tachycardias, only 25% were truly focal. The other three quarters involved a 1-2 cm circuit with greater than 75% of the tachycardia cycle length mappable. It is unknown whether these localised reentrant circuits are drivers for AF or whether they are just the result of previous ablation.

1.3 Atrial fibrillation

AF is a supraventricular tachyarrhythmia characterised by uncoordinated atrial activation with consequent deterioration of atrial mechanical function.[29] It is the most common cardiac arrhythmia, with an increasing prevalence with age. AF affects an estimated 2.2 million adults in the United States[30] and each year around

46,000 people in the United Kingdom are newly diagnosed with the condition.[31] It is a leading cause of stroke and with an increasingly elderly population, the prevalence of AF is set to rise, conferring substantial mortality, morbidity and economic burden. In the Framingham study, the presence of AF independently increased mortality in men by 1.5 fold and in women by 1.9 fold.[32] Although the AFFIRM study demonstrated that rhythm control conferred no prognostic benefit when compared with rate control, a sub-study of this trial has shown that if sinus rhythm can be achieved without the use of anti-arrhythmic drugs, there is a substantial mortality benefit.[33] Until recently, the mainstay of treatment for AF has been pharmacological but this is limited by concerns about efficacy, side effects and safety.

1.3.1 Electrical remodelling in AF

The natural history of AF is characterised by a gradual worsening over time, with an increasing frequency and/or duration of arrhythmia episodes. Eventually, the AF does not terminate and becomes persistent*. The finding that AF itself produces changes in atrial function and structure has provided a possible explanation for the progressive nature of AF.

The concept of tachycardia-induced atrial electrical remodelling was introduced in 1995 by two independent experimental studies.[34, 35] In a dog model of prolonged rapid atrial pacing the atrial refractory period was reduced by about 15%. In goats, AF was maintained by implanting a pacemaker, which automatically delivered

*According to ACC/AHA/ESC guidelines: paroxysmal AF involves self-terminating episodes that last <7 days (usually <24 hours); persistent AF does not self-terminate; long-standing persistent AF is persistent AF for >1 year; permanent AF is where DC cardioversion does not terminate the arrhythmia (or is not attempted due to low anticipated chance of success). Lone AF is AF that occurs in young patients (<65 years) with structurally normal hearts and no evidence of other causative pathology (such as hypertension or diabetes).

bursts of atrial stimuli as soon as sinus rhythm occurred. This resulted in an even more marked shortening in atrial refractoriness from 146 ± 19 ms to 81 ± 22 ms after two to four days of AF and a loss (or even reversal) of the normal rate adaptation of the refractory period. More importantly, these studies showed that long-term rapid atrial pacing led to a progressive increase in the susceptibility to AF. After six weeks of rapid atrial pacing, episodes of AF lasting >15 min could be induced in 82% of the dogs. In ten out of 11 goats, after maintaining AF for 7.1 ± 4.8 days, the arrhythmia sustained itself for >24 hours. In contrast, at the start of the experiment, episodes of AF induced by burst pacing only self-sustained for 6 ± 3 s. This observation of tachycardia-induced electrical remodelling creating a substrate for persistent AF, led to the concept that "AF begets AF".[34]

1.3.2 Structural remodelling in AF

In addition to electrical remodelling, structural remodelling, involving myocardial fibrosis (the most common histological feature of the failing heart) is a hallmark of, and fundamental to, the progression of AF.[36, 37] Structural remodelling contributes synergistically with electrical remodelling to form the arrhythmogenic substrate in AF. There is an increase in atrial fibrosis, not only in patients with AF and underlying heart disease, but also in patients with lone AF[38-41] and there is a positive correlation between the amount of fibrosis and the persistence of AF.[41] Even when the ventricular rate is controlled, rapid atrial activation in a dog causes atrial fibrosis,[42] perhaps due to the secretion of chemokines by atrial myocytes, which enhance collagen synthesis by atrial fibroblasts.[43]

Ventricular tachypacing induces congestive heart failure in dogs by causing a tachycardiomyopathy,[44] and produces atrial interstitial fibrosis comparable with many forms of clinical AF.[45] In the dog model, atrial fibrosis causes localised

regions of conduction slowing, increasing conduction heterogeneity and providing a substrate for AF.[45]

1.3.3 Catheter ablation of paroxysmal AF

In recent years, catheter ablation has emerged as an effective and potentially curative approach for patients with symptomatic paroxysmal AF. The 2012 Heart Rhythm Society, European Heart Rhythm Association and European Cardiac Arrhythmia Society consensus statement on catheter and surgical ablation of AF recommends catheter ablation as a reasonable first-line therapy for selected patients with paroxysmal AF.[46] However, this is an expert consensus, which is not necessarily supported by clinical trials, and it is still common practice to try antiarrhythmic drug therapy before proceeding to catheter ablation. Furthermore, the consensus document specifies that catheter ablation should be performed in experienced high-volume centres by experienced operators to maximise success and minimise complications. In patients who are highly symptomatic, catheter ablation can improve quality of life,[47] but as there is no randomised controlled trial demonstrating a reduction in stroke risk or mortality with catheter ablation, patients with no or minimal symptoms should be offered drug therapy for rate control. However, the Catheter Ablation versus Anti-arrhythmic Drug Therapy for Atrial Fibrillation (CABANA) Trial aims to answer this question in a prospective randomised multi-centre international study with a primary endpoint of all-cause mortality, and secondary endpoints of cardiovascular mortality and stroke.

The demonstration that paroxysmal AF is frequently triggered by ectopy arising from within the PVs has led to the emergence of PV isolation as a widely practised therapy for this arrhythmia.[48] In the early days of AF ablation, only spontaneously firing PVs were ablated. However, high recurrence rates, the increasing recognition

that all PVs can initiate AF and technological developments mean it is now routine practice to isolate all four PVs.[49]

Pulmonary vein isolation (PVI) requires transseptal access to the LA and identification of the PV ostia, following which ablation lesions are deployed in a continuous and circumferential manner to isolate the left and right PVs, either individually or in pairs, with the endpoint of electrical disconnection from the LA. Incomplete or non-transmural circumferential ablation lesions may lead to immediate or delayed reconnection of the PVs, which can be documented in the majority of cases of AF recurrence.[50]

One possible mechanism for reconnection is that the application of RF energy to the LA wall causes an acute inflammatory response. Tissue oedema during this inflammatory response may result in temporary electrical isolation of the PVs, but may prevent delivery of sufficient RF energy to cause tissue necrosis.[51] Electrical reconnection between the LA and PVs occurs once the oedema has resolved. These gaps in ablation lines are thought to be one of the reasons for the relatively modest success rates of AF ablation – a meta-analysis suggested single and multiple procedure success rates (off antiarrhythmic drug therapy) of 57% and 71% respectively,[52] whilst more recent studies have reported five-year success for multiple procedures in 80-92% of patients.[53-55]

1.3.4 Catheter ablation of persistent AF

The mechanisms responsible for persistent AF are less clear, and whilst PV foci may be involved in initiation of AF in a subset of patients, mechanisms involved in the maintenance of AF are most likely more important. Comorbidities including heart failure, hypertension, valvular heart disease and obstructive sleep apnoea are all responsible for electrical and structural remodeling of the LA with the

development of regional fibrosis, providing a substrate for persistent AF.[56] Animal studies have shown the importance of atrial rotors in maintaining AF,[57, 58] and recent human studies have suggested that ablation targeting these rotors may be able to terminate persistent AF. [59-61]

The uncertainty in the mechanisms involved in persistent AF has led to the development of many different empirical ablation strategies with often disappointing success.[62] These strategies include PV isolation, linear ablation, substrate modification targeting complex fractionated atrial electrograms, ablation of autonomic ganglia, and isolation of the SVC and CS. Stepwise procedures involving two or more of these approaches have been described with evidence for a cumulative effect.[63] However, these are based on unproven assumptions about the mechanism of AF, which contrasts with catheter ablation of AT and paroxysmal AF. A systematic review comparing multiple techniques in 32 studies suggested single procedure success rates of between 11% and 74% (mean 47%), increasing to 17% to 84% (mean 65%) with multiple procedures,[62] confirming that the optimal ablation technique for persistent AF remains unclear.

The next chapter discusses the role of CMR in providing non-invasive insights into the underlying substrate responsible for atrial arrhythmias and how CMR can be used both before and after catheter ablation procedures.

2 Atrial cardiac magnetic resonance

2.1 Introduction

Over the past two decades, CMR has evolved as a non-invasive imaging technique that allows comprehensive assessment of cardiac anatomy and function. More recently, late enhancement CMR using gadolinium-based contrast agents has enabled the imaging of myocardial tissue composition and therefore myocardial fibrosis. However, the overwhelming majority of CMR work has focused on the ventricles and it is only in the past few years that technical advancements in CMR have made late enhancement imaging of the thin atrial wall possible. In turn, the significant increase in catheter ablation for AF in the past decade has resulted in an increasing focus on CMR assessment of atrial structure and function and their potential link to arrhythmia substrate.

2.2 Atrial late gadolinium enhancement

2.2.1 Imaging myocardial fibrosis

The first clinical application of myocardial LGE was in acute and chronic myocardial infarction[64-66] and animal studies suggest a close correlation between areas of LGE in the ventricle and areas of scar on histology.[67] During the chronic phase of infarction, when dense fibrotic scar replaces infarcted myocardium, it has been shown that LGE accurately and reproducibly determines infarct size.[68] Furthermore, studies have shown the higher sensitivity for infarct detection by LGE compared with single-photon emission computed tomography.[69, 70]

Over the past ten years, many studies have been published assessing myocardial fibrosis by LGE in non-ischaemic cardiomyopathies. Different patterns of LGE have been demonstrated according to the underlying aetiology, and LGE CMR now forms an important assessment of new-onset myocardial dysfunction.[68, 71, 72]

2.2.2 Limitations of late gadolinium enhancement

LGE allows a sensitive and reproducible qualitative assessment of myocardial fibrosis, but is limited in its accuracy in quantifying myocardial fibrosis. In addition, the assessment of diffuse myocardial fibrosis is more challenging than discrete fibrosis due to the relatively lower image contrast. With conventional LGE imaging sequences, signal intensity (SI) is expressed on an arbitrary scale that differs from one imaging study to another and is not suitable for quantification between patients. Image contrast is generated by the difference in SI between normal and abnormal myocardium and, during post-processing, an arbitrary intensity threshold is defined to make this differentiation.[73] There is no consensus on the intensity threshold to use for the clinical assessment of myocardial fibrosis and various methods have been described.[73-76] This might explain why studies examining the same cardiomyopathy have reported significantly different frequencies of myocardial fibrosis and questions the reliability and reproducibility of LGE for myocardial fibrosis quantification in a clinical setting. To try and overcome this significant limitation of LGE imaging, this thesis explores the use of pathologically-validated SI thresholds to distinguish between normal and abnormal atrial myocardium.

2.2.3 Left atrial late gadolinium enhancement

Atrial wall imaging poses a greater challenge than LV imaging since the wall of the LA is several times thinner than the LV myocardium, and, therefore, greater spatial resolution is required. Over the past few years, technological developments and novel imaging sequences have made LA LGE CMR possible.[77, 78] A recent series of studies has suggested that LA LGE both before and after catheter ablation can help predict the chance of recurrence of AF by identifying the extent of pre-existing fibrosis and post-ablation injury.[51, 78-86] It has been proposed that this may allow a more individualised approach to AF ablation.

Imaging sequences for LA LGE imaging begin with an anatomical scan for LA and PV segmentation. Fifteen to twenty minutes after the administration of a gadolinium-based contrast agent, 3D LGE imaging is performed with a respiratory-navigated, ECG-triggered acquisition with a typical in-plane spatial resolution of 1.3x1.3 mm^2 and a slice thickness of 2.5-3 mm. The inversion time (TI) is determined using a preceding Look-Locker sequence to achieve optimal suppression of ventricular myocardium. The scan is typically acquired in an axial orientation, with 30-40 slices to achieve complete coverage of the LA. The length of the acquisition window is restricted to minimise motion artefacts. The two most important predictors of poor LA LGE image quality are the presence of AF (particularly with a rapid ventricular response rate) and an inconsistent respiratory navigator signal (Figure 2-1).

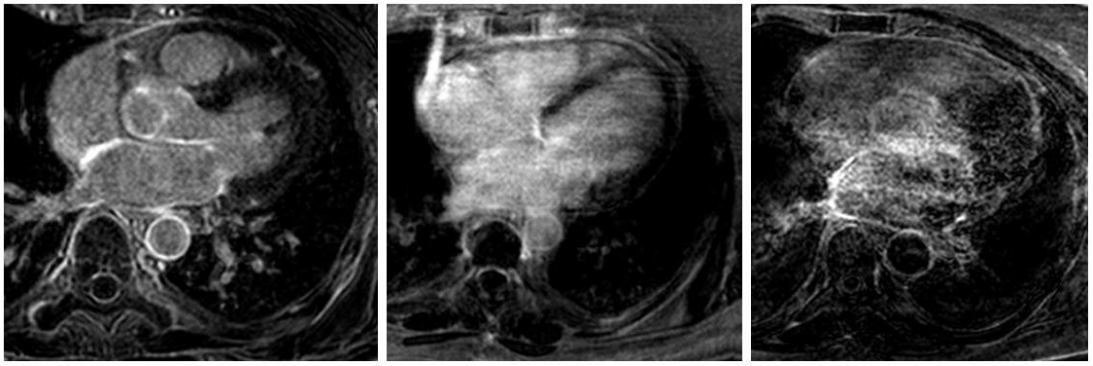

Figure 2-1: Examples of good (left) and poor (middle and right) image quality in 3D LA LGE acquisitions.

2.2.3.1 Image processing

This is one of the most challenging areas in LA LGE imaging and several methods have been suggested.[77, 80, 87] Clinical interpretation of 2D images is extremely difficult given the complex anatomy, and 3D reconstructions have been employed in most publications to date. These require both an accurate segmentation of the LA and PVs, as well as the more challenging segmentation of the LGE information from the 2D slices and registration of this information to the reconstructed shell.

In the LV, there is good image contrast between the healthy myocardium and areas of LGE. This is not the case in the much thinner-walled atrium, where it is more difficult to differentiate normal myocardium from areas of LGE, primarily due to greater susceptibility to image artefacts (motion and partial volume effect).

The method used in this thesis (Figure 2-2)[87] first involves image registration of the 2D information from the LGE scan to the b-SSFP whole heart acquisition. A

semi-automatic segmentation of the LA 3D anatomy from the b-SSFP whole heart acquisition is then performed and the registered 2D data is projected on to the 3D shell. Once fused, a maximum intensity projection (MIP) technique is used, whereby the maximum SI within ±3 mm of the 3D surface is selected as the intensity for that point on the shell. The MIP is performed in both endocardial and epicardial directions to account for potential errors in image fusion and the projection range is chosen to be large enough to extend into the LA myocardium but not so far as to project SI from other locations in the image. At ±3 mm, the projection should sufficiently account for all enhancement in the LA myocardium, which is approximately 1–4 mm thick. Signal intensities are then displayed as a number of standard deviations (SD) from the mean intensity of the atrial blood pool.

An alternative method involves manually segmenting the epicardial and endocardial borders of the LA on each slice of the 3D LGE volume (Figure 2-3).[80] This defines the LA wall as the region of interest and the SI histogram for the entire LA wall can then be determined. Based on the histogram, an SI threshold is chosen to distinguish between enhanced and non-enhanced voxels. However, the selection of this cut-off value is to some extent arbitrary, will vary from patient to patient (depending on image quality and image contrast) and influences any further data interpretation or analysis. Setting a lower threshold/cut-off value will produce a processed image showing more 'abnormal' areas, whereas a higher threshold will have the opposite effect.

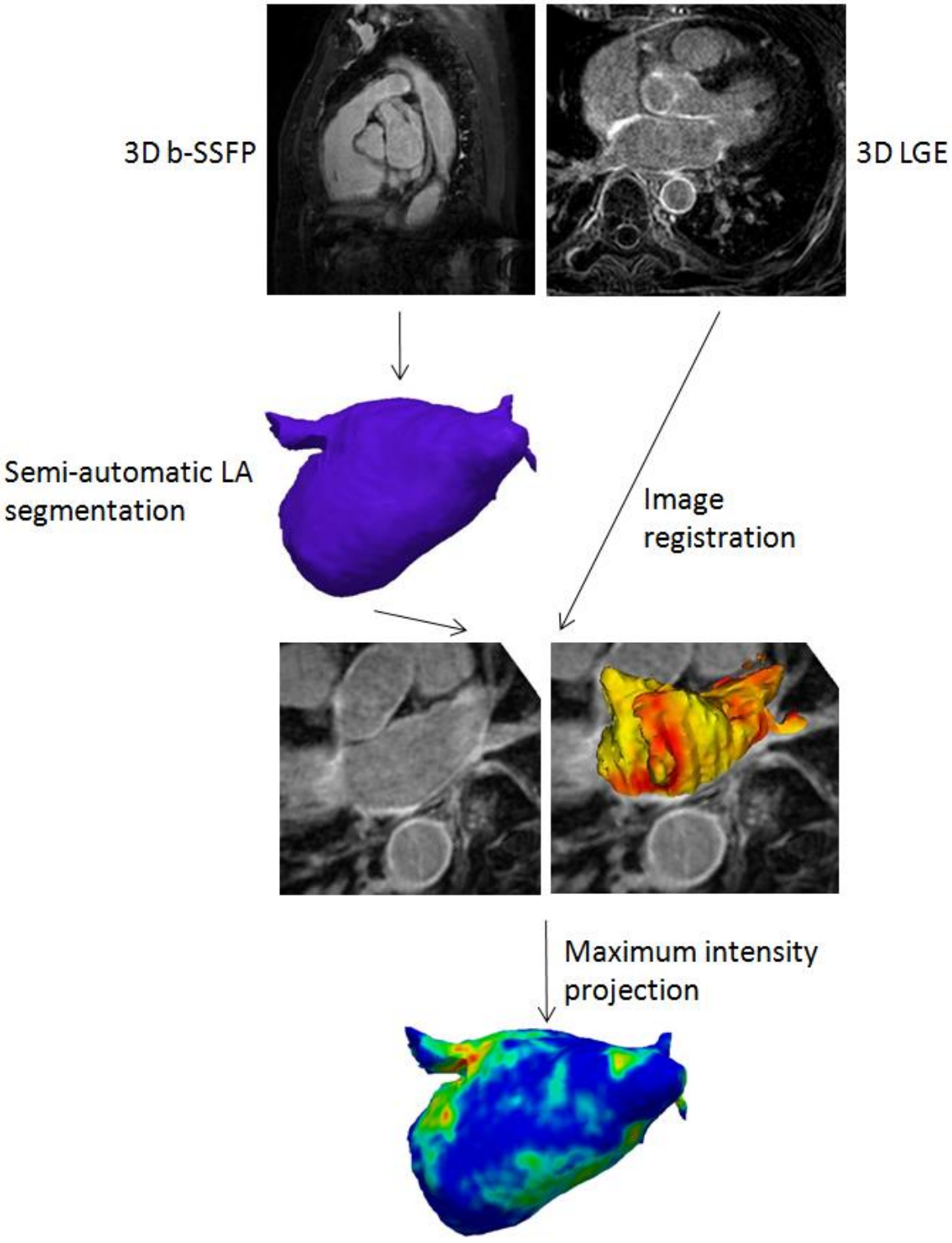

Figure 2-2: An algorithm for the 3D reconstruction of LA LGE.

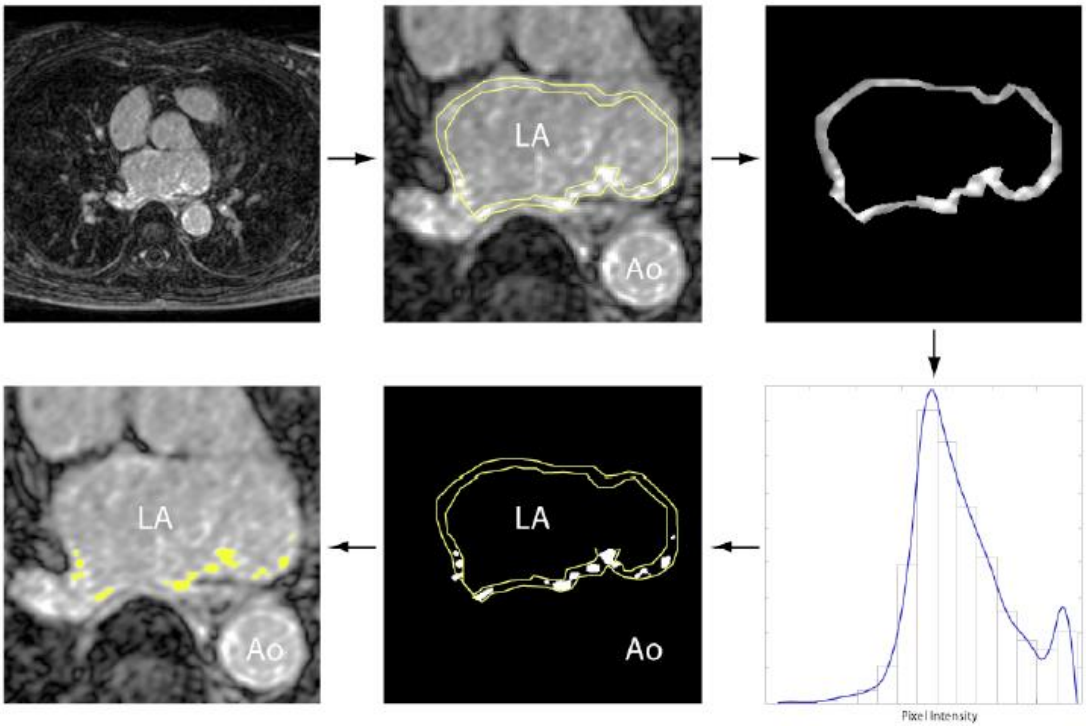

Figure 2-3: An algorithm for the detection of LGE. The epicardial and endocardial borders of the LA are first segmented to extract the LA wall. The SI histogram of the LA wall is derived and a threshold is selected to distinguish between enhanced and non-enhanced voxels.[80]

There are many potential sources of error in producing 3D representations of LGE of the LA (original image quality, image registration and selection of a threshold) and this has to be taken into account when making clinical inferences from the data, particularly those requiring high resolution information, such as small gaps in ablation lines.

2.2.3.2 Pre-ablation imaging

Irreversible remodelling of the LA is thought to limit the effectiveness of PV isolation for AF and to be an important factor impacting the success of the

procedure.[88] Endomyocardial atrial biopsies in patients with lone AF show fibrosis in the LA wall.[41] A non-invasive method of detecting the location and extent of these fibrotic areas before AF ablation might be able to predict the long-term success of the procedure in an individual patient.

A landmark study assessed the role of LA LGE CMR in detecting the extent of atrial remodelling in 118 patients before AF ablation for either paroxysmal or persistent AF.[80] Image quality was insufficient in 37 patients, leaving 81 patients in the study. The authors identified varying degrees of LGE in the LA wall, with 43 patients having mild enhancement (<15% of the LA wall area), 30 with moderate enhancement (15-35% of the LA wall area) and 8 with severe enhancement (>35% of the LA wall area). At six month follow-up, AF recurrence increased with pre-ablation enhancement, with 14% recurrence in the mild enhancement group, 43% in the moderate enhancement group and 75% in the severe enhancement group. The study concluded that LA LGE CMR is able to offer a non-invasive means of predicting disease severity and response to AF ablation.

The same group later revised the extent of LA enhancement into a 4-stage classification system: Utah I (<5% enhancement), Utah II (5-20% enhancement), Utah III (21-35% enhancement) and Utah IV (>35% enhancement).[83, 84] These studies once again suggested that the extent of pre-existing LGE is proportional to the incidence of AF recurrence, despite there being comparable LGE across the four Utah stages on follow-up scans three months after ablation. There was no difference in this finding between patients with lone and those with non-lone AF. They further stated that a more extensive

ablation strategy was appropriate in those with more enhancement, and that in Utah IV ablation was unlikely to be successful.

This non-invasive pre-ablation imaging has recently been extended to predicting the risk of stroke in AF. It is known that LA structural remodelling in AF increases the risk of thromboembolism[89] and, therefore, the extent of LGE in the LA wall may be a predictor of stroke risk. Investigators used the Utah staging system to show that patients with more LA enhancement were more likely to have had a previous stroke and have a higher $CHADS_2$ score[90] than those with less LA enhancement.[91] However, this has not yet been assessed prospectively.

2.2.3.3 Post-ablation imaging

The technique of LA LGE CMR after catheter ablation for AF was first described in 2007 in 23 patients in a study that attempted to quantify the extent of circumferential enhancement of the PVs on 2D reconstructions of the PV ostia.[77] However, unlike the studies in the previous section, this study did not show pre-ablation LGE in any patients.

A similar technique was then used to assess the relationship between AF recurrence and the extent of post-ablation LGE at three months.[78, 81] These studies, in cohorts of 46 and 86 patients, reported significantly less total LA wall enhancement in patients with AF recurrence. They also showed complete encirclement of only 39% of PVs at three months post-ablation, with the number of PVs encircled being proportional to procedural success. In the first of these studies, the authors did not report any significant pre-ablation enhancement, with only mild enhancement in four patients.[78]

The authors of these two studies suggested that certain patients may be more 'resistant' to scar formation, although the mechanisms responsible are not understood. It may be that those with more pre-existing LA remodelling are less likely to form scar, although this would not be consistent with the finding of comparable LGE at three months across the four Utah stages.[83]

Insights into the temporal formation of LA scar have also been revealed by LGE imaging.[79] CMR scans at 24 hours post-ablation were repeated at three months in ten patients (and at six and nine months in 16 patients). This showed that LGE imaging within 24 hours of ablation overestimates the extent of enhancement at three months, suggesting a transient inflammatory response, which then resolves. This is due in part to LA wall oedema, shown on T2-weighted (T2W) imaging, which has resolved by three months.[51, 87] This thesis explores these LGE and T2W imaging findings in an animal model of acute and chronic atrial ablation injury.

2.3 Atrial anatomy, volume and function

The assessment of LA and PV anatomy by CMR can be used to help plan ablation procedures and monitor for their complications. These structures can be imaged using standard black-blood spin echo CMR techniques, which are sufficient to identify the LA and proximal PVs and their relationships to the surrounding structures. Further anatomical detail, particularly of the PVs, can be obtained using contrast-enhanced MR angiography, with protocols typically involving short TR, high flip angles and fractional echoes to provide highly T1-weighted images with minimal flow artefacts.[92-100] Spatial resolution is typically 1-2 mm^2 in plane with 2-4 mm slices, and a single 3D volume can be acquired in

a 10-20 second breath-hold. The sequence is not ECG-triggered, which can cause motion artefact of both the LA and PVs (the position of the PVs changes throughout the cardiac cycle[97, 101]). A gadolinium-based contrast agent is injected at 1-2 ml/s and a pre-contrast subtraction mask can be used, although this is not necessary since the background signal from the lungs is low. Acquisition timing is critical and this is achieved using a bolus timing scan[102] and multiple dynamics to ensure acquisition during peak contrast in the LA.

An alternative anatomical protocol involves a non-contrast-enhanced 3D b-SSFP acquisition with a 2-3 mm isotropic resolution.[87] This sequence uses the respiratory navigator to minimise motion artefacts and to ensure acquisition at end-expiration for all slices. The acquisition is ECG-triggered, with the length of the acquisition window set to maximum of 150 ms to minimise motion artefacts.

Thereafter, either acquisition can be viewed on a workstation using multi-planar reformatting to dynamically view 2D slices of the 3D dataset in any orientation (Figure 2-4). However, it is difficult to produce a single summary image of the anatomy; techniques employed include a MIP or 3D reconstructions to produce shaded or volume-rendered images (Figure 2-5).

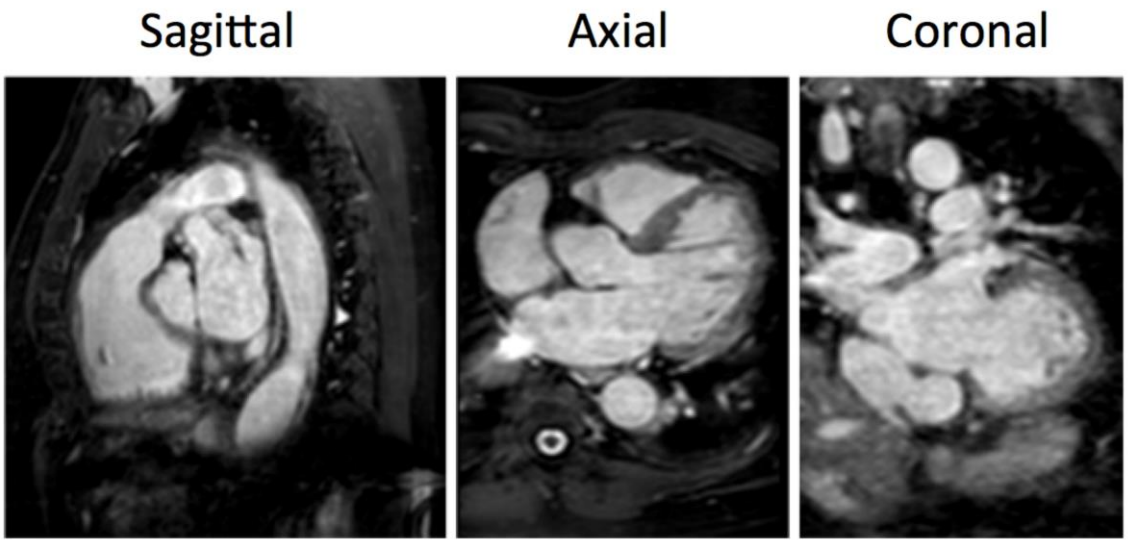

Figure 2-4: Multiplanar reformat of a 3D b-SSFP acquisition.

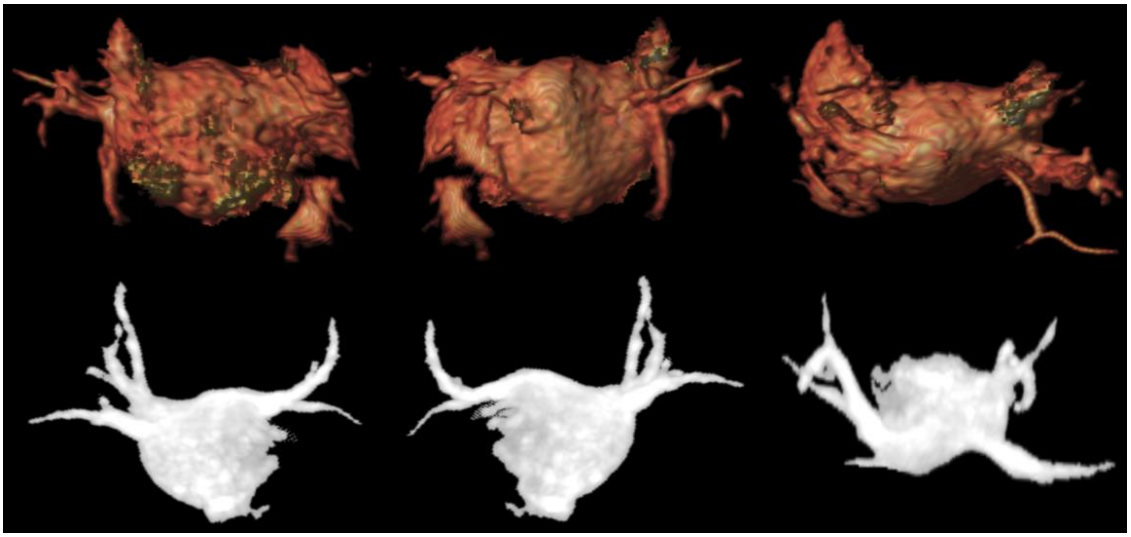

Figure 2-5: LA volume-render of a b-SSFP acquisition (top row) and MIP of an MR angiogram (bottom row) from the same patient, in three different views.

2.3.1 Atrial volume and function

Atrial enlargement is seen in a wide range of cardiac and pulmonary conditions and plays an important role in the development and maintenance of AF.[103, 104] Atrial size is a marker of LA structural remodelling, a predictor of AF and mortality, and a key determinant of therapeutic strategy in the management of AF.[89]

Atrial volumes measured by cine CMR show a good correlation with volumes measured in cadaveric casts.[105] The most accurate method of measuring atrial volume and function is the multiple slice method, whereby manual tracings of the atria are made on each cross-sectional image.[106] However, this method is time-consuming and so simplified methods have been employed, using the single-plane area length method. This measurement is taken on a four-chamber acquisition, a technique previously used to determine LA and LV size using echocardiography[107] and LV volume and function using CMR.[108-110] However, one study found that the area length method underestimated LA volume and overestimated LA function compared with the multiple slice method.[106]

CMR has been used to compare LA volumes in patients with paroxysmal AF with healthy controls, with one study showing significantly larger volumes in paroxysmal AF patients[111] and another finding no significant difference.[112] Whilst CMR-measured LA volumes are significantly greater in patients with persistent AF than those with paroxysmal AF,[113] there is no difference between patients with persistent and permanent AF, suggesting that LA dilatation stabilises once AF becomes persistent.[114]

CMR has also shown the immediate reduction in atrial systolic volumes following cardioversion.[115] There was a further recovery of atrial dimensions at 30 days and 180 days. However, only the RA volumes were completely normalised 180 days after cardioversion.

Pre-ablation LA volume measured by CMR has been shown to be the main determinant of the outcome of PV isolation and linear ablation in a study of 240 patients undergoing ablation for drug-refractory AF,[116] whilst another CMR study suggested that, in a multivariate analysis, LA volume was not statistically significant in determining outcome from PV isolation for paroxysmal AF.[117] CMR has also demonstrated a reduction in LA volume three to four months after PV isolation,[118, 119] however there was no relationship between LA volume reduction and AF recurrence.[118]

There are few data on the CMR assessment of LA function after AF ablation. In one of the aforementioned studies, there was a mild reduction in LA function following PV isolation.[119] This finding is supported by another study of 33 patients who underwent ablation for paroxysmal or persistent AF, in whom there was a mean reduction in LA ejection fraction of 14% following ablation.[120] However, another study, using velocity-encoded CMR, demonstrated an improvement in LA and LA appendage function six months following stepwise ablation for persistent AF.[121]

2.3.2 Pulmonary venous anatomy and stenosis

PV imaging is important for planning LA ablation procedures and for diagnosing PV stenosis following ablation. PV diameters are normally measured on the multi-planar reformat of the contrast-enhanced MR angiogram or the 3D b-SSFP

acquisition in a single plane at the ostia of the PV.[92, 122-124] However, reproducibility is poor and identification of the true PV ostia can be difficult, because there is no well-defined border with the LA. Furthermore, the PV ostia are ovoid, not round, so measurements depend on the imaging plane.[92, 93] Measuring the PV diameter in the sagittal plane has been suggested to be the most reproducible method, which may be advantageous for serial examination.[93] Additional measurement error can be introduced in non-cardiac-gated angiography, because the PV diameter varies over the cardiac cycle with a maximum diameter during ventricular diastole.[97, 125]

A 2D multi-slice breath-hold ECG-gated SSFP cine acquisition has been shown to have comparable precision with contrast-enhanced MR angiography.[126] However, both methods showed a significant range of intraobserver and interobserver agreement. No study has compared PV measurements using contrast-enhanced MR angiography and 3D b-SSFP acquisitions.

Despite these potential inaccuracies in the measurements of PV diameters, CMR can provide an accurate assessment of the branching pattern of the PVs. In a study of 28 patients, variant PV anatomy was found in 38% of patients and patients with AF had larger PV diameters than matched controls.[111] Another study, in a much larger cohort of 437 patients, found that only 40% of patients had a typical PV branching pattern of two left and two right PVs.[113] A short and long common left trunk was found in 20% and 11% of patients respectively. A right middle PV was found in 30% of patients and two right middle PVs were found in 1.5% of patients. Atypical accessory PVs were documented in 6% of patients and 9% had a common left trunk with a right middle PV.

In the early years of AF ablation, RF ablation was delivered within the PVs and PV stenosis was not an infrequent complication.[127] When severe, this complication can cause pulmonary hypertension and severe breathlessness. This complication led to a change in practice to deliver RF energy outside of the PVs, towards the PV antra. CMR can be used to diagnose PV stenosis, albeit with the caveats mentioned above, and several studies have used contrast-enhanced MR angiography in these circumstances.[122, 128, 129]

2.3.3 Stroke risk

Stroke is one of the most devastating complications of AF and thrombus formation within the LA appendage is thought to be the origin of most thromboemboli in AF.[130] Whilst transoesophageal echocardiography (TOE) is the clinical standard for diagnosing LA appendage thrombus, TOE is invasive and has a small risk of serious complications. CMR is an alternative, non-invasive technique for assessing the LA appendage. A study of 50 patients compared TOE with CMR and found that the LA appendage was easily visualised in all patients with CMR.[131] Concordance between the detection of a high SI mass with CMR and thrombus with TOE was high. Another study of 97 patients undergoing PV isolation showed 100% concordance between the two imaging modalities.[132] However, in a study of 25 patients, contrast-enhanced CMR lacked diagnostic accuracy compared with TOE as the gold-standard.[133]

CMR can also be used to predict stroke risk in patients with AF. 144 patients with non-valvular AF underwent CMR to assess LA appendage volume and dimensions.[134] Patients with a history of stroke or transient ischaemic attack had higher LA appendage volumes and dimensions than those with no previous

history. Velocity-encoded CMR may be able to determine 3D flow patterns within the LA and LA appendage, providing insight into the mechanism of stasis and thrombus formation, however this remains a research tool.[135]

The next chapter describes the physical principles of the CMR sequences described in this chapter.

3 Principles of cardiac magnetic resonance

3.1 Introduction

CMR is ideally suited to imaging the thin atrial wall – it is non-invasive, does not involve ionising radiation or have any known long-term harmful effects, has excellent spatial resolution and is able to distinguish between different tissue types based on their different physical properties.

3.2 Nuclear spins in a magnetic field

A hydrogen atom consists of a central nucleus that contains one proton, surrounded by a single electron. Nuclei have a quantum mechanic property called nuclear spin and a magnetic moment proportional to the nuclear spin.

When an external magnetic field (the B_o field) is applied, the magnetic moments align in the direction of the external field (spin-up) or in the opposite direction (spin-down). In thermal equilibrium, more spins are in the spin-up state than in the spin-down state. The difference between the numbers of spins in each state is determined by a Boltzmann distribution and, at room temperature, this difference is in the order of a few parts per million.

Once in an external magnetic field, the protons do not remain static. They precess akin to the cone shape formed by a spinning-top. The frequency at which they precess is known as the Larmor frequency (ω_0) and is determined by the magnetic field strength (B_0) and gyromagnetic ratio (γ), as described in the Larmor equation ($\omega_0 = \gamma.B_0$).

The precession frequency is measured in (M)Hz, the gyromagnetic ratio in (M)Hz/Tesla and the field strength in Tesla. The gyromagnetic ratio is different for different materials/atoms – the value for hydrogen nuclei is 42.5MHz/Tesla.

The z-axis is denoted as being parallel to the external magnetic field, whilst the x-axis and y-axis are perpendicular to the external magnetic field. As already described, more magnetic moments align in the direction of the magnetic field than in the opposite direction and so there is a net magnetisation in the z-axis once a subject is placed in the MR scanner. This is known as longitudinal magnetisation.

3.3 Radiofrequency excitation

CMR is performed by placing the patient within a strong and modifiable magnetic field. Once the subject is in the magnetic field, an RF pulse is applied to disturb the equilibrium state of the nuclear spins. This is only possible if the frequency of the RF band of the electromagnetic spectrum corresponds to the precession frequency of protons (they are in resonance), such that energy exchange from RF to the nuclear spins is possible. As the precession frequency of the protons is determined by the Larmor equation, this also dictates the frequency of RF required. The application of an RF pulse that is on resonance with the precessing hydrogen nucleus is termed excitation.

When RF is applied, some spins go from the low to the high energy state. Furthermore, the RF pulse causes the spins to precess in step – it puts the protons in phase. This leads to a measurable transverse magnetisation. The angle between the z-axis and the new net magnetisation vector is known as the flip angle and its magnitude depends upon the amplitude and duration of the RF

pulse. Once the RF pulse is removed, the protons continue precessing at their precession frequency and this change in magnetic flux induces an electric voltage, which can be detected by an RF antenna – the MR signal.

3.4 T1 and T2 relaxation

After the RF field is switched off, the protons from the higher energy state return to the lower energy state. However, this is not an instantaneous process and not all protons do this at the same time. During this relaxation, energy is transferred from the protons to their surroundings, known as the lattice. Longitudinal relaxation is also, therefore, known as spin-lattice relaxation. A graph of longitudinal magnetisation against time is known as a T1 curve (Figure 3-1) and the time constant of this process is the T1 time or longitudinal relaxation time. The T1 time is defined as the time to reach 63% of the equilibrium longitudinal magnetisation.

Following removal of the RF pulse, the protons progressively become out of phase (they lose phase coherence). As a result, transverse magnetisation decreases and this is also known as spin-spin relaxation. A graph of transverse magnetisation against time is known as a T2 curve (Figure 3-1) and the time constant of this process is the T2 time or transverse relaxation time. The T2 time is defined as the time at which transverse magnetisation has reduced to 37% of its original value.

The T1 and T2 values depend on the properties of the tissue and can therefore provide physical information. Water has a long T1 and long T2 value, whilst fat has a short T1 and short T2. T1 values are also strongly dependent upon the magnetic field strength.

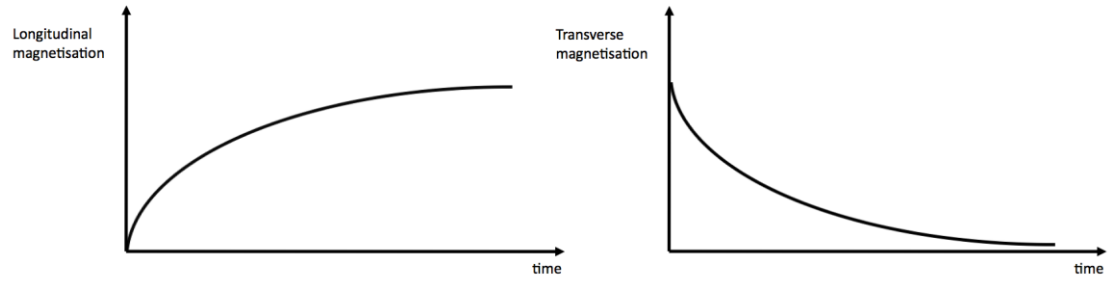

Figure 3-1: The amount of magnetisation in the longitudinal plane gradually increases back to its original state and this is called T1 relaxation (left). At the same time the amount of magnetisation in the transverse plane gradually decreases, and this is called T2 relaxation (right).

3.5 Pulse sequences

Pulse sequences comprise a combination of RF pulses and/or gradient fields. The time from one RF excitation to the next is known as the repetition time, TR.

3.5.1 Spin echo sequences

Spin echo sequences begin with a 90 degree excitation pulse to flip the net magnetisation vector into the transverse plane. When the 90 degree pulse is removed, a free induction decay (FID) signal is produced. T2* dephasing also occurs, which describes the dephasing of transverse magnetisation caused by the combination of spin-spin interactions (T2 decay) and macroscopic magnetic field (B_0) inhomogeneities. If a 180 degree pulse is applied at a time TE/2 (TE is the echo time) after the 90 degree pulse, the protons will start precessing in the opposite direction and the faster protons will begin to 'catch-up' with the

slower protons. At time TE, the protons will be temporarily almost back in phase, resulting in increased transverse magnetisation and, therefore, signal. This resulting signal is called a spin echo. The 180 degree pulse only compensates for the constant inhomogeneities of the external magnetic field, with no effect on temporally-varying inhomogeneities. Therefore, the obtained signal is T2 weighted.

It is possible to keep repeating 180 degree pulses to give a series of spin echoes, however each one will have a lower intensity than the previous one (due to T2 effects). A pulse sequence consisting of a 90 degree pulse followed by a 180 degree pulse is known as a spin echo sequence.

3.5.2 Gradient echo sequences

The problem with spin echo sequences is that the acquisition time is relatively long because of the duration of RF and the long TR required. Gradient echo sequences are a faster imaging technique, which do not require a 180 degree pulse and use smaller flip angles (which require a shorter duration of RF) for data acquisition. Therefore, only part of the longitudinal magnetisation is converted into transverse magnetisation. A temporary additional magnetic field gradient is superimposed on the existing magnetic field to increase field inhomogeneities and dephase nuclear spins. The gradient is then applied in the opposite direction to rephase the spins and produce a gradient echo signal (Figure 3-2). Since the gradients can be applied rapidly, the minimum TE is much shorter than in spin echo sequences, and so the TR can also be reduced. However, gradient echo sequences are more susceptible to magnetic field

inhomogeneities than spin echo sequences. The obtained signal is dependent on T2*.

With fast gradient echo imaging, the TR is usually shorter than $T2^*$ in most tissues. This means the transverse magnetisation may not have fully decayed before the next RF pulse occurs. The following RF pulses may then tip this residual magnetisation towards the longitudinal plane. If this process is not very well controlled the contribution of the transverse magnetisation can corrupt the image contrast. The easiest way to resolve this problem is to eliminate the transverse magnetisation before the subsequent RF pulse, a process called spoiled gradient echo. Another approach is known as balanced steady state free precession (b-SSFP), which has an improved signal to noise ratio (SNR) and contrast to noise ratio (CNR).

3.5.2.1 Spoiled gradient echo

A gradient echo sequence can be spoiled by either RF spoiling or spoiler gradients (or both). If RF spoiling is used, a phase is added to each successive RF pulse to avoid coherence. With spoiler gradients, an extra gradient is added at the end of the readout and slice selection gradient before the next RF pulse. This gradient causes dephasing of the residual transverse magnetisation. After a number of RF pulses and assuming that perfect spoiling is achieved, the transverse magnetisation is zero before each RF pulse and the magnetisation reaches a steady state.

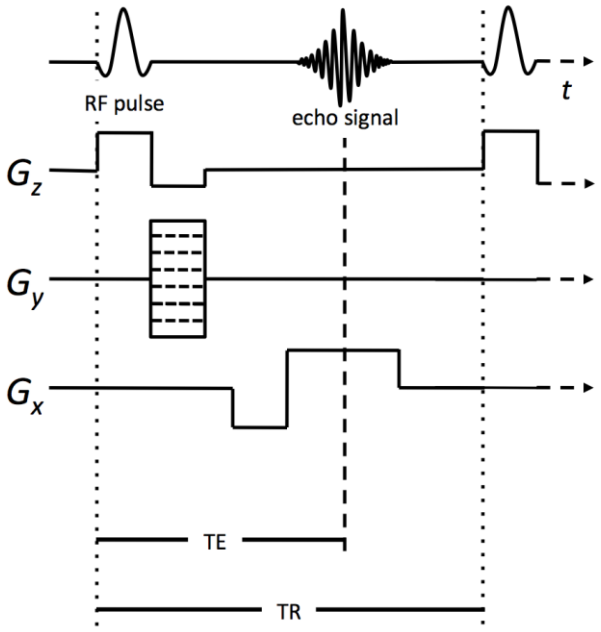

Figure 3-2: A gradient echo pulse sequence uses an RF excitation pulse that is variable. The magnetic moments within the transverse component of the magnetisation are dephased and are then rephased by a gradient pair.

3.5.2.2 Balanced steady state free precession

Balanced steady state free precession acquisitions are gradient echo sequences in which the net phase shift introduced by the gradients is exactly zero after each TR. In these sequences, the gradients are compensated by applying a gradient pulse with the opposite polarity at the end of each TR, which results in a net magnetisation vector that is not dephased. The images provided by b-SSFP sequences have an SI proportional to the T2/T1 ratio. Furthermore, due to the lack of net dephasing, the entire magnetisation vector contributes to the MR signal, giving higher SNR.

These characteristics have played an important role in cardiovascular imaging since the T2/T1 ratio is approximately four-fold higher for blood than myocardium. The b-SSFP sequence, therefore, provides a much higher contrast between blood and myocardium and an improved SNR compared to other gradient echo sequences. However, B_0 inhomogeneities can cause additional dephasing and modification of the steady state signal. The resulting off resonance can result in dephasing of the magnetisation and collapse of the steady state signal, causing so-called banding artefacts.

3.6 Cardiac MR sequences

3.6.1 Inversion recovery sequences

Inversion recovery (IR) sequences begin with a 180 degree pulse, which inverts the longitudinal magnetisation. After a given time, known as the inversion time (TI), data acquisition is carried out. Tissues with a shorter T1 value will have regained more longitudinal magnetisation by the time data is acquired and so the transverse magnetisation and obtained signal is dependent on tissue T1 values. The contrast of the image depends primarily on the length of the TI. Inversion recovery can be used to produce heavily T1-weighted images as the 180 degree inverting pulse achieves full saturation.

3.6.1.1 Late gadolinium enhancement

Late gadolinium enhancement (LGE) imaging uses a T1-dependent IR technique to exploit the significant shortening of T1 by gadolinium contrast agents, the SI being dependent upon the local tissue gadolinium concentration. Gadolinium is a small paramagnetic molecule and can enter the interstitial space in the

myocardium. In normal myocardium, the interstitial space is minimal, but is expanded in certain pathological states (e.g. fibrosis, inflammation, infarction and infiltration), so that sufficient gadolinium is present to be detected. Furthermore, gadolinium washes out of tissue capillary beds within minutes, but takes 10-30 minutes to wash out from the interstitial space. By imaging within this window using a TI where normal myocardium has a net magnetisation vector of zero (and therefore appears black or 'nulled'), the difference with normal myocardium (from which gadolinium has washed out) can be exploited (Figure 3-3).

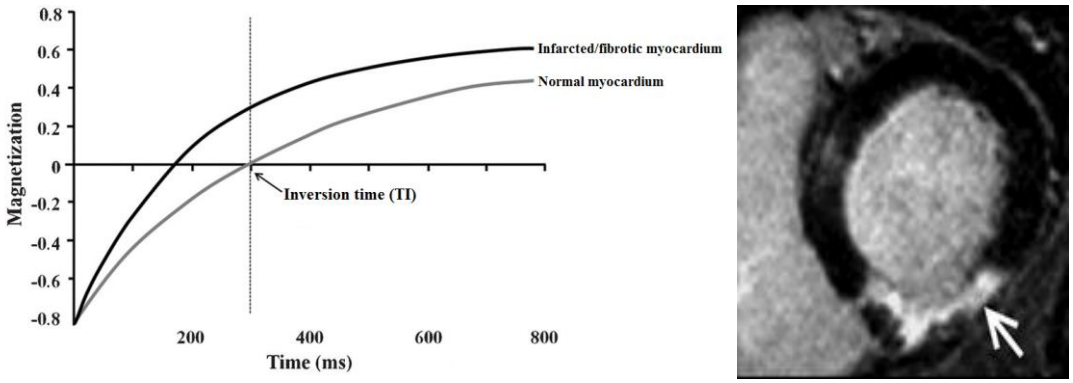

Figure 3-3: If a TI is chosen at which normal myocardium has a net magnetisation vector of zero, gadolinium-containing tissues will have greater SI, maximising the contrast between the two tissue types.

3.6.2 Contrast-enhanced magnetic resonance angiography

Magnetic resonance angiography is a commonly used imaging technique for imaging cardiac and vascular anatomy. The relatively short scan time means that the acquisition can be performed within a single breath-hold, minimising respiratory motion artefacts. Using T1-weighted sequences, gadolinium

contrast agents improve the SNR by creating a high intravascular signal. Timing the MR acquisition with the arrival of contrast in the area of interest is crucial. There are many strategies to optimise the synchronisation of the acquisition and the arrival of the contrast bolus. Real-time low-resolution T1-weighted sequences can be used to track the arrival of contrast from the arm to the ascending aorta, and the scan is either automatically or manually triggered. Alternative methods include the use of a test bolus and automated bolus detection algorithms.

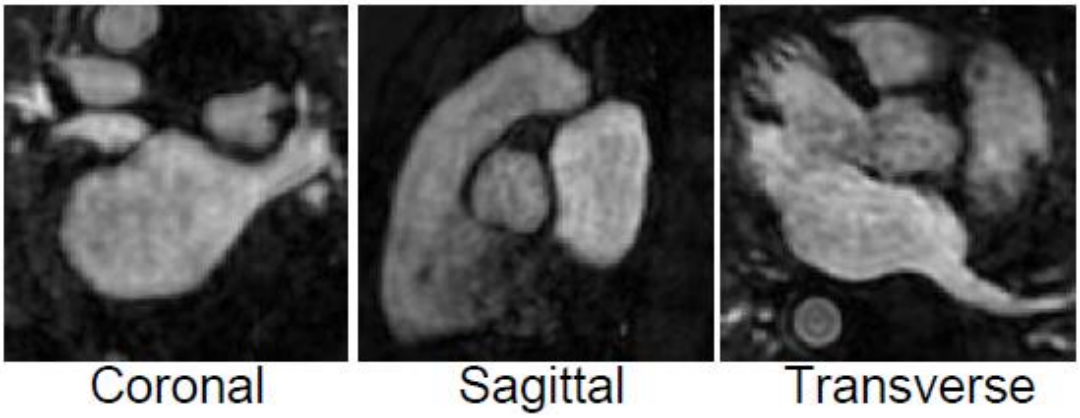

Figure 3-4: Coronal, sagittal and transverse (axial) slices of a 3D MR angiogram, with the brightest SI in the LA.

3.7 Encoding and image information

To create an MR image, it is first necessary to localise the MR signal in three dimensions. The first step is slice selection, followed by locating (encoding) the signal along both axes of the image (frequency and phase encoding). These processes are performed by additional magnetic fields, which are superimposed on the external magnetic field, with location-varying strengths, known as

gradient fields. Therefore, different parts of the body experience different field strengths and so the precession/resonant frequency of protons is different, a process called spatial encoding.

An RF pulse with a particular range of frequencies (bandwidth) can be applied to selectively excite a particular slice; the wider the range of frequencies, the thicker the slice. Alternatively, if the bandwidth is kept constant, the slice thickness can be altered by adjusting the slope of the gradient field along the slice encoding direction. Normally, in spin echo sequences, the slice selection gradient is switched on during application of the 90 degree excitation pulse and during the 180 degree refocusing pulse, to excite and rephase each slice selectively. In gradient echo sequences, the slice select gradient is switched on during the excitation pulse only.

The frequency encoding gradient alters the field strength and, therefore, precession frequency along the axis of the gradient. The gradient, therefore, produces a frequency shift along its axis and the signal can be located along the axis of the gradient according to its frequency. The frequency encoding gradient is switched on when the signal is received and is often called the readout gradient. Equally, when the phase encoding gradient is switched on, the magnetic field strength, and therefore the precession frequency of protons along its axis, is altered. The phase encoding gradient is typically switched on between excitation and signal collection.

The application of all gradients selects an individual slice and produces a frequency shift along one axis of the slice and a phase shift along the other. An individual signal within the image can now be located by their measured

frequency and phase. The data points are acquired in an array known as *k*-space. Usually *k*-space is filled linearly but it can also be filled with other patterns, for example radial. Data acquired in the central lines contribute the lower frequencies in the image (image contrast), while data acquired in the outer lines contribute higher frequencies (resolution). The scan time is the time to obtain all the required *k*-space information. Following data acquisition, *k*-space is converted into an interpretable MR image by Fourier transformation.

3.8 Image quality

The choice of pulse sequence determines the weighting and quality of the images, and their sensitivity to different tissues/pathologies. Two of the main considerations for determining image quality are the SNR and CNR.

The SNR is commonly determined as the ratio of the mean SI of a region of interest to the SD of the background signal. Many factors affect the signal strength such as the magnetic field strength, voxel volume, TR, TE and flip angle, receive bandwidth, coil type and contrast agents. CNR is defined as the difference in SNR between two adjacent areas and is therefore influenced by some of the same factors.

3.9 Motion artefacts

Cardiac and respiratory motion of the heart can strongly impair image quality. Several approaches have been presented to address this problem.

3.9.1 Cardiac motion

Cardiac synchronisation

Cardiac synchronisation is used to minimise motion artefacts arising from the beating heart and from pulsatile blood flow. The MR data acquisition is synchronised with the cardiac cycle using the ECG. The pulse sequence is triggered when the amplitude of the R-wave reaches its maximum voltage. Although the ECG signal obtained during MR scanning can be used for cardiac synchronisation, it suffers from artefacts due to magnetohydrodynamic effects and cannot, therefore, be used diagnostically.

The ECG signal can be used in several ways to guide the acquisition. Prospective gating detects the R-wave and starts RF excitation and data acquisition after a certain delay time (known as the trigger delay). When using prospective cardiac gating, data acquisition must be completed before the start of the next cardiac cycle. If the acquisition overruns into the next cardiac cycle, the next R-wave is ignored, prolonging the scan.

In retrospective cardiac gating, data are continuously acquired throughout the scan whilst monitoring the ECG signal. During reconstruction, time points are assigned to the acquired profiles with respect to the cardiac cycle. An interpolation process is then performed in order to reconstruct the desired number of cardiac phases. The advantage of this technique over prospective cardiac gating is that data for the entire cardiac cycle is obtained.

3.9.2 Respiratory motion

In order to avoid image degradation from breathing artefacts, motion-compensation strategies are normally employed. These include breath-holding, the use of a respiratory belt and respiratory navigator echoes.

Breath-holding

Image artefacts caused by respiration can be reduced by breath-holding. However, for high-resolution imaging, and especially for 3D imaging, it is often not possible to acquire the data in a single breath hold. Patients may be unable to hold their breath repeatedly and changes in the breath-hold position can cause misregistration of the images in multi-slice acquisitions and artefacts in 3D acquisitions.

Respiratory belt

The respiratory belt system is based on a pressure sensor fixed with a belt, which is placed around the waist of the patient. Due to the movement of the abdomen during a breathing cycle, the pressure on the sensor changes over time, which is used as a respiratory signal. The signal from the pneumatic belt sensor is normally used to gate the image acquisition to particular breathing phases.

Respiratory navigator

A one dimensional navigator is used in which the RF excitation pulse excites a slab or pencil beam of spins. The data is acquired along a single dimension (readout direction) and, by obtaining this information frequently, these projections can be used to determine diaphragmatic motion. With prospective

gating, image data are only acquired when the respiratory phase is within the predefined acceptance window (a window location near the end-expiratory phase is usually chosen). The acceptance window width (typically 3-6 mm) and window location are determined from navigator data acquired over a period before image acquisition starts. An acceptance window that is too wide will result in poor image quality, whilst a smaller acceptance window improves image quality, but results in longer scanning times as more data is rejected.

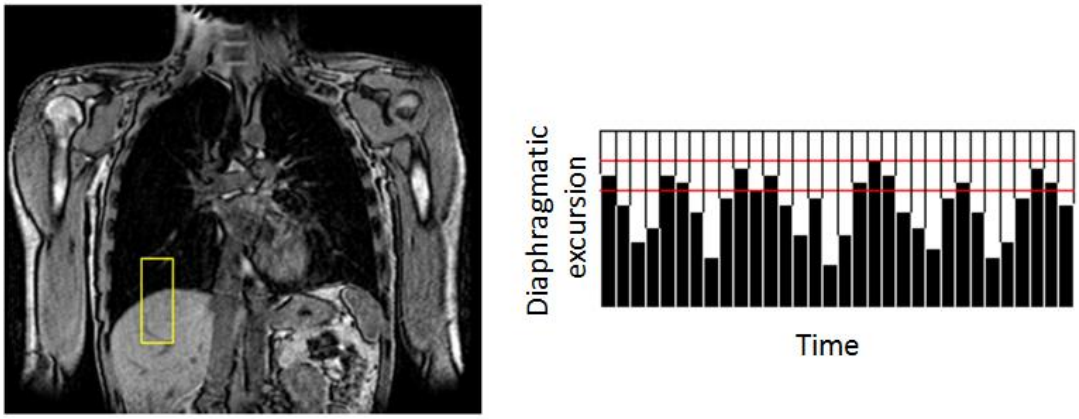

Figure 3-5: A diagram showing the position of the respiratory navigator with respect to the diaphragm (left) and an idealised profile produced by the navigator, showing movement of the diaphragm (right). Red lines indicate the acceptance window.

Whereas the physical principles and CMR sequences described in this and the previous chapter have principally been used for atrial imaging before and after ablation, the next chapter discusses how they can be applied to real-time MR-EP.

4 Magnetic resonance-guided electrophysiology

4.1 Introduction

The use of CMR to guide EP procedures has several potential advantages over x-ray fluoroscopy and conventional EAM systems. Perhaps the most significant potential advantage is the ability to image ablation lesion formation during the procedure, using a variety of imaging techniques. Furthermore, CMR allows rapid imaging in any plane, with the potential to visualise EP catheters in relation to real-time, high resolution cardiac anatomy. This avoids the errors of using pre-acquired CMR images with possible image registration errors. Finally, MR-EP eliminates patient and physician exposure to ionising radiation.

A number of recent technical advances have allowed the development of comprehensive MR-EP systems, although translation into human studies remains limited.

4.2 Intraprocedural ablation lesion imaging

Traditional endpoints of EP procedures are conduction block across an ablated region or inability to induce a previously inducible arrhythmia. While these endpoints may be appropriate for simple arrhythmias including atrioventricular node- or atrioventricular reentrant tachycardia, they do not necessarily determine long-term procedural success for more complex substrate-dependent arrhythmias such as AF or ventricular tachycardia where electrical reconnection and arrhythmia recurrence are common.[50, 136, 137] CMR

imaging techniques may be able to visualise areas of permanent damage, rather than relying on potentially transient electrophysiological endpoints.

The first description of MR-EP was a study in 2000, in which continuous real-time interactive CMR was used to position non-ferromagnetic catheters at the RV apex of six mongrel dogs.[138] RF ablation was performed and ablated tissue imaged with T2W fast spin-echo and gadolinium contrast-enhanced T1-weighted gradient-echo sequences. Lesion size by CMR was determined and compared with measurements at gross pathological examination. Ablated areas of myocardium appeared as hyperintense regions directly adjacent to the catheter tip and could be detected two minutes after RF delivery. Lesions reached maximum size approximately five minutes after ablation. Lesion size by CMR correlated well with postmortem lesion size (r=0.958).

A subsequent study further investigated CMR imaging patterns following RF ablation.[139] Using a power-controlled, cooled-tip ablation system, RF ablation lesions were created on the RV epicardium of ten mongrel dogs. T1- and T2W CMR images were acquired during a 12-hour follow-up period and compared with gross pathology. Lesions were successfully visualised with T1- and T2-weighted images 30 minutes to 12 hours after RF ablation. T2 images were more consistent, displaying an elliptical, high-intensity core with a surrounding low-intensity rim, corresponding to zone of tissue necrosis and the transition zone, respectively. T1-weighted images had a lower contrast and there was no surrounding low-intensity rim. Lesion size and appearance were well defined and unchanged during the 12-hour follow-up.

Gadolinium-enhanced CMR has also been investigated for imaging ablation lesion formation. Using the same animal model as in the previous study, investigators performed T1-weighted fast gradient echo CMR following RF ablation and the injection of gadolinium contrast.[140] In this study, four distinct phases of signal enhancement were observed. After gadolinium injection, RF lesions were initially seen as areas of low SI. Signal enhancement then progressed from the lesion periphery towards the lesion centre. Maximum enhancement was observed after one to two hours. During the ten-hour follow-up period, contrast started to decrease but the lesions remained detectable. During the first three phases of enhancement (up to two hours after contrast), CMR lesion measurements correlated well with pathological findings. However, the time required for full renal clearance and the maximum allowable dose of gadolinium-containing contrast agents limit their use in serial lesion assessment during a procedure.[141] Nevertheless, contrast-enhanced CMR may still be useful in evaluating gaps in ablation lesions at the end of a procedure.

4.3 Increasing temporal resolution

CMR can generate excellent spatial resolution by spreading data collection over multiple heartbeats. However, real-time CMR requires a careful balance of increased temporal resolution at the expense of spatial resolution. An in-plane resolution of 2x2 mm is needed for catheter visualisation and the target temporal resolution is 7 frames per second (fps), equivalent to conventional x-ray fluoroscopy used in EP procedures. The first study of MR-EP used a temporal resolution of 1 fps, but the development of faster and stronger gradients permits increased frame rates. Improved gradient performance and

magnetic field homogeneity allows real-time imaging to be performed with b-SSFP sequences, providing increased CNR compared with gradient echo sequences.[142] Furthermore, parallel imaging techniques can improve temporal resolution without sacrificing spatial resolution.[143, 144]

4.4 Catheter navigation and visualisation

X-ray fluoroscopy images are 2D projection images, which lack depth information. This means that it is possible to see the entire catheter body and tip in a single image. However, 2D CMR depicts a slice through the body, such that curved catheters may pass in and out of the imaging plane. This can lead to misinterpretation of the catheter tip position, with consequent complications and inaccurate placement of ablation lesions.

The catheter tip location can be visualised using interactive real-time sequences with manual adjustment of the imaging plane. However, for navigation within cardiac chambers, where the catheter tip is relatively mobile, this requires frequent image plane manipulation, which can reduce workflow efficiency.

An alternative technique involves automatically directing the imaging plane to the catheter tip location using position sensors in the catheter. Three one-dimensional projections along the x, y and z axes are taken sequentially and combined to identify the 3D position of the receiver coils in the catheter tip.[145] The tracking sequence can be interleaved with real-time imaging sequences so that the imaging plane is updated during device manipulation.[144, 146] Alternatively, the tracking position can be used to define the catheter tip in a multi-planar reformatted image or 3D surface reconstruction of a previously acquired 3D dataset.

4.5 Electroanatomical mapping

CMR is able to produce detailed 3D images in any orientation and is, therefore, well-suited to navigating complex anatomy. However, this flexibility can also lead to potential operator disorientation or information overload, particularly if real-time imaging intersects the anatomy in an unfamiliar plane. Appropriate displays, user interfaces and 3D visualisations are, therefore, crucial to maximising workflow efficiency.

4.6 Safety

The most important consideration for translation of MR-EP from animal to human studies is demonstrating safety. The most straightforward safety aspect of MR-EP procedures (which applies to all procedures in an MR environment) is the avoidance of ferromagnetic materials. Defibrillation, not infrequently required during EP procedures, must be performed a safe distance from the scanner bore and monitoring systems, ablation and pacing sources and anaesthetic equipment must be placed outside the main static magnetic field.

An additional safety concern of MR-EP procedures is significant heating due to RF-induced currents in long metallic objects (guide wires and metal braided catheters).[147, 148] The simplest way to avoid this is to construct devices from non-metallic components. However, in structures requiring conductivity, significant heating can be avoided by the use of high-resistance wires.[149]

SECTION TWO:

METHODS AND

EXPERIMENTAL DATA

5 Methods

Where methods are applicable to more than one of the following chapters, the details are given below to avoid repetition. However, the individual study protocols are retained within the individual chapters.

5.1 Animal model

All animal studies were undertaken at Aarhus University Hospital Skejby, approved by the Danish Animal Experiments Inspectorate and fully complied with Danish law on animal experiments (Dyreforsøgstilsynet approval number: 2012/561-148).

Female Danish Landrace pigs (approximately 40 kg) were used for all experiments without a recovery phase, whilst female Ellegaard Göttingen minipigs (approximately 30 kg) were used for all experiments with a recovery phase. Minipigs were used as, unlike the Danish Landrace pigs, they are already fully grown and so there is minimal weight change during the recovery period, which would invalidate pathological findings.

5.1.1 General anaesthesia

After an overnight fast the animals were pre-sedated with an intramuscular injection of azaperone (4 mg/kg) and midazolam (0.5 mg/kg). Intravenous cannulae (20 G) were placed in both ears and general anaesthesia was induced with intravenous ketamine (5 mg/kg) and midazolam (0.5 mg/kg). The animals were intubated and mechanically ventilated (Datex-Ohmeda ventilator, GE Healthcare; tidal volume 450 ml; respiratory rate 12/min). General anaesthesia

was maintained with a continuous intravenous infusion of propofol (3 mg/kg/hr) and fentanyl (15 mcg/kg/hr). During anaesthesia, the animals were monitored using a continuous three-lead ECG, pulse oximetry (sited on the tail) and end-tidal CO_2 measurements. Urinary catheters were placed for the duration of the experiments and the animals were kept hydrated with a continuous intravenous infusion of 0.9% normal saline (125 ml/hr).

5.1.2 Femoral venous access

Using a handheld Doppler probe (Huntleigh Healthcare, UK), the right femoral artery and vein were located. Using a Seldinger technique, two 8/9F sheaths were inserted into the right femoral vein, followed by an intravenous injection of 100 IU/kg heparin.

5.1.3 Additional medication

Where necessary, the heart rate was kept below 80 beats per minute using boluses of 5 mg of intravenous metoprolol. Episodes of AF lasting longer than five minutes were pharmacologically cardioverted with 50-100 mg of intravenous flecainide.

5.1.4 Animal recovery

For chronic experiments, minipigs were recovered from general anaesthesia and given a single dose of intravenous antibiotic (600 mg benzylpenicillin). Once fully conscious, the animals were returned to the farm, where they were fed a restricted diet for eight weeks to minimise growth during the recovery period.

5.1.5 Euthanasia

At the end of the experiment, animals were euthanised with an intravenous bolus of phenobarbital (80 mg/kg).

5.2 EP setup

A clinical grade interventional EP setup was designed for these experiments (Figure 5-1), comprising CartoXPress (Biosense Webster, Diamond Bar, CA, USA) EAM system (COM Unit, Patient Interface Unit, computer workstation, repeater screen, location pad, location reference patch), x-ray fluoroscopy (GE Healthcare), pacing stimulator, RF generator (Stockert, Biosense Webster), RF indifferent electrode, 6F decapolar CS catheter and an 8F bidirectional ablation catheter (Thermocool SF, D curve, Biosense Webster, Diamond Bar, CA, USA).

5.3 Macroscopic and microscopic examination

The hearts were explanted and the RA was opened and photographed (Figure 5-2). The hearts were then fixed in formaldehyde. Next, the ablation line and surrounding tissue were excised *en bloc* (Figure 5-3) and cut into 4 mm sections perpendicular to the ablation line (Figure 5-4). Each cross section was photographed and then dehydrated, embedded in paraffin, sectioned (3 μm sections) and stained with hematoxylin and eosin or Masson's Trichrome for microscopic examination (Figure 5-5).

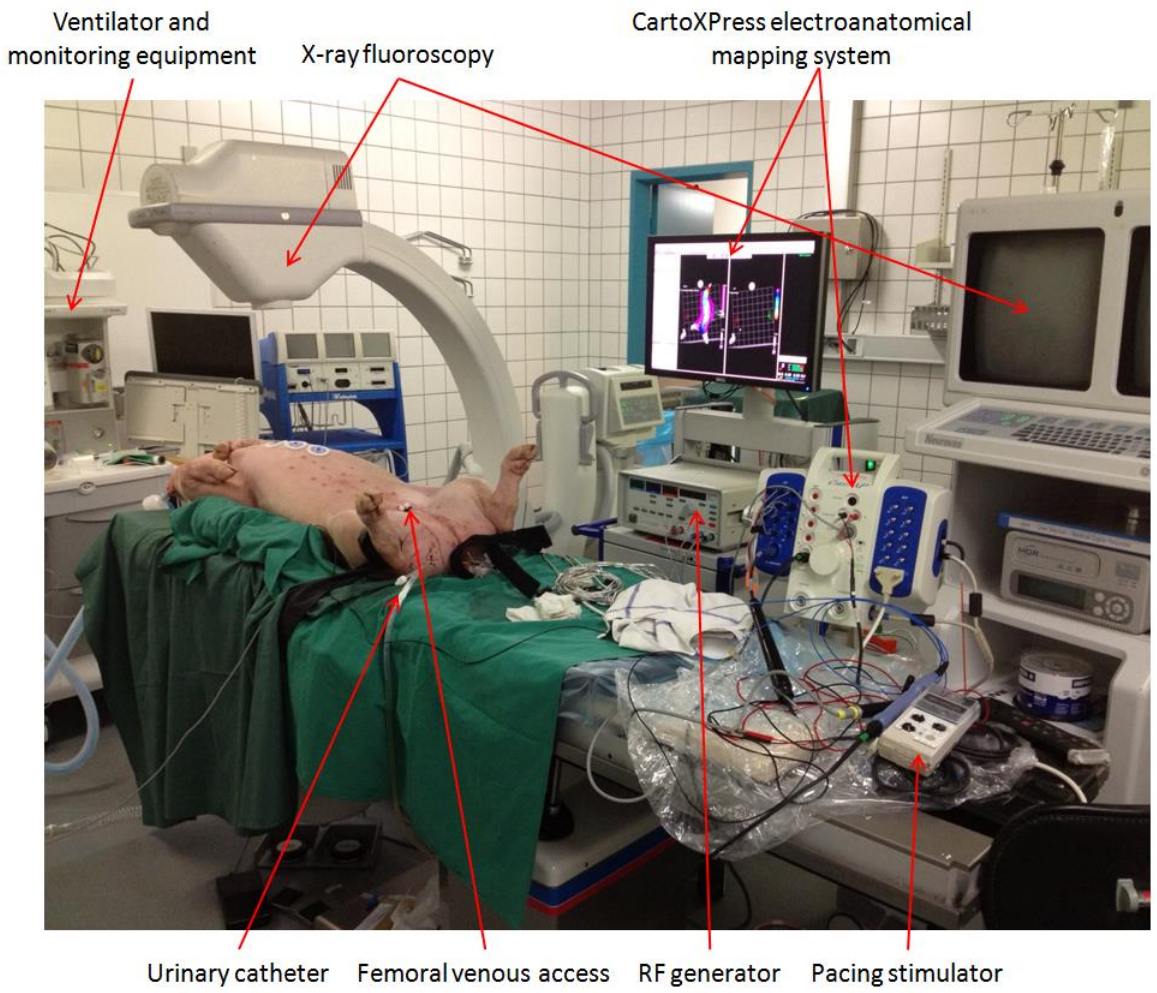

Figure 5-1: Interventional EP setup used for animal experiments.

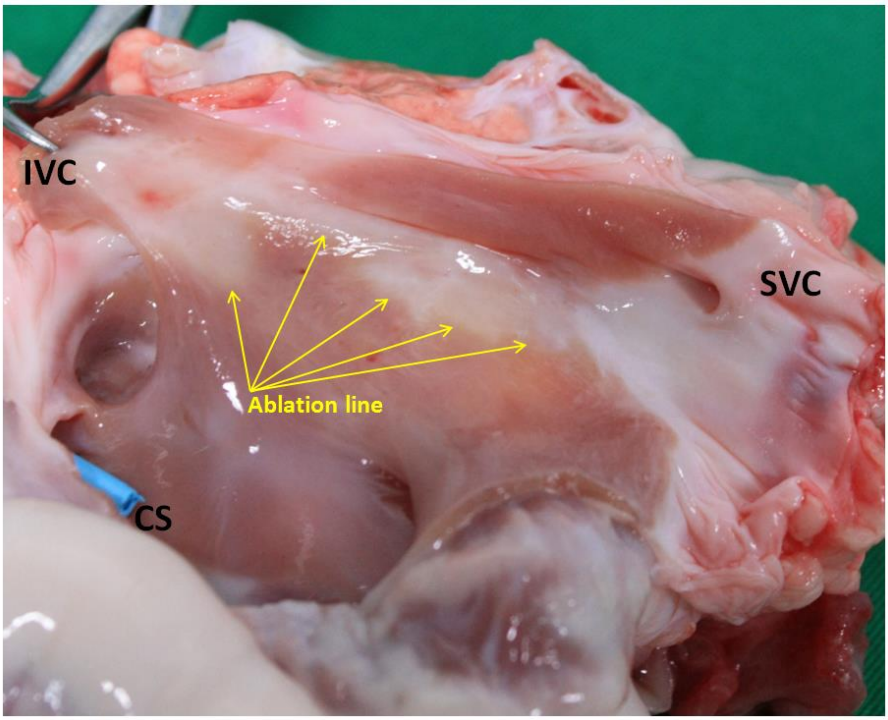

Figure 5-2: Explanted heart photographed immediately after explantation. The RA has been opened. SVC=superior vena cava; IVC=inferior vena cava; CS=coronary sinus.

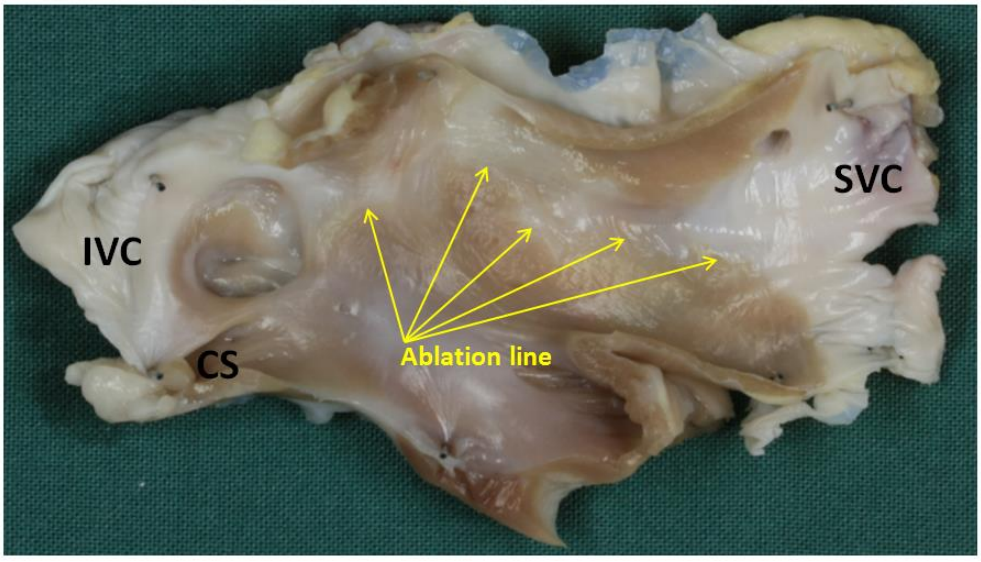

Figure 5-3: The same specimen as in Figure 5-2, after fixation in formaldehyde. The ablation line and surrounding tissue have been excised. SVC=superior vena cava; IVC=inferior vena cava; CS=coronary sinus.

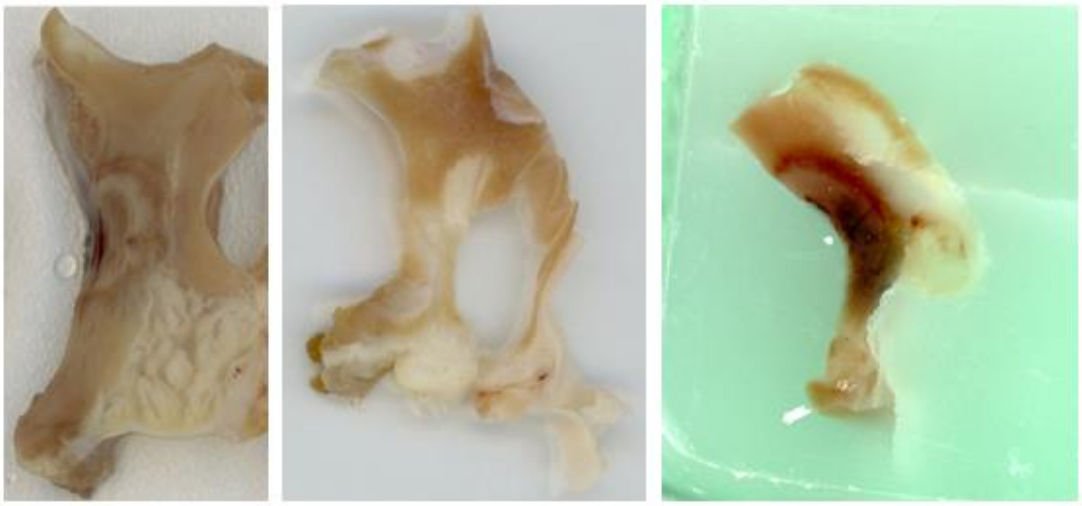

Figure 5-4: Cross-sections (4 mm thick) through acute (left) and chronic (middle) ablation lines. An acute ablation lesion has been embedded in paraffin (right) in preparation for histological staining and examination.

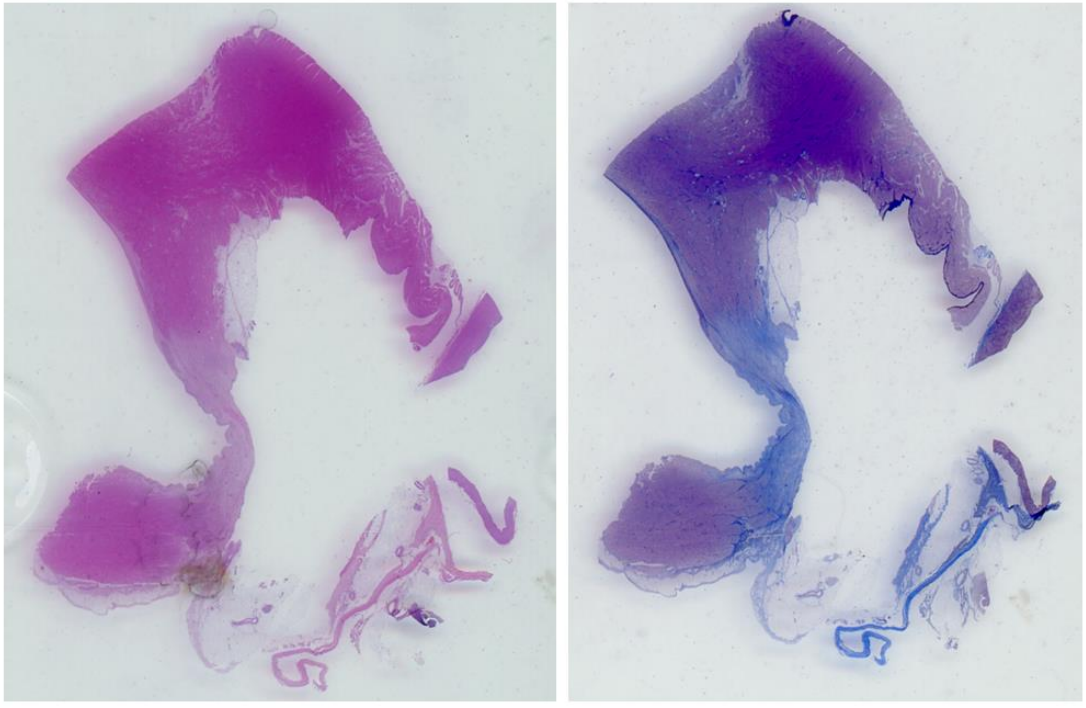

Figure 5-5: Paraffin-embedded 3 µm sections stained with haematoxylin and eosin (left) or Masson's Trichrome (right).

5.4 Cardiac magnetic resonance

All CMR acquisitions were performed on a 1.5 Tesla MR system (Achieva, Philips Medical Systems, Best, The Netherlands) and a five (for animal studies) or 32 (for human studies) element cardiac phased array coil.

5.4.1 Planning

First, survey and sensitivity encoding (SENSE) reference scans were obtained followed by a 2D multi-cardiac phase cine scan acquired in an approximate four-chamber orientation. From this scan, the trigger delay was determined for all subsequent scans. In order to minimise artefacts from atrial wall motion, the length of the acquisition window was set to maximum of 150 ms for all subsequent scans and the respiratory navigator was used to ensure acquisition at end-expiration for all slices.

5.4.2 3D T2-weighted sequence

Sagittal T2W images were acquired using a multi-slice Turbo Spin Echo (TSE) acquisition technique with a double IR pre-pulse to suppress the blood pool signal. Spectral pre-saturation with inversion recovery (SPIR) fat suppression was applied. The effective TE was set to 45 ms using linear profile ordering. The TR was twice the cardiac cycle length. The spatial resolution was 1.5x1.5 mm^2, reconstructed to 1.0x1.0 mm, with a slice thickness of 3 mm. Approximately 20-25 slices were acquired to provide complete coverage of the LA/RA.

5.4.3 3D balanced steady state free precession sequence

Sagittal whole heart b-SSFP images were acquired with 2 mm isotropic resolution, reconstructed to 1.3 mm resolution, with a T2 preparation pulse (TE 50 ms), a flip angle of 90 degrees and TE/TR of 4.3/2.2 ms.

5.4.4 3D late gadolinium enhancement sequence

Twenty minutes after the administration of 0.2 ml/kg Gadovist (Bayer HealthCare Pharmaceuticals, Berlin, Germany), 3D LGE imaging was performed with a respiratory-navigated, ECG-triggered IR turbo field echo (TFE) acquisition. The spatial resolution was 1.3x1.3x4 mm^3, reconstructed to 0.6x0.6x2 mm^3, using TE/TR of 3.0/6.2 ms and a flip angle of 25 degrees. The TI was determined using a preceding Look-Locker sequence to achieve optimal suppression of ventricular myocardium. The scan was acquired in an axial orientation, typically with 30-40 slices to achieve complete coverage of the LA/RA.

6 Cardiac magnetic resonance and electroanatomical mapping of acute and chronic atrial ablation injury in the pig – a histological validation study

6.1 Introduction

Left atrial RF catheter ablation, of which PVI is the cornerstone, is a widely practised procedure for the treatment of AF.[46] However, it is now apparent that acute achievement of PVI is seldom durable, and this has refocused the field on the mechanisms of RF injury in the LA. In turn, there has been a recent increase in the use of CMR to provide pre- and post-procedural non-invasive atrial tissue characterisation to assess patient suitability and response to catheter ablation[51, 77-80, 82-85, 87] and to guide both repeat catheter ablation[82, 86] and real-time MR-EP procedures.[150-153]

The use of CMR to characterise acute and chronic ventricular myocardial injury only became clinically accepted and in widespread use following comprehensive pathological validation,[67] yet there has been no fundamental validation work on the CMR assessment of the atrium. This is of particular importance as controversy remains regarding the reproducibility and diagnostic ability of atrial CMR.[154] Validation of atrial CMR would benefit from defining SI thresholds, which can distinguish between healthy and injured atrial tissue, rather than arbitrarily chosen SI thresholds used in clinical studies to date.[51, 78, 80, 82-84, 87]

Furthermore, invasive atrial endocardial voltage mapping, the current clinical gold standard for characterising the atrial substrate, has not been pathologically validated or systematically compared with CMR findings. Voltage thresholds in common clinical use have been extrapolated from ventricular studies comparing EAM with post-myocardial infarction scar[155, 156] and not ablation-induced injury.

This chapter provides a comprehensive histopathological validation of CMR and endocardial voltage mapping of acute and chronic atrial ablation injury and explores the possibility of defining SI thresholds for T2W and LGE CMR immediately following, and eight weeks after, linear RF ablation in the porcine RA.

6.2 Methods

6.2.1 Protocol

Under general anaesthesia, as described in section 5.1.1 (page 77), eight female Danish Landrace pigs (mean weight 39 ± 1.8 kg) underwent pre-ablation CMR, followed by EAM and ablation according to the protocols described below. These animals were then immediately transferred for post-ablation CMR according to the same protocol, before they were euthanised.

Eight Göttingen mini-pigs (mean weight 31 ± 2.9 kg) underwent the same protocol, but were recovered from general anaesthesia after post-ablation CMR and returned to the farm for eight weeks. After eight weeks these animals were anaesthetised again and underwent chronic CMR and EAM (without ablation), before they were euthanised.

6.2.2 Electroanatomical map and ablation

Two 8F sheaths were placed percutaneously in the right femoral vein, followed by an intravenous injection of 100 IU/kg heparin. Fluoroscopy was used to position a 6F decapolar reference catheter in the CS. An 8F bidirectional ablation catheter (Thermocool SF, D curve, Biosense Webster, Diamond Bar, CA, USA) was advanced to the RA. A 3-dimensional (3D) geometry of the RA was created using CartoXPress (Biosense Webster, Diamond Bar, CA, USA) and a high-density pre-ablation peak-to-peak bipolar voltage map was constructed during proximal CS pacing. Linear RF ablation (25 W, 38^{o}C, 8 ml/min irrigation) was performed from the SVC to the IVC along the posterior wall of the RA. Ablation was performed as a continuous drag with the catheter moved every 30 seconds. The SVC to IVC line was chosen as the aim of this study was to create a reproducible transmural linear ablation lesion in all animals, so as to demonstrate signal intensity and voltage thresholds for complete, rather than incomplete, scar.

Following completion of the intercaval linear lesion, a second high-density post-ablation voltage map was immediately acquired during proximal CS pacing. Chronic voltage maps were created in the same way, but without ablation.

Continuity of the intercaval lesion was confirmed by the presence of double potentials along the line, absence of pace capture (at 3 mA) and the presence of a new activation detour during CS pacing. However, as the aim of the study was to evaluate the relationship between ablation injury, voltage and CMR appearances, an absolute insistence on the presence of bidirectional conduction block was not made.

6.2.3 CMR

Each CMR study included 3D T2W, 3D b-SSFP and 3D LGE imaging, as described in section 5.4 (page 83).

6.2.4 Macroscopic and microscopic examination

After the animals were euthanised, the hearts were explanted for macroscopic and microscopic examination as described in section 5.3 (page 79).

6.2.5 Data analysis

6.2.5.1 Electroanatomical maps

Pre-ablation, post-ablation and chronic voltage maps were exported from CartoXPress and imported into software custom-written with Matlab. This allowed the voltage maps and data collection points to be reconstructed for off-line analysis. Axial slices (perpendicular to the ablation line) were placed on the voltage maps at 4 mm intervals (the same as the macroscopic cross-sections) along the ablation line. For each slice, the centre of the ablation line was identified by minimising the weighted distance to the ablation points (Figure 6-1). For the chronic voltage maps, which unavoidably had a different anatomical shell from the pre-/post-ablation maps, 'ablation points' were added manually to the estimated centre of the low voltage zone to represent the ablation line. A graph of endocardial voltage against distance from the centre of the ablation line (from -25 mm to +25 mm) was constructed for each slice.

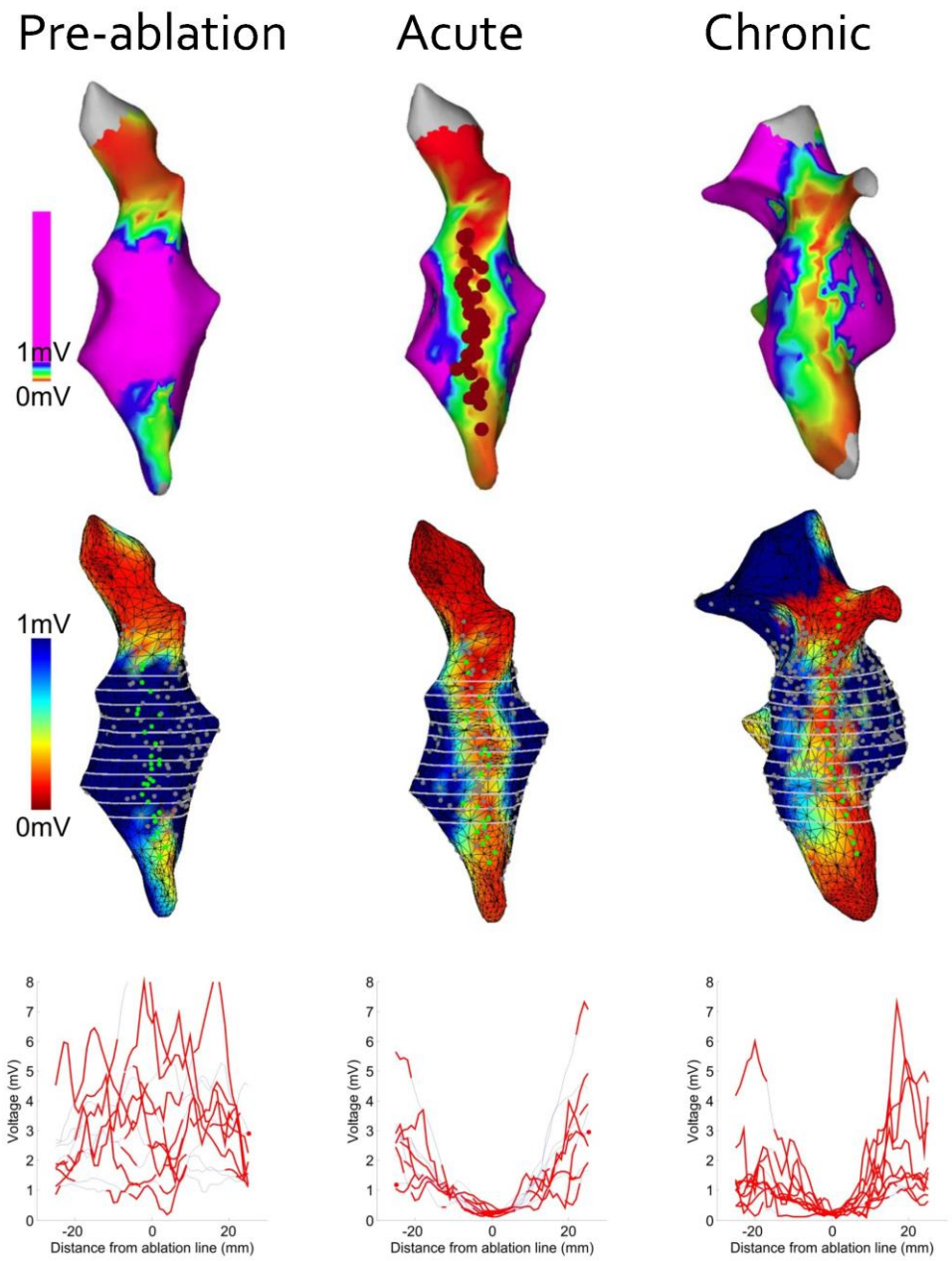
Pre-ablation
Acute
Chronic
1mV
0mV
1mV
0mV
Voltage (mV)
Distance from ablation line (mm)
Voltage (mV)
Distance from ablation line (mm)
Voltage (mV)
Distance from ablation line (mm)

Figure 6-1: Top row – Pre-ablation, acute (immediately after ablation) and chronic (eight weeks after ablation) CartoXPress endocardial bipolar voltage maps in a posteroanterior view (all from the same animal). Voltages ≥1.0 mV are denoted in pink. Red circles indicate the site of linear RF ablation from the SVC to the IVC. Middle row - the same voltage maps have been imported in Matlab and reconstructed. Voltages ≥1.0 mV are denoted in blue. Green circles indicate the site of ablation. Grey circles indicate data sampling points. Axial slices (perpendicular to the ablation line) in white are shown at 4 mm intervals along the ablation line. For each slice, the centre of the ablation line was identified by minimising the weighted distance to the ablation points. For the chronic voltage maps, which unavoidably had a different anatomical shell from the pre-/post-ablation maps, 'ablation points' were added manually to the estimated centre of the low voltage zone to represent the ablation line. Bottom row - graphs of endocardial voltage against distance from the centre of the ablation line (from -25 mm to +25 mm) for each axial slice. Red and blue lines indicate that values are ≤3 mm (non-interpolated) and ≥3 mm (interpolated) from a grey data sampling point respectively. Only non-interpolated values were used for summary analysis in Figure 6-5.

6.2.5.2 CMR

Pre-ablation, post-ablation and chronic T2W and LGE images were analysed using 3D medical image segmentation software (itk-SNAP Version 2.2.0). First, two blinded expert observers independently selected a reference region (LV myocardium for T2W and the atrial blood pool for LGE images) and the mean (and SD) SI for the reference region was calculated. Next, the two observers manually segmented the RA wall in the 3D volume by consensus (Figure 6-2A). Thresholds from 0 to 15 SD (at 0.1 intervals) above the reference SI were applied to the RA wall. A 3D segmentation was created for each threshold (where all pixels above the threshold SI were included in the segmentation) and the volume of the segmentation plotted against the SI threshold (Figure 6-2B).

6.2.5.3 Macroscopic examination

Using Image J image processing software (National Institutes of Health), two blinded expert observers manually segmented the total area of injury for each 4 mm cross-section on the gross pathological digital photographs taken after fixation in formaldehyde, but before dehydration and staining for histological examination. For the acute specimens, the ablation lesion was defined as both the zone of pallor and the surrounding haemorrhagic border zone, whilst for the chronic specimens, the ablation lesion was defined as the zone of pallor alone (as there is no surrounding haemorrhagic border zone) (Figure 6-3). The total volume of injury for each animal was calculated by summing the cross sectional areas and multiplying by the slice thickness. The mean value for the two observers was then taken.

6.2.6 Statistical analysis

Variables are expressed throughout as mean ± SD, except for voltages, which are expressed as geometric mean and 95% confidence interval (CI). Student's *t*-test for paired data was used to compare pre-ablation, post-ablation and chronic CMR segmentations. Student's *t*-test for unpaired data was used to compare pre-ablation, post-ablation and chronic endocardial voltages. A significance level of $p<0.05$ was considered statistically significant. Interobserver variability for macroscopic pathological examination was assessed by the intraclass correlation coefficient.

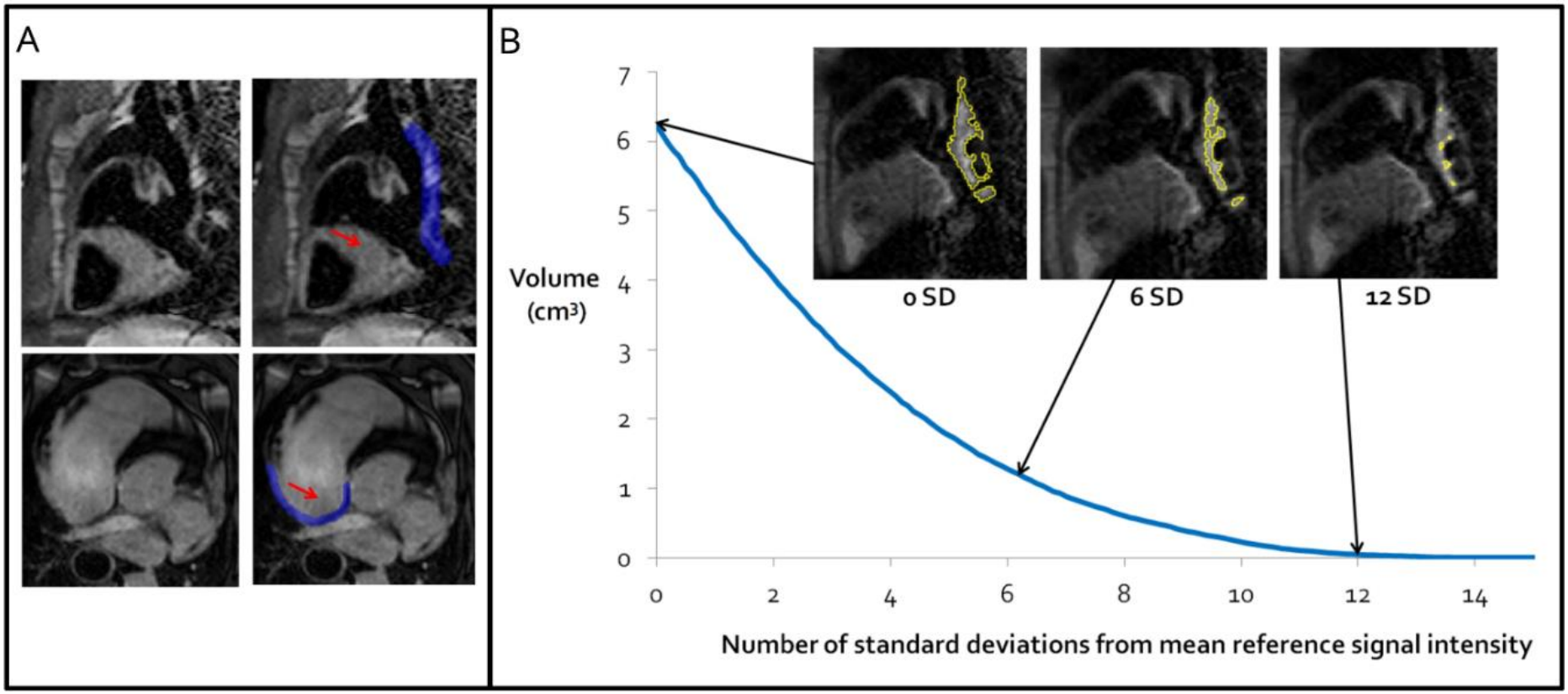
A
B
Volume (cm³)
0
1
2
3
4
5
6
7
0
2
4
6
8
10
12
14
0 SD
6 SD
12 SD
Number of standard deviations from mean reference signal intensity

Figure 6-2: A - Sagittal T2W (top row) and axial LGE (bottom row) CMR images. The red arrows indicate the reference region against which SI were compared (LV myocardium for T2W and the atrial blood pool for LGE images). The blue overlay indicates the region segmented as the RA wall (in this particular slice). These images are all pre-ablation, but the same technique was used for all image analyses. B - A graph for one post-ablation T2W image of segmentation volume (in cm^3) against the SI threshold (expressed as the number of SD above the reference SI). Sample images are included to show the segmentation created (outlined in yellow) at 0, 6 and 12 SD above the reference SI.

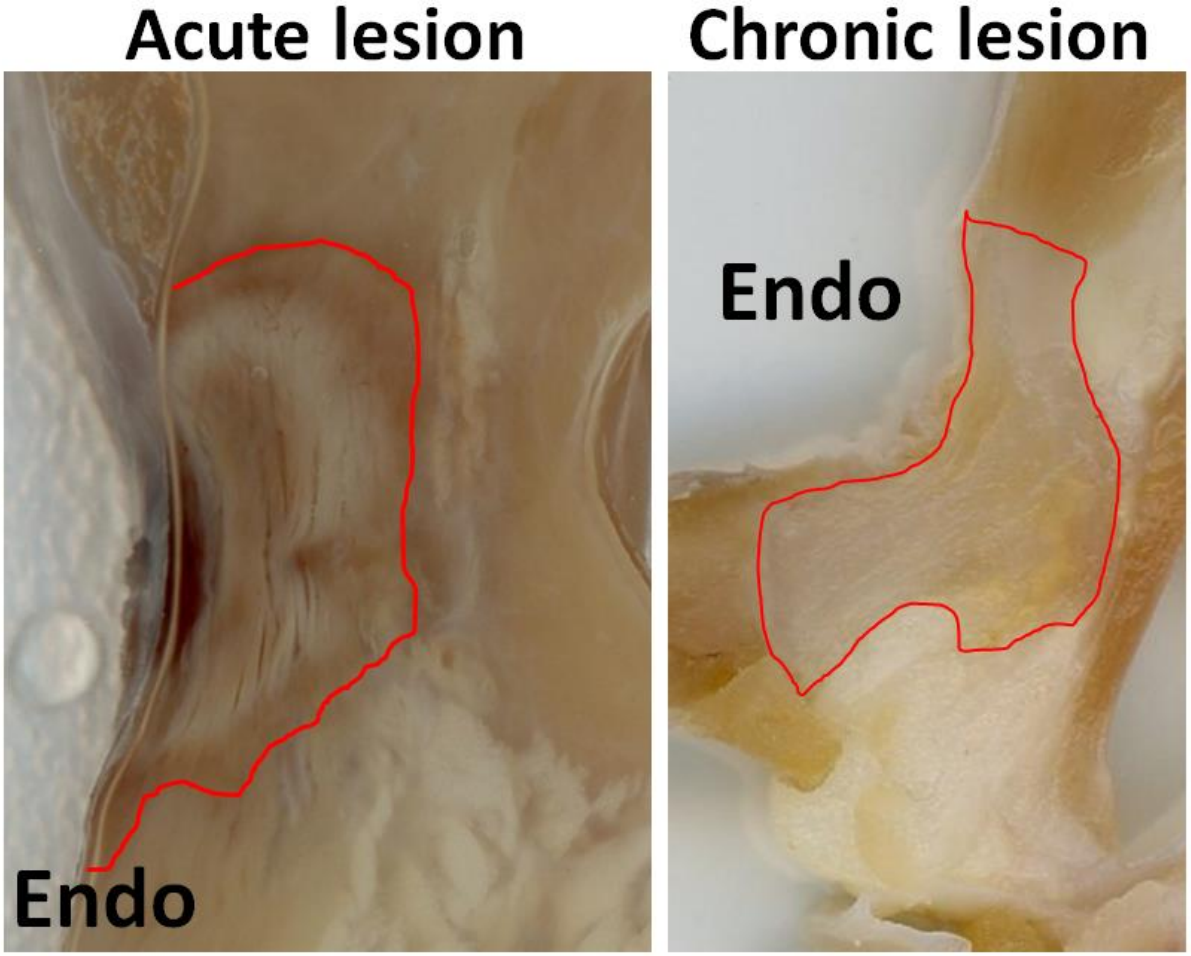

Figure 6-3: Manually contoured acute (left) and chronic (right) ablation lesions.

6.3 Results

6.3.1 Electroanatomical maps

All 16 animals survived until the end of the protocol and no animals were excluded from analysis due to premature death. Percutaneous femoral venous access could not be achieved in one animal and a femoral venous cutdown was required. Otherwise, there were no complications during any of the studies.

There were a total of 16 pre-ablation, 16 post-ablation and eight chronic electroanatomical maps with an average of 545 ± 400 points per map. The average time to create a high-density map was 18.5 ± 9.5 minutes and the average duration of RF application was 11.6 ± 4.2 minutes. Whilst a new atrial activation pattern (Figure 6-4) and double potentials were seen in all 16 animals immediately after ablation and also in the eight chronic animals, there was no change in the latest atrial activation time point (pre ablation 135 ± 30 ms, post-ablation 142 ± 25 ms, chronic 131 ± 24 ms) (Table 1).

Animal	Pre-ablation (ms)	Post-ablation (ms)	Chronic (ms)
1	101	108	
2	133	124	
3	117	114	
4	135	122	
5	122	139	
6	177	163	
7	150	173	
8	130	169	
9	111	108	166
10	129	136	137
11	169	180	145
12	200	169	95
13	96	161	106
14	133	120	122
15	92	154	123
16	165	133	150

Table 1: Latest atrial activation time points (as measured from the CS pacing artefact) for all 16 animals.

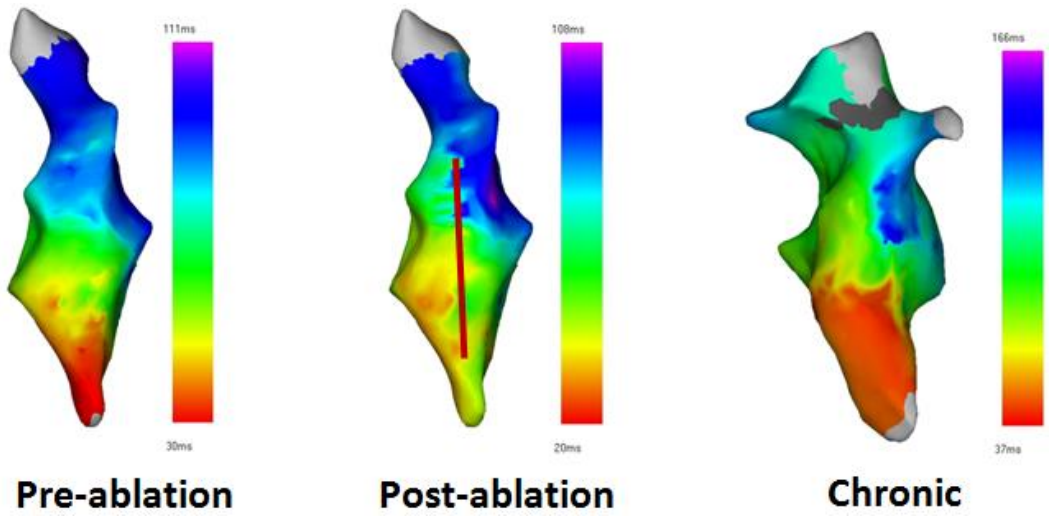

Figure 6-4: Isochronal local activation time maps before, immediately after and eight weeks following SVC-IVC ablation. The red line in the post-ablation map indicates the site of the ablation line.

6.3.2 CMR

There were a total of 16 pre-ablation, 16 post-ablation and eight chronic 3D T2W and LGE scans. Example images showing the site of ablation are shown in Figure 6-6. Qualitatively, no appreciable pre-ablation T2W or LGE enhancement was seen in any of the animals, but both T2W and LGE enhancement were seen in all animals post-ablation. Chronically, T2W enhancement had reduced, whilst LGE enhancement remained.

The summary data and statistical significance values for the eight pigs are shown in Figure 6-7 A and B. For T2W and LGE images, segmented volumes were significantly greater for post-ablation images compared with pre-ablation images.

The summary data and statistical significance values for the eight mini-pigs are shown in Figure 6-7 C and D. For T2W and LGE images, segmented volumes were significantly greater for post-ablation images compared with pre-ablation images. When compared with acute post-ablation images, there was a significant reduction in the segmented volume for chronic T2W images, but no statistical difference for chronic LGE images.

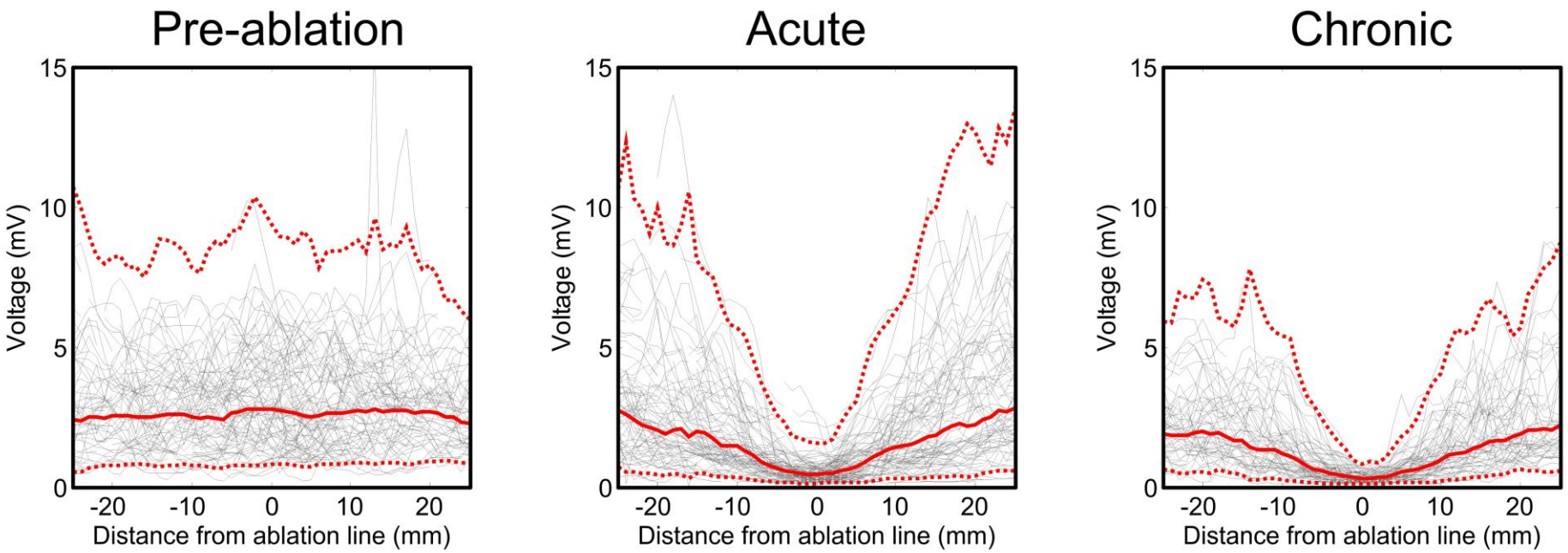

Figure 6-5: Average results for the 16 pre-ablation (left), 16 post-ablation (middle) and eight chronic (right) electroanatomical maps. The solid red line indicates the mean, whilst the dashed red lines indicate the 95% CI. Black lines indicate the raw data for all of the animals.

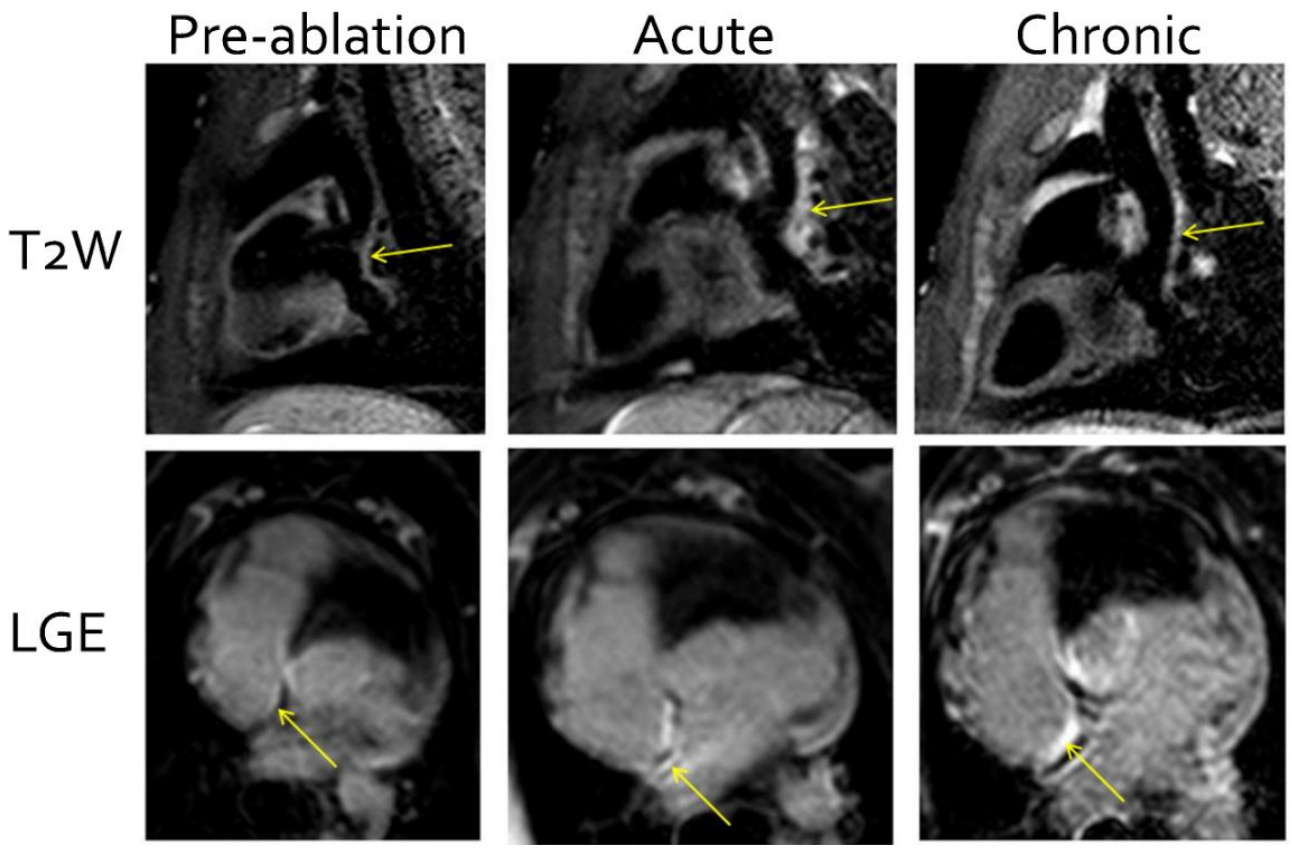

Figure 6-6: Sagittal T2W (top row) and axial LGE (bottom row) CMR images pre-ablation (left column), acutely post-ablation (middle column) and chronically (right column). The site of ablation at the posterior RA wall is indicated by the arrow.

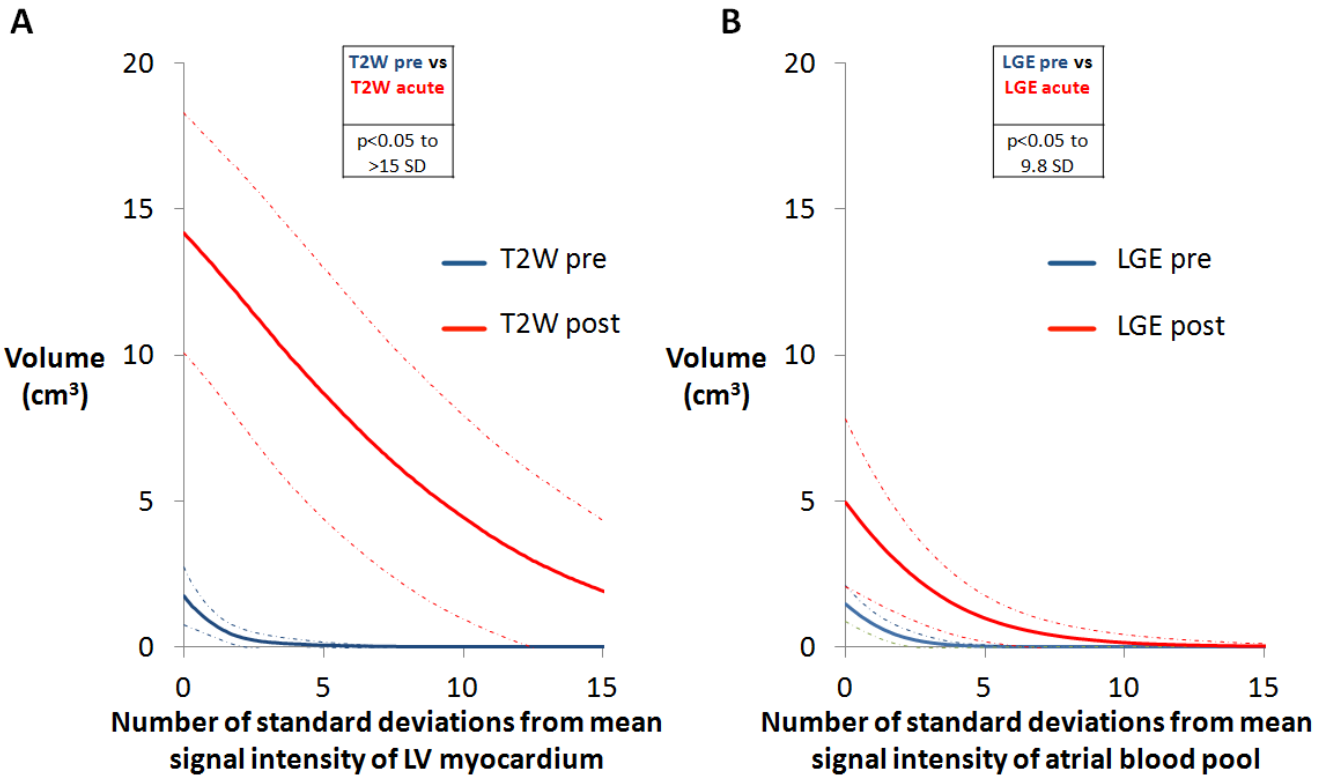
A
T2W pre vs
T2W acute
p<0.05 to
>15 SD
T2W pre
T2W post
Volume
(cm³)
20
15
10
5
0
0
5
10
15
Number of standard deviations from mean
signal intensity of LV myocardium
B
LGE pre vs
LGE acute
p<0.05 to
9.8 SD
LGE pre
LGE post
Volume
(cm³)
20
15
10
5
0
0
5
10
15
Number of standard deviations from mean
signal intensity of atrial blood pool

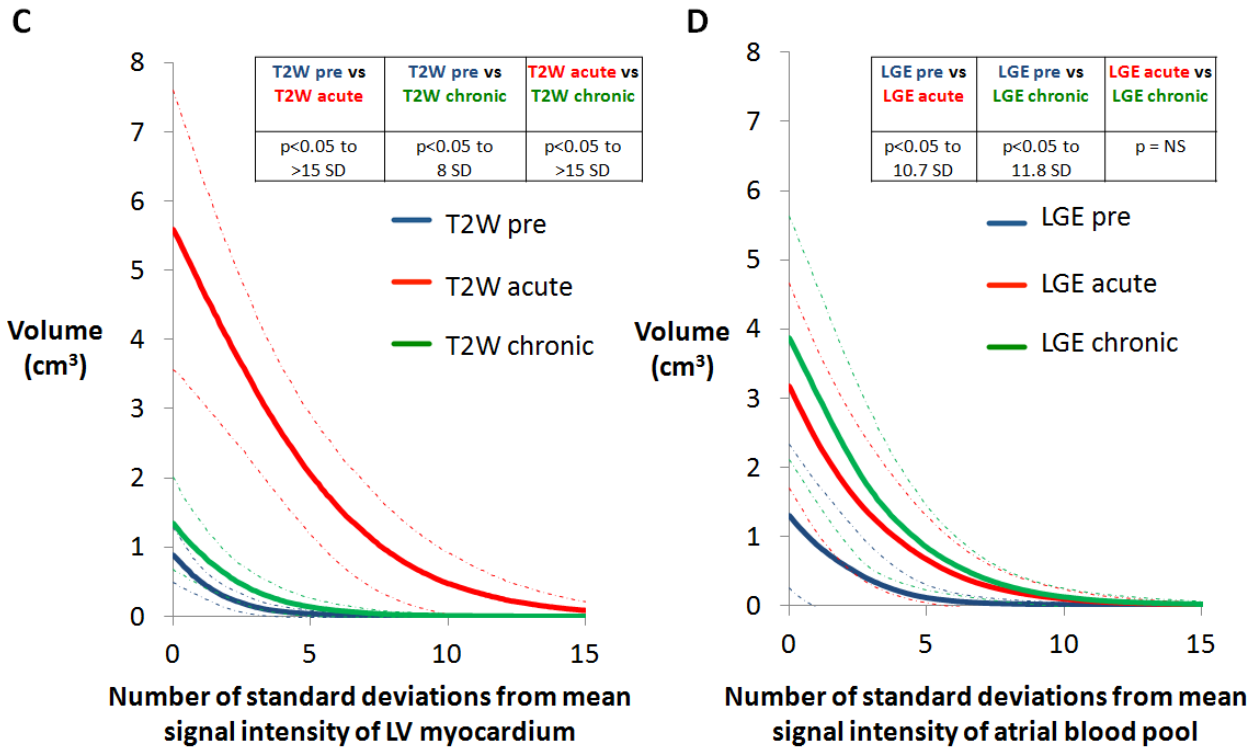

Figure 6-7: Signal intensity thresholds from 0 to 15 SD above a reference SI were applied to the RA wall for T2W and LGE images and a 3D segmentation was created for each threshold. A and B show the results for the eight pigs, whilst C and D show the results for the eight mini-pigs. Values in the tables show the statistical comparison within each graph. Dashed lines indicate ±1 SD.

6.3.3 Macroscopic and microscopic examination

Macroscopic photographs of acute and chronic ablation lesions, both immediately after heart explantation and after fixing in formaldehyde, are shown in Figure 6-9. Microscopic histology of acute ablation injury confirmed transmural injury with coagulative necrosis, haemorrhage and interstitial oedema, whilst chronic histology demonstrated transmural replacement of normal atrial wall with fibrous scar tissue (Figure 6-10).

The mean acute volume of injury measured on the cross sections in the eight pigs was 2.75 ± 1.26 cm^3, whilst the mean chronic volume of injury in the eight mini-pigs was 1.51 ± 0.53 cm^3. However, when corrected for the difference in atrial area between the pigs and mini-pigs (7.48 ± 0.85 cm^2 vs 4.39 ± 1.05 cm^2), there was no significant difference (p=0.9) (Figure 6-8). The interobserver variability for acute and chronic measurements was 0.95 (95% CI 0.69-0.99) and 0.87 (95% CI 0.53-0.97) respectively.

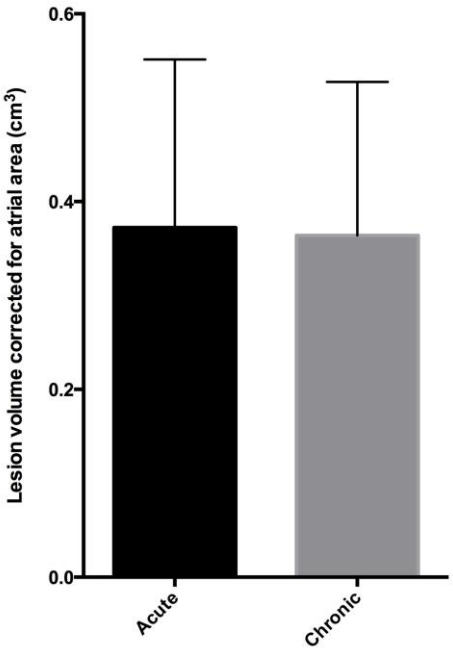

Figure 6-8: Mean lesion volumes for the acute and chronic animals. Error bar indicates 1 SD.

6.3.3.1 Comparison with CMR segmented volumes

When the CMR segmented volumes were compared with the macroscopic volumes of injury, the SI thresholds that best approximated macroscopic volumes were: 2.3 SD above the mean atrial blood pool SI for LGE post-ablation; 3.3 SD above the mean atrial blood pool SI for LGE chronically; and 14.5 SD above the mean LV myocardium SI for T2W post-ablation (Figure 6-11). Chronically, T2W always underestimated the lesion volume, even at 0 SD above the reference SI. Thresholds were determined by the intersection with the line y=1 on Figure 6-11, which indicated the best match between average CMR segmented volumes and average macroscopic volumes. The individual thresholds for each animal are shown in Figure 6-12.

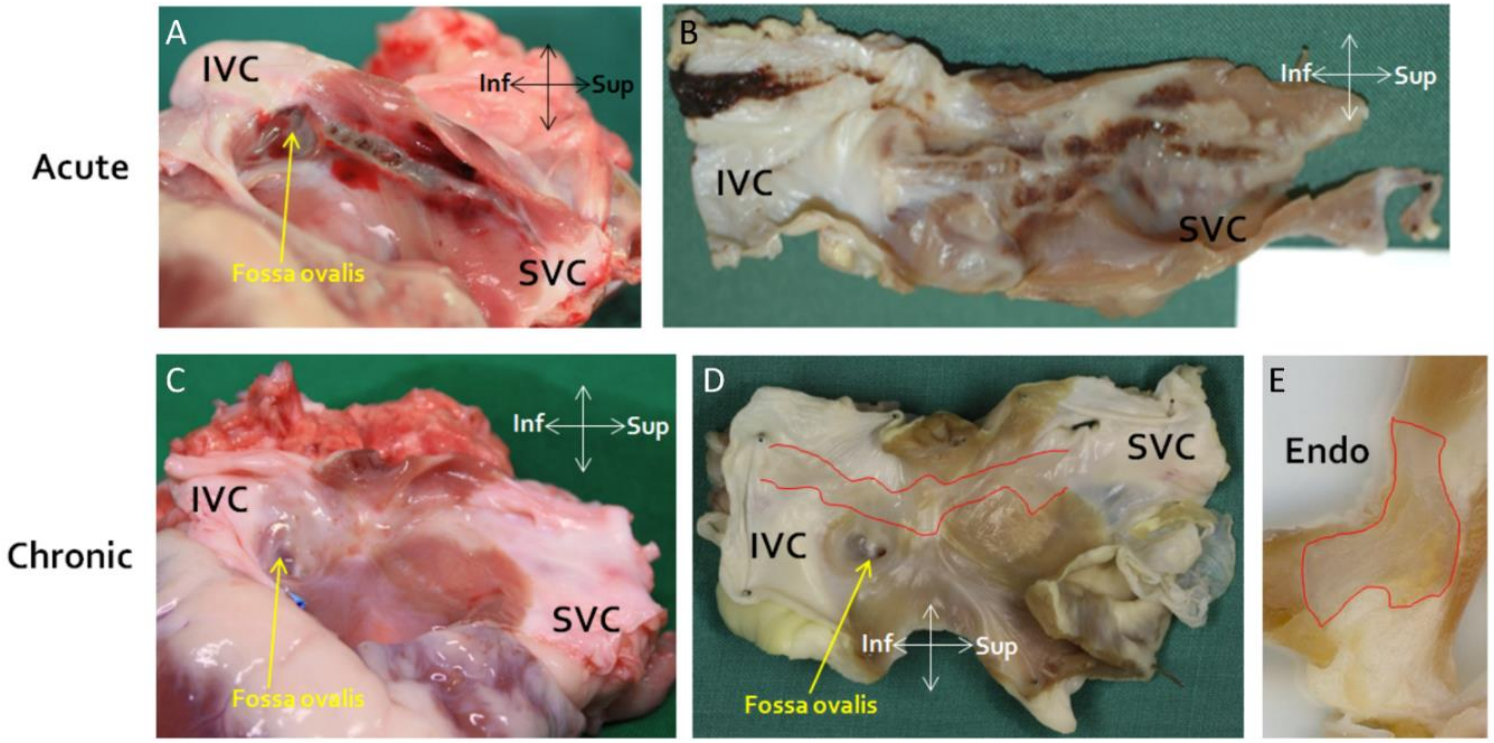

Figure 6-9: A and B - Macroscopic photographs from animals euthanised acutely after ablation. 'A' is immediately after heart explantation, whilst 'B' is after fixation in formaldehyde. C and D - Macroscopic photographs from an animal euthanised eight weeks after ablation. 'C' is immediately after heart explantation, whilst 'D' is after fixation in formaldehyde (the ablation lesion is outlined in red). E - Cross-section through 'D' with the chronic ablation lesion outlined in red. Inf = inferior, Sup = superior, Endo = endocardial surface.

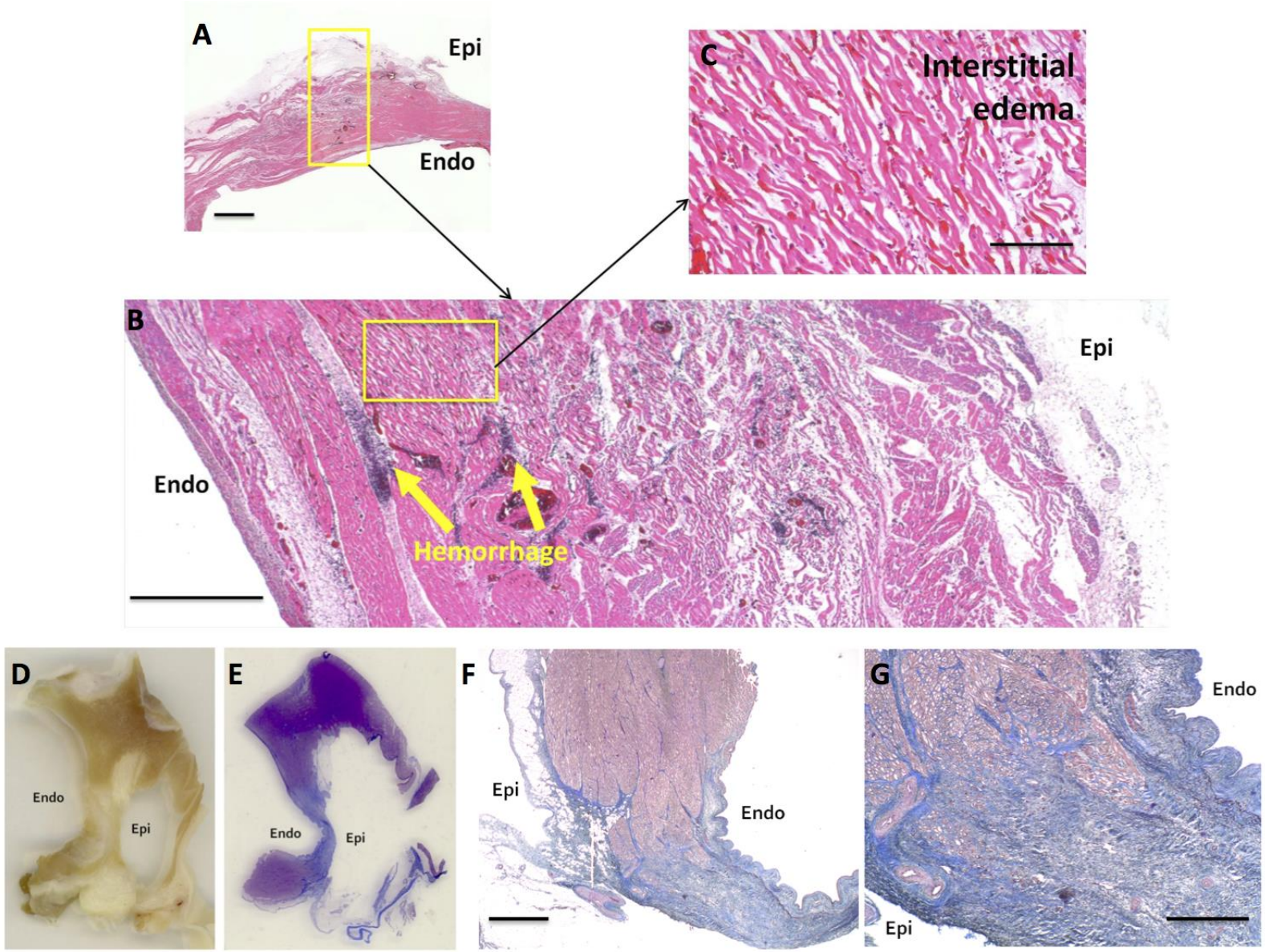
A
Epi
Endo
C
Interstitial
edema
B
Epi
Endo
Hemorrhage
D
Endo
Epi
E
Endo
Epi
F
Epi
Endo
G
Endo
Epi

Figure 6-10: A, B and C - Histology (stained with hematoxylin and eosin) of an acute ablation line at increasing levels of magnification demonstrating transmural injury with coagulative necrosis, haemorrhage and interstitial oedema. Scale bars in A, B and C are 1 mm, 500 µm and 100 µm respectively. Macroscopic cross-sections through a chronic ablation line (D - 4 mm section after fixation in formaldehyde; E - 3 µm section after staining with Masson's Trichrome, with which fibrous collagen appears blue). F and G - Microscopic histology of a chronic ablation line stained with Masson's Trichrome), demonstrating transmural replacement of normal atrial wall with fibrous scar tissue. Scale bars in F and G are 1 mm and 500 µm respectively.

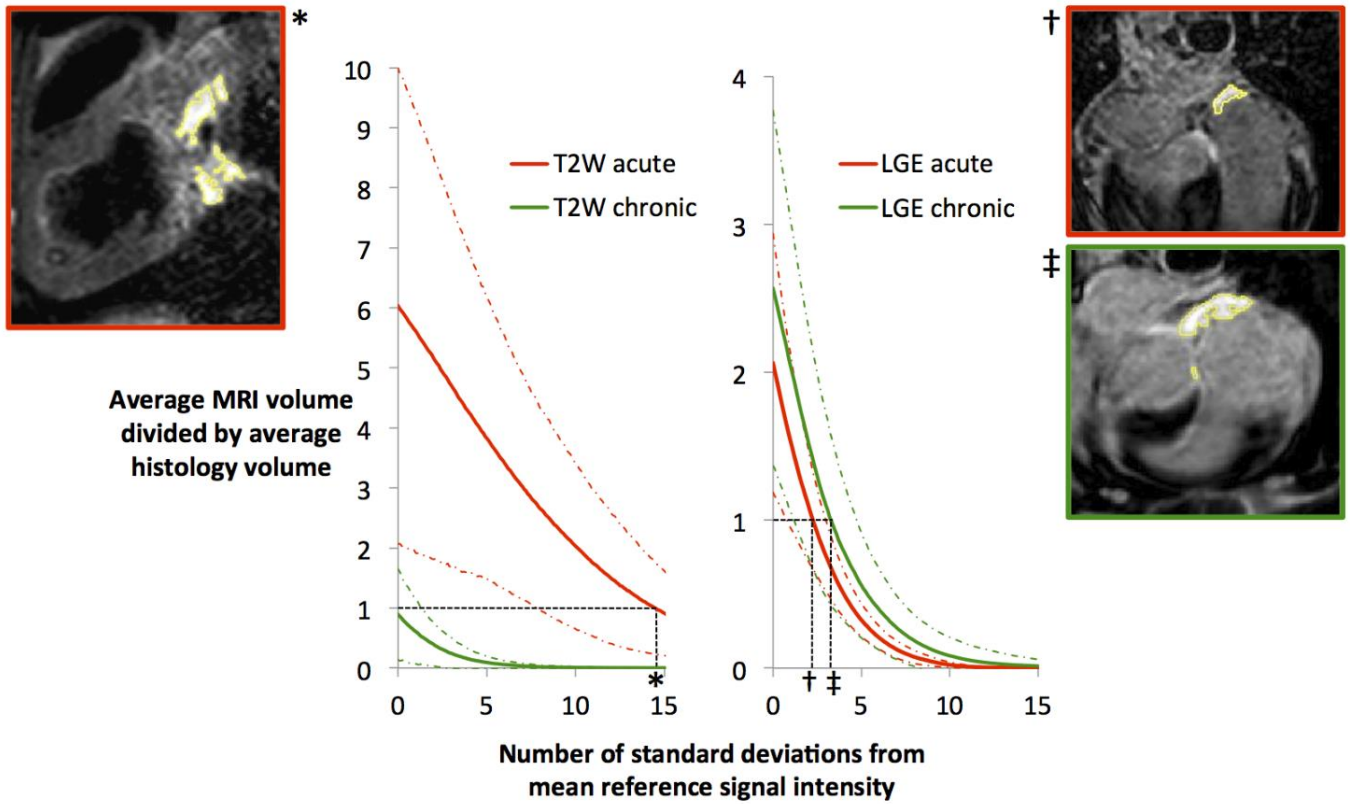

Figure 6-11: Graphs showing the comparison of CMR segmented volumes with macroscopic volumes of injury for T2W (left) and LGE (right). A value >1 on the y-axis suggests that CMR is overestimating the macroscopic volume, whilst a value of <1 suggests underestimation. Thresholds are determined by the intersection with the line y=1. Sample images are included to show the segmentation created (outlined in yellow) at these thresholds. Red and green dashed lines indicate ±1 SD. *=14.5 SD, †=2.3 SD, ‡=3.3 SD.

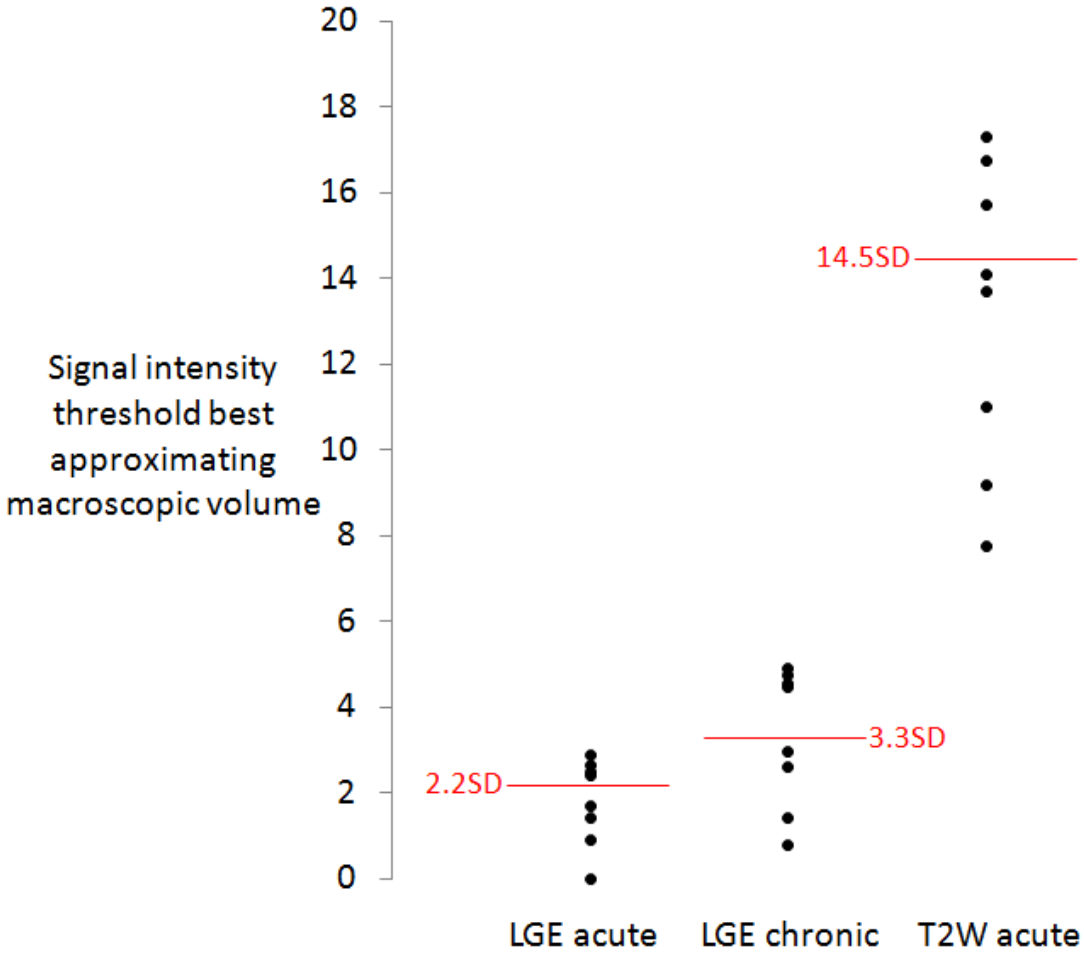

Figure 6-12: Signal intensity thresholds that best approximate macroscopic volumes for each individual animal. The average thresholds derived from Figure 6-11 are indicated with the horizontal red lines.

6.4 Discussion

This study was prospectively designed to provide objective T2W and LGE CMR SI and endocardial voltage thresholds for defining acute and chronic atrial ablation injury, by comparison with macroscopic and microscopic pathological examination. The principal findings can be summarised as follows: 1) LGE CMR SI thresholds of 2.3 SD (acutely) and 3.3 SD (chronically) above the mean SI of the atrial blood pool best approximate macroscopic volumes of injury; 2) T2W CMR overestimates the volume of ablation injury acutely, up to 14.5 SD above the mean SI of the LV myocardium, whilst T2W CMR underestimates the volume of ablation injury chronically regardless of the SI threshold used; 3) mean endocardial voltage at the centre of a CMR-confirmed linear atrial ablation lesion is 3.3 mV before ablation, 0.6 mV immediately after ablation and 0.3 mV chronically; 4) microscopic examination of a CMR-confirmed ablation line shows transmural coagulative necrosis acutely and transmural fibrosis chronically.

6.4.1 CMR of ablation injury

Several animal studies have shown that atrial and ventricular ablation lesions can be acutely visualised with CMR following thermal injury, but CMR visualisation of chronic ablation injury in an animal model has not previously been reported. T2W and contrast-enhanced T1-weighted CMR demonstrated a strong correlation between CMR lesion size and macroscopic examination following ablation at the right ventricular (RV) apex of six dogs.[138] Another study described the gadolinium-enhanced T1-weighted appearances of acute RF ablation lesions created on the RV epicardium of eight dogs.[140] Four distinct

phases of signal enhancement were observed over a follow up period of ten hours, which correlated well with pathological findings.

However, visualising lesions in the thinner walled atria is inherently more challenging. Even at the current limits of CMR spatial resolution, the atrial wall is covered by only a few voxels and the contrast between acute injury or chronic scar/fibrosis and healthy atrium is less easily visualised than in the ventricle. Published studies investigating atrial CMR lesion measurements and pathological examination are limited and have been in the context of real-time MR-EP.[150-152] One study showed a correlation between the size of four focal atrial ablation lesions, measured by T2W CMR and macroscopic examination, but only 30% of lesions could be visualised.[151] Another demonstrated a correlation between the size of eight focal atrial and ventricular ablation lesions measured by T2W and LGE CMR and macroscopic examination, with a trend towards larger lesion size measured by T2W CMR.[152] However, only the lesion diameter was measured in these studies - lesion volume was not taken into account. Most recently, investigators demonstrated the ability of CMR to visualise deliberate gaps in acute ablation lesions up to 1.4mm in size with a strong correlation between gap length identified using CMR and gross pathology.[150]

Gadolinium-enhanced CMR has also demonstrated areas of atrial (and ventricular) non-enhancement within one hour of RF ablation,[140, 157] which are most likely due to non-perfused necrotic atrial myocardium, analogous to the 'no-reflow' phenomenon seen with CMR following acute myocardial infarction.[64] Investigators have shown that these non-enhancing areas appear

to predict permanent LGE at three months following ablation, providing a potential early imaging marker of effective ablation injury.[157] However, these non-enhancing regions progressively enhance as the time from gadolinium injection (and ablation) increases, with a marked difference between images acquired at 13 minutes and 27 minutes after injection. Investigators used an arbitrary SI threshold of more than three SD below the SI of normal LA wall to define non-enhancing regions. However, this would not be detected by the thresholding technique used in this study as the SI would be lower than the reference SI. In these animals, the volume of LGE acutely after ablation may, therefore, have been underestimated.

6.4.2 CMR SI thresholds

The aforementioned animal studies used arbitrary SI thresholds/image windowing to define areas of T2W and LGE enhancement, and changes in these values could make a significant difference to the lesion measurements. Whilst studies have suggested CMR SI thresholds to quantify myocardial scar in a range of conditions, including acute and chronic myocardial infarction and hypertrophic cardiomyopathy,[74, 158] no studies have attempted to validate similar thresholds for acute or chronic atrial (or ventricular) ablation injury. As a result, a variety of SI thresholds to distinguish between healthy and injured atrial tissue have been used: two to four SD above the normal atrial wall SI to quantify LA pre-ablation fibrosis[80] and three SD to quantify post-ablation injury.[78, 82] In these and indeed any study, an alteration in the threshold would change the quantification.

6.4.3 Atrial endocardial voltage thresholds

Endocardial voltage mapping before catheter ablation for atrial arrhythmias can help to characterise the underlying atrial substrate and identify areas of previous ablation injury.[88] Most commonly, atrial scar is identified by a bipolar voltage of ≤0.05 mV – this threshold originates from the baseline noise in early EAM systems[25] and has been propagated through the literature and clinical practice without published pathological validation. Equally, thresholds to identify "low voltage", but not scarred, atrial tissue have generally been extrapolated from ventricular studies of post-myocardial infarction scar. In animal models, bipolar voltages of ≤1.0 mV and ≤0.5 mV best correlated with pathological infarct size.[155, 156] In a human study of ischaemic and non-ischaemic cardiomyopathy, authors defined abnormal endocardium as a bipolar electrogram of <1.5 mV and "densely scarred" endocardium as <0.5 mV.[159]

In this study, the mean bipolar voltage at the centre of the ablation line was 0.6 mV acutely and 0.3 mV chronically. These values would suggest that using a threshold of ≤0.05 mV to define atrial scar could significantly underestimate the extent of previous ablation injury, perhaps leading to inaccurate interpretation of voltage data and even unnecessary ablation during a redo atrial ablation procedure.

There was a statistically significant reduction in voltage (compared with pre-ablation voltages) almost 2 cm either side of the centre of the line. There are several potential reasons why the area of recorded low voltage may be greater than the actual size of the ablation line: 1) at any point, the measured bipolar voltage depends on the tissue in the surrounding area, even if outside of the

zone of histological damage; 2) when creating an intercaval ablation line in the porcine RA, the catheter sits in a concave groove, such that the contact area may be larger than if perpendicularly opposed to a flat piece of tissue; 3) catheter, cardiac and respiratory motion may cause inaccuracies in the electroanatomical shell.

6.4.4 Pathology of acute and chronic atrial ablation injury

The pathology of acute RF atrial ablation injury in animal models is well established and is characterised by coagulation necrosis,[160] as seen in this study. However, the microscopic features of chronic atrial ablation injury are much less well described due to the increased complexity in performing recovery animal experiments. Transmural myocardial fibrosis with areas of chronic inflammatory cell infiltration was seen in pigs four weeks after linear non-irrigated ablation in the RA.[161] In open-chest beating heart sheep and dog models of RF ablation, there was replacement of the atrial myocardium with a fibrin and collagen matrix 30 days after ablation.[162, 163] In the present study, animals were recovered for eight weeks to ensure a representative model of chronic ablation injury and histological findings were in keeping with the aforementioned studies, with transmural fibrous scar. Whilst CMR findings were compared with macroscopic volumes of injury, the microscopic histology in this study provided confirmation of transmural acute and chronic atrial ablation lesions.

6.4.5 Limitations

1) Extrapolation of results to humans is always a potential limitation of animal models. The LA is the predominant target of catheter ablation for AF and so

clinical CMR studies have focused on LA ablation. The porcine LA does not closely resemble the human LA and its structure is not conducive to the reproducible deployment of a linear ablation lesion. For this reason, ablation was performed on the thin posterior RA wall, which is more comparable to the human LA.

2) The CMR thresholds identified in this study are for the identification of post-ablation injury and are not applicable to quantification of *de novo* atrial fibrosis, for which a specific animal model would be required.

3) Determining volumes of injury on CMR images and pathological examination are challenging, particularly in the thin-walled atrium. Both require a subjective judgement (to segment the RA wall on CMR and to segment the ablation lesion on pathology), which was reduced as far as possible by the use of two blinded expert observers for each measurement. Furthermore, shrinkage of the pathological specimens may also occur during the preserving process.

4) Surface coil proximity, sequence parameters, body mass index, haematocrit, renal function and field strength can all affect T2W and LGE SI. Furthermore, there is currently no consensus on the optimum timing of atrial LGE CMR after contrast administration, or on the choice and dose of contrast agent, which can also affect SI. In this study, these parameters were chosen based on previously published studies of atrial CMR and clinical experience. The clinical applicability of the SI thresholds derived in this study would have to take these considerations into account and these variables may explain the variation of the SI thresholds between animals.

6.5 Conclusions

This study presents the first histopathological and electroanatomical validation of CMR to define acute and chronic atrial ablation injury, including SI thresholds that best match histological lesion volumes. However, the wide range of individual SI thresholds across the animals suggests that these values should be applied cautiously and that larger numbers would be needed to define these more accurately. Whilst continuous infusions of gadolinium (to achieve contrast equilibrium) have been shown to quantify diffuse ventricular myocardial fibrosis,[164] this technique would not be suitable for atrial LGE quantification due to the high blood pool signal. In the future, further validation of SI thresholds of atrial injury is likely to require the development of high-resolution non-contrast enhanced T1 mapping techniques.

The endocardial voltage thresholds defined in this study challenge currently used clinical values and application of these thresholds may allow a more accurate assessment of the underlying atrial substrate immediately after ablation and before repeat catheter ablation for atrial arrhythmias, potentially preventing unnecessary ablation.

In the next chapter, the SI and voltage thresholds defined in this chapter are applied to a cohort of patients who underwent CMR prior to repeat catheter ablation for AF or AT.

7 Atrial arrhythmias following catheter ablation – cardiac magnetic resonance prediction of endocardial voltage and gaps in ablation lesion sets

7.1 Introduction

In appropriately selected patients with paroxysmal and persistent AF, catheter ablation is an effective treatment with freedom from AF reported in 56-89% of cases at one year.[18] However, following ablation, a significant proportion of patients re-present with either AF or AT, often necessitating repeat procedures. Pulmonary vein reconnection is common and conduction across previously complete linear and circular ablation lesions is frequently seen at repeat catheter ablation procedures,[136, 137] providing a possible explanation for the modest success rates.

LGE CMR has been used to assess patient suitability and response to catheter ablation[51, 77-80, 82-85, 87] and to guide repeat catheter ablation.[82, 86, 165, 166] Previous studies in a relatively small number (n=11-13) of patients undergoing repeat catheter ablation have suggested a qualitative[82] and quantitative[165, 166] relationship between areas of LGE and areas of low endocardial voltage. However, there is controversy regarding the reproducibility and diagnostic ability of atrial LGE CMR to reliably identify ablation lesions and their distribution.[167] Furthermore, while one study demonstrated that LGE CMR can predict electrical reconnection by identifying gaps in ablation lesions,[82] another has shown the opposite.[165]

Given these conflicting findings, this chapter investigates atrial LGE CMR to determine its relationship with atrial bipolar voltage recording, and also to investigate its potential as a predictor of electrical reconnection in patients undergoing repeat catheter ablation.

7.2 Methods

7.2.1 Patients

Twenty patients requiring a clinically indicated repeat LA catheter ablation were studied. All had previously undergone LA catheter ablation for paroxysmal AF, persistent AF or AT. The index procedure for patients with paroxysmal AF was a PV wide area encirclement alone. For patients with persistent AF, the index procedure was a stepwise ablation approach incorporating wide area PV encirclement, electrogram-guided ablation and linear lesions at the LA roof, mitral isthmus and CTI as deemed appropriate. Patients presenting in AF on the day of the repeat procedure or with any contraindication to CMR were excluded from the study.

7.2.2 CMR

CMR was performed 2-3 weeks prior to repeat catheter ablation and included 3D b-SSFP and 3D LGE imaging, as described in section 5.4 (page 83). Example LGE images are shown in Figure 7-1.

7.2.3 Ablation procedure

Class I and III antiarrhythmic medications, with the exception of amiodarone, were discontinued at least five half-lives prior to the procedure. Patients taking warfarin discontinued this five days before the procedure and were

administered with subcutaneous low molecular weight heparin for three days before ablation. In two patients, the procedure was performed on uninterrupted warfarin.[168] In patients with an original diagnosis of persistent AF or a $CHADS_2Vasc$ score ≥2, transoesophageal echocardiography was performed prior to the procedure to exclude intracardiac thrombus.

At the start of the ablation procedure, a 6F decapolar catheter was placed in the CS to provide a reference for EAM. For procedures performed under general anaesthesia, TOE was used to guide transseptal puncture. For those performed under conscious sedation, fluoroscopy alone was used to guide a single transseptal puncture through which two SRO sheaths were passed to the LA. Immediately after needle access to the LA, intravenous heparin was administered to achieve an activated clotting time ≥300 seconds. The SRO sheaths were used to place a 3.5 mm tip irrigated ablation catheter (Thermocool, Biosense Webster) and a 20-pole circumferential mapping catheter (Lasso, Biosense Webster) in the LA.

A 3D geometry of the LA was created using the Carto 3 EAM system (Biosense Webster). A high-density pre-ablation peak-to-peak bipolar voltage map was constructed using points acquired with the ablation catheter in order to give coverage of the entire LA. Tissue contact was determined by electrogram amplitude and distance from the endocardial shell. The catheter was held in each position for 5-10 seconds. The voltage map was constructed in either sinus rhythm or AT, according to the presenting arrhythmia.

The circumferential mapping catheter was positioned sequentially in the PVs to assess for PV-LA reconnection. In sinus rhythm, conduction across the LA roof

and left lower PV-mitral isthmus line ('mitral line') was also assessed using previously validated pacing techniques.[169, 170]

For patients with an original diagnosis of paroxysmal AF and in sinus rhythm, the procedural endpoint was re-isolation of the PVs, achieved by targeting the site(s) of PV reconnection(s) and verification of conduction block at the sites of any previous linear lesion. For patients presenting in AT, the procedural endpoint was termination of tachycardia, re-isolation of incompletely isolated PVs and achievement of conduction block across linear lesions.

7.2.4 CMR image processing

CMR images were not analysed before repeat ablation and the procedure was performed without any of the CMR anatomical or LGE information available to the operator.

CMR images were processed according to previously described methods.[51, 87] Following creation of the 3D volumes, the first step was to perform an automatic segmentation of the LA using model-based segmentation (Philips segmentation plug-in for Graphical Interface for Medical Image Analysis and Simulation (GIMIAS), Universitat Pompeu Fabra, Barcelona). This technique aims to fit a standardised cardiac model (created as an average from a patient library) to the b-SSFP acquisition using contrast boundaries. The LA segmentation was extracted, but invariably required slice-by-slice manual correction using 3D medical image segmentation software (itk-SNAP Version 2.2.0).

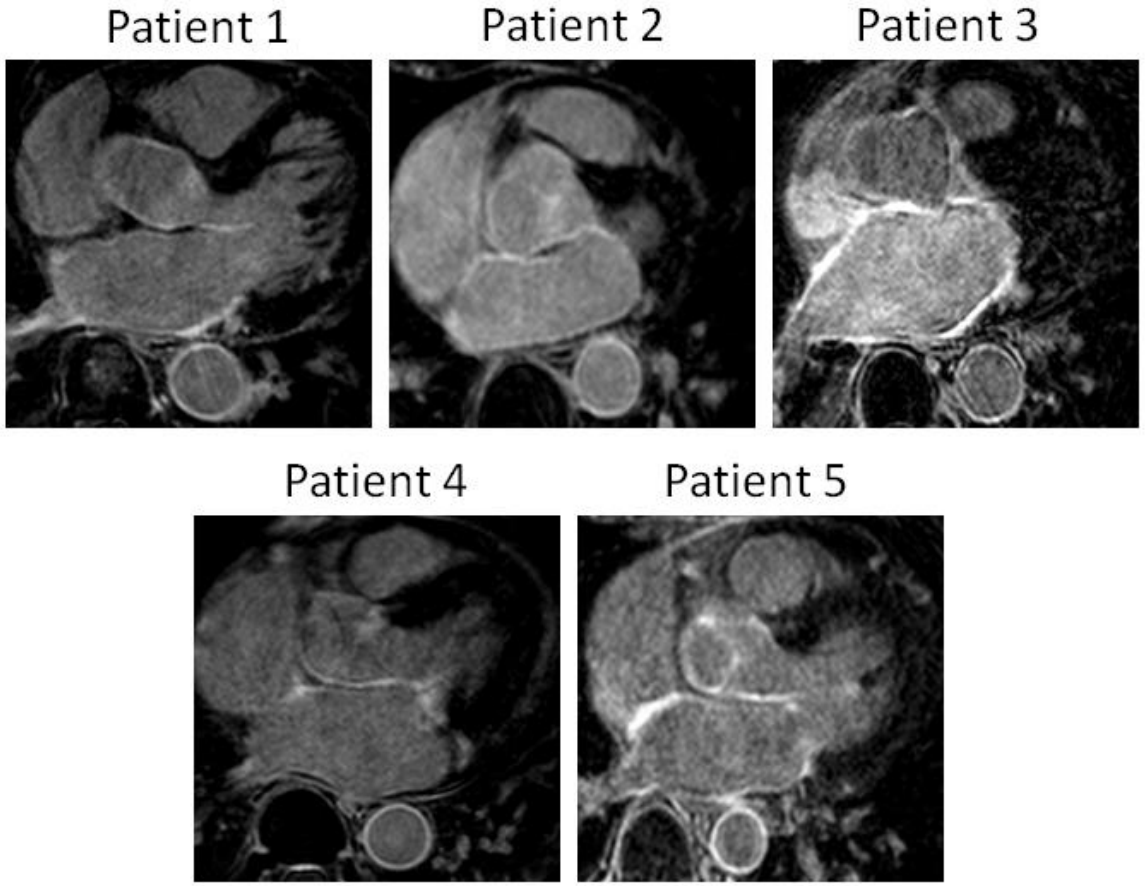

Figure 7-1: Transverse slices from 3D LA LGE CMR scans from five different patients

The second step involved image registration between the LGE and b-SSFP acquisition, using the information stored in the DICOM headers and the Image Registration Toolkit (Department of Computing, Imperial College). As the b-SSFP and LGE acquisitions have different resolutions (both in-plane and in the slice direction), the LGE acquisition is interpolated during this registration process to fit the resolution of the b-SSFP acquisition.

The final step was the projection of the image-registered LGE acquisition on to the segmented LA shell. Vectors at a normal to each vertex on the LA shell (a triangular mesh) were projected and the maximum SI within 3 mm of the surface was selected as the intensity for that vertex (a MIP). Signal intensities were then displayed on the 3D LA shell as a number of SD from the mean SI of the atrial blood pool to avoid the need for thresholding (Figure 7-2).

7.2.5 Comparison of CMR signal intensity and endocardial voltage

Voltage maps were exported from Carto 3 and imported into software custom-written with Matlab (The Mathworks, Matick, USA), so that the voltage maps and data collection points could be reconstructed for off-line analysis. The CMR-segmented LA shells were registered to the Carto 3 LA shells using a two-step process: 1) landmark registration (using the PVs and LA appendage as landmarks) and 2) iterative closest point registration. This allowed the LGE CMR SI to be projected on to the Carto 3 LA anatomy using point correspondence between the two LA shells (Figure 7-3). Thereafter, for each Carto 3 sampling point, the bipolar endocardial voltage and LGE CMR SI were extracted to allow a point-by-point comparison.

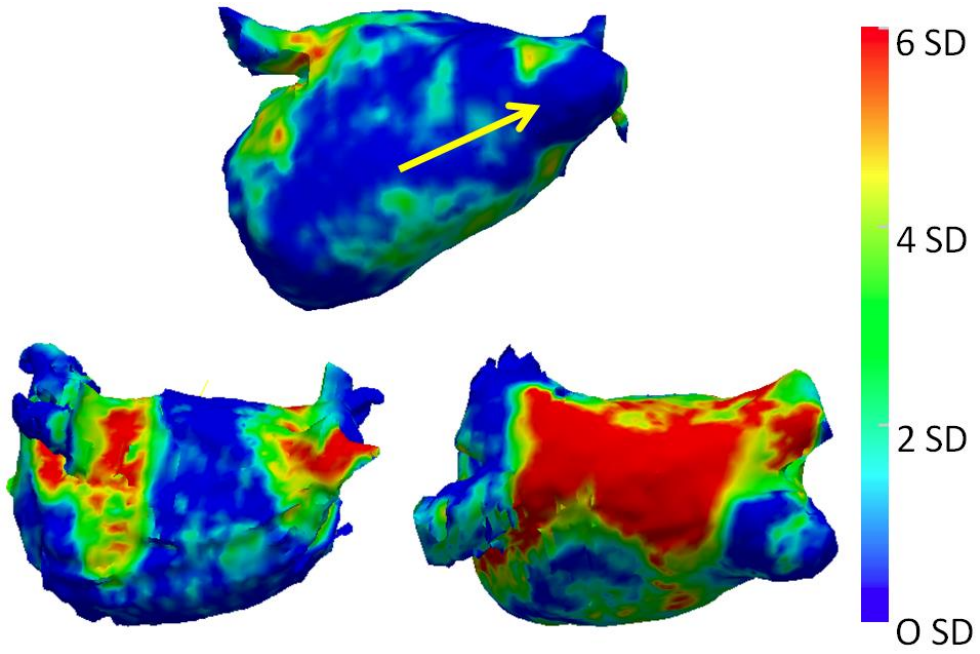

Figure 7-2: Top row - 3D LA LGE CMR reconstruction showing an SI 'gap' at the inferior right lower PV-LA junction (arrow). Bottom left - 3D reconstruction of a patient with previous PV isolation for paroxysmal AF. Bottom right - 3D reconstruction of a patient with previous roof line ablation. The scale bar applies to all three reconstructions and SI are expressed as the number of SD from the mean SI of the atrial blood pool.

7.2.6 CMR analysis of gaps in ablation lesions

The presence or absence of gaps in ablation lesions on 3D CMR reconstructions depends on the SI threshold chosen to denote 'scar'. A lower threshold will result in more 'scar', whereas a higher threshold will result in more 'gaps'. In order to avoid selecting an arbitrary threshold, it was necessary to develop an objective user-independent method for detecting gaps.

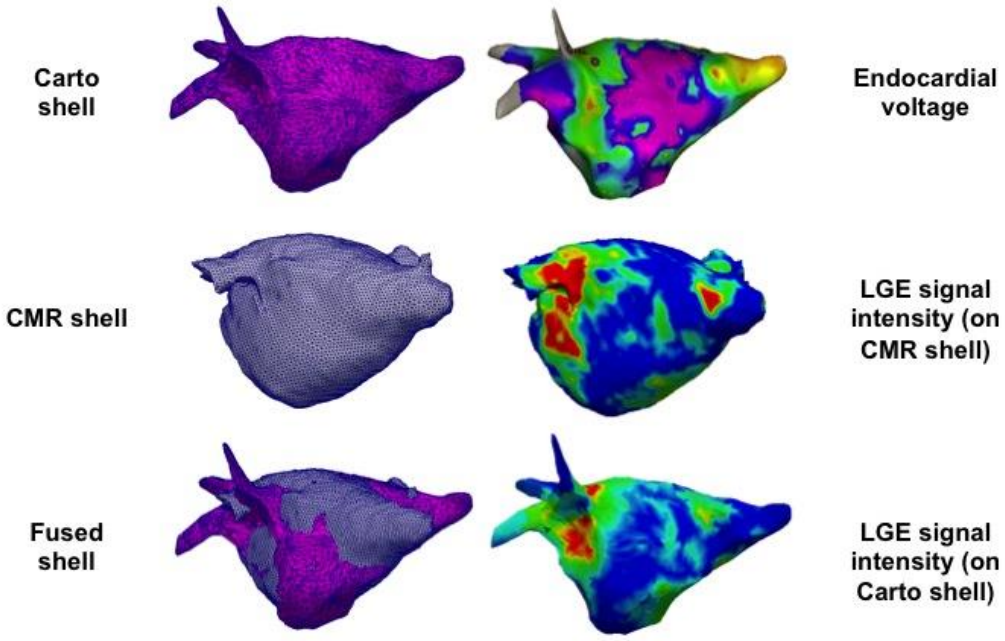

Figure 7-3: Top row - Carto LA anatomical shell (left) and bipolar endocardial voltage map (right). Middle row: CMR LA anatomical shell (left) and LGE SI map. Bottom row - Fusion of the Carto and CMR LA anatomical shells by landmark and iterative closest point registration (left) and LGE SI map projected on to the fused Carto shell (right).

Using custom-written software, a path was traced around the left and right PV antra, the LA roof line and the mitral line on the CMR-segmented LA shell (without registration to the Carto 3 shell). For each vertex along these paths, the mean SI within 10 mm was extracted. The minimum intensity (LGE_{min}) recorded on these paths represents the 'weakest link in the chain' and the most likely site for reconnection, on the basis of LGE information (Figure 7-4). The mean SI (LGE_{mean}) of the path gives an assessment of the total scar burden along the

path. The values of LGE_{min} and LGE_{mean} were compared with the electrical integrity of the lesion sets (assessed at the time of repeat catheter ablation).

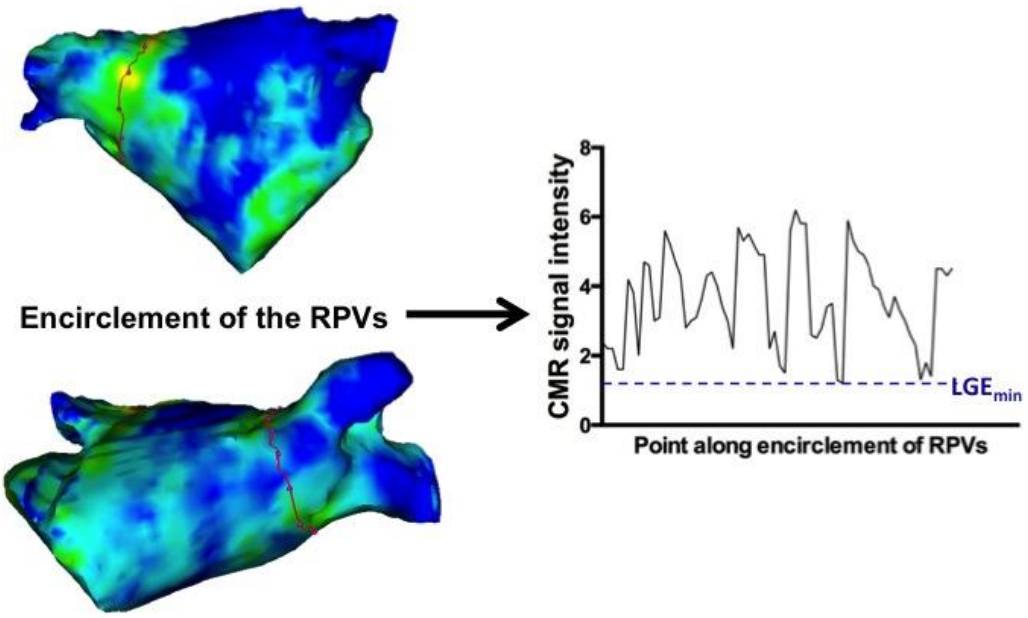

Figure 7-4: A path was traced around the left and right PV antra, the LA roof line and the mitral line on the CMR-segmented LA shell (the right PV antra is shown for example purposes). For each point along these paths, the mean SI within 10 mm was extracted. The minimum intensity (LGE_{min}) recorded on these paths represents the 'weakest link in the chain' and the most likely site for reconnection, on the basis of LGE information.

7.2.7 Statistical analysis

Continuous variables are expressed throughout as mean ± SD, except where stated otherwise, and were compared using Student's *t*-test for unpaired data.

One-way ANOVA with a post test for a linear trend was used for multiple comparisons. A significance level of $p<0.05$ was considered statistically significant.

7.3 Results

7.3.1 Patients

Twenty patients (17 male, 3 female; mean age 59 ± 7 years) completed the study. Patient characteristics are shown in Table 2. The median number of previous ablation procedures was 2 (range 1-5). The original diagnosis was paroxysmal AF in 11 patients, persistent AF in eight patients and AT in one patient. The arrhythmia at the time of the redo procedure was paroxysmal AF in ten patients and AT in ten patients.

7.3.2 Comparison of CMR signal intensity and endocardial voltage

There were a total of 6767 voltage measurements in the twenty patients (mean number of points per patient was 342 ± 214). 119 (1.8%) of the points were ≤0.05 mV (the current clinical thresholds to define atrial scar), whilst 1819 (27%) of the points were ≤0.3 mV (the threshold defined in the previous chapter). To demonstrate a qualitative comparison between the two datasets, voltage maps thresholded to these two values are shown in Figure 7-5, alongside corresponding non-thresholded voltage maps and 3D CMR reconstructions.

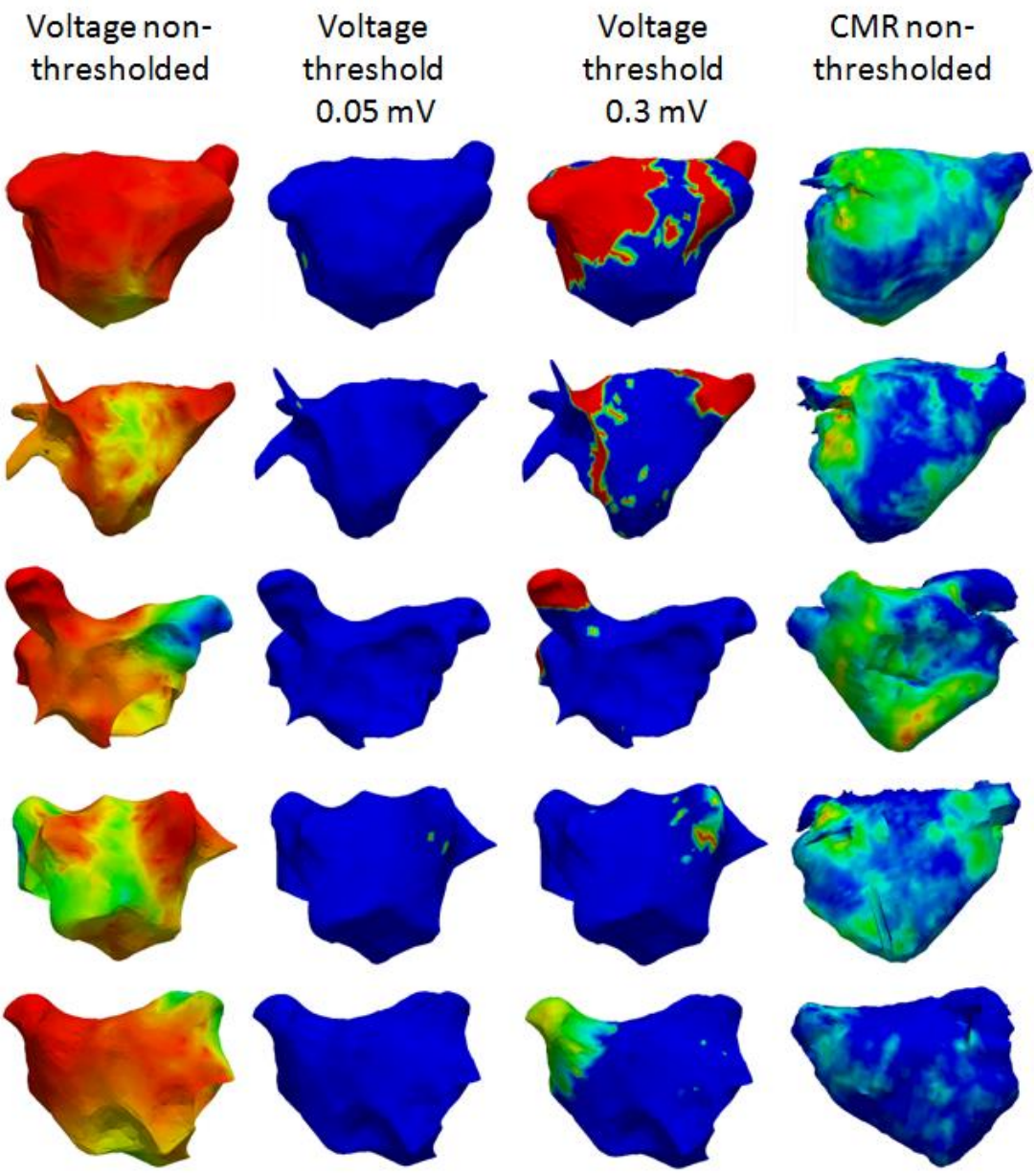
Voltage non-thresholded
Voltage threshold 0.05 mV
Voltage threshold 0.3 mV
CMR non-thresholded

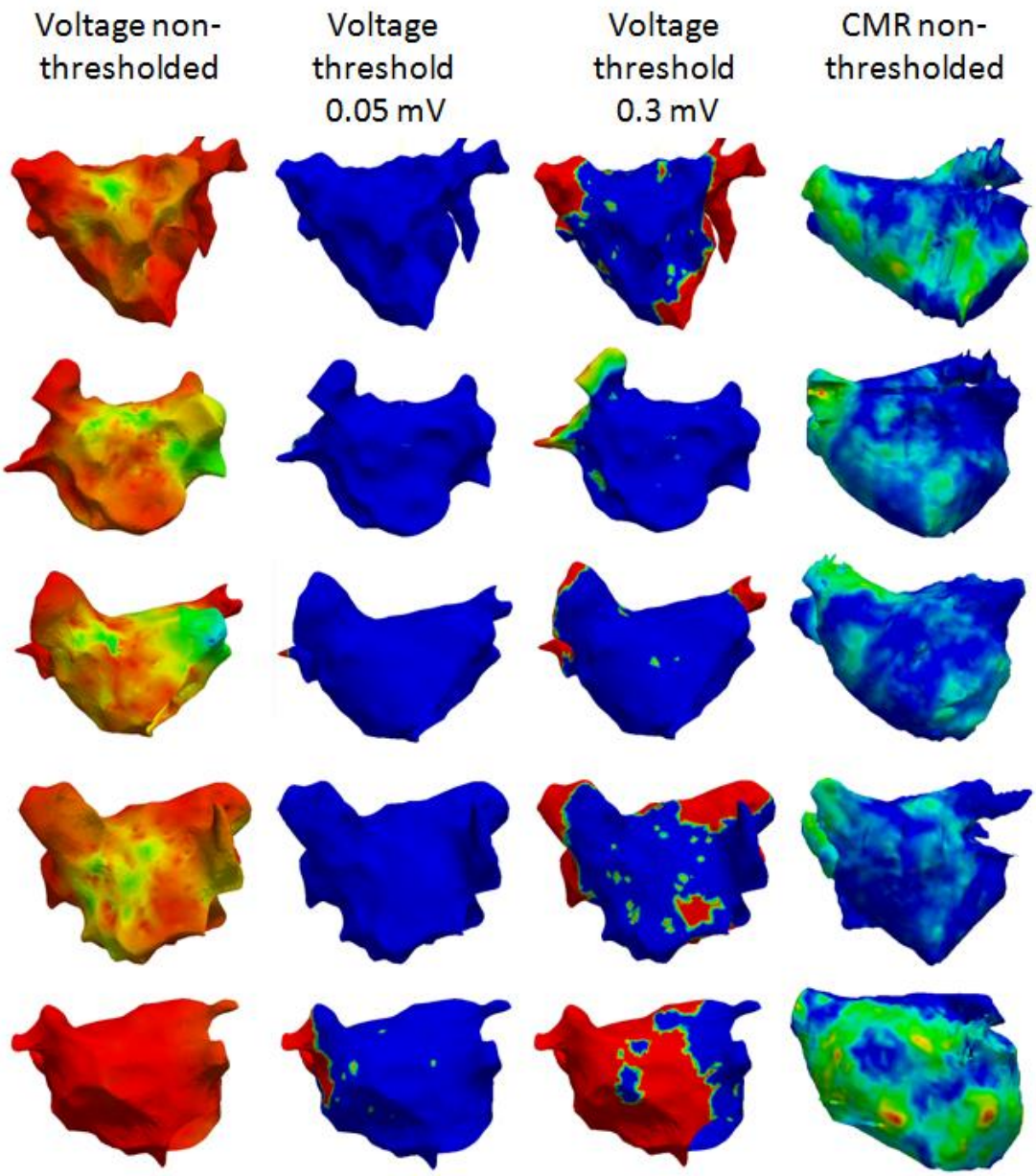
Voltage non-thresholded
Voltage threshold 0.05 mV
Voltage threshold 0.3 mV
CMR non-thresholded

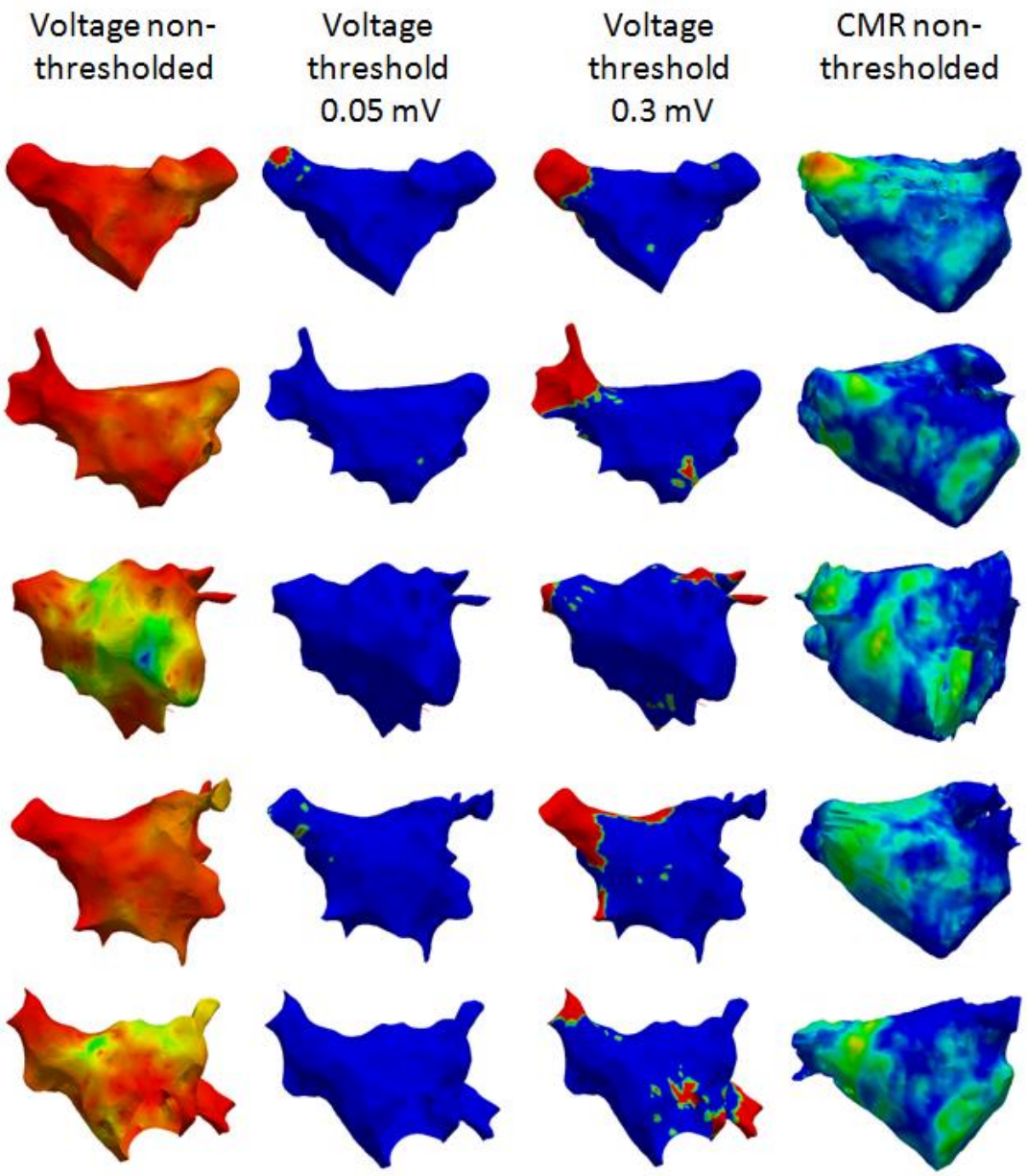
Voltage non-thresholded
Voltage threshold 0.05 mV
Voltage threshold 0.3 mV
CMR non-thresholded

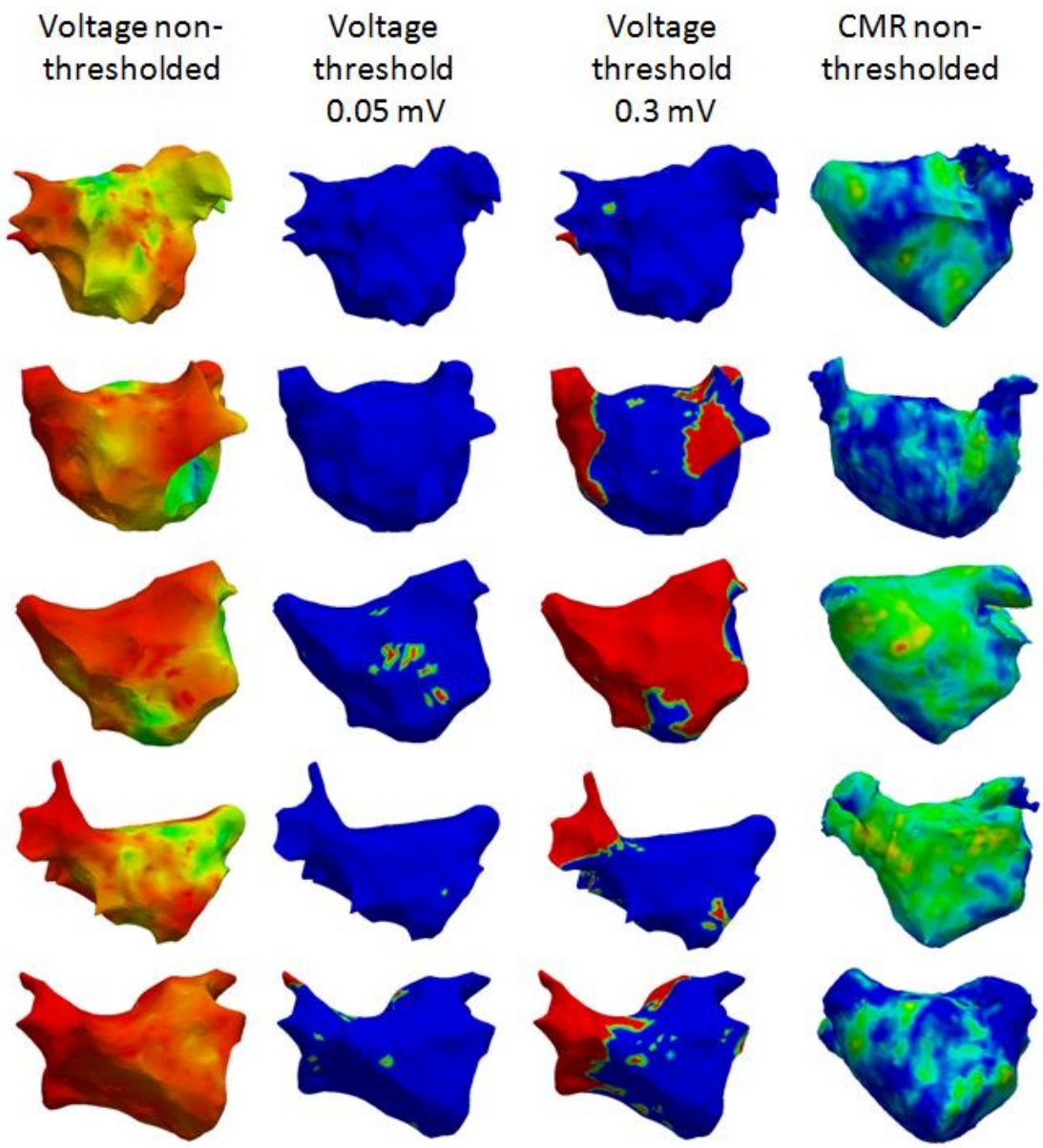

Figure 7-5: For all 20 patients, endocardial voltage maps are shown without thresholding and at two different thresholds (where blue indicates values greater than the threshold and red/green indicates values less than the threshold). Corresponding 3D CMR reconstructions are shown without thresholding.

For each of the voltage points, the corresponding CMR SI was extracted as described to allow point-by-point comparison of bipolar voltage and CMR SI. Examples of co-registered voltage maps and CMR SI maps are shown in Figure 7-3. The summary data are shown in Figure 7-6. There is a very weak correlation between the two measurements (R^2=0.018) with low voltage occurring across a large range of SI.

Age (years)	59 ± 7
Gender (n)	
Male	17 (85%)
Female	3 (15%)
Original diagnosis (n)	
Paroxysmal AF	11 (55%)
Persistent AF	8 (40%)
AT	1 (5%)
Recurrent arrhythmia (n)	
Paroxysmal AF	10 (50%)
AT	10 (50%)
Coronary artery disease (n)	0 (0%)
Smoking (n)	1 (5%)
Valve disease (n)	1 (5%)
Hypertension (n)	2 (10%)
Diabetes mellitus (n)	2 (10%)
CVA/TIA (n)	2 (10%)
LVEF (%)	53 ± 3
LVEF <40% (n)	0 (0%)
$CHADS_2Vasc$ (n)	
0	14 (70%)
1	2 (10%)
2	3 (15%)
3	1 (5%)
>3	0 (0%)
Number of previous LA ablations (n)	
1	9 (45%)
2	6 (30%)
3	3 (15%)
>3	2 (10%)

AT=atrial tachycardia; CVA=cerebrovascular accident; TIA=transient ischemic attack; LVEF=left ventricular ejection fraction; LA=left atrial

Table 2: Patient demographics

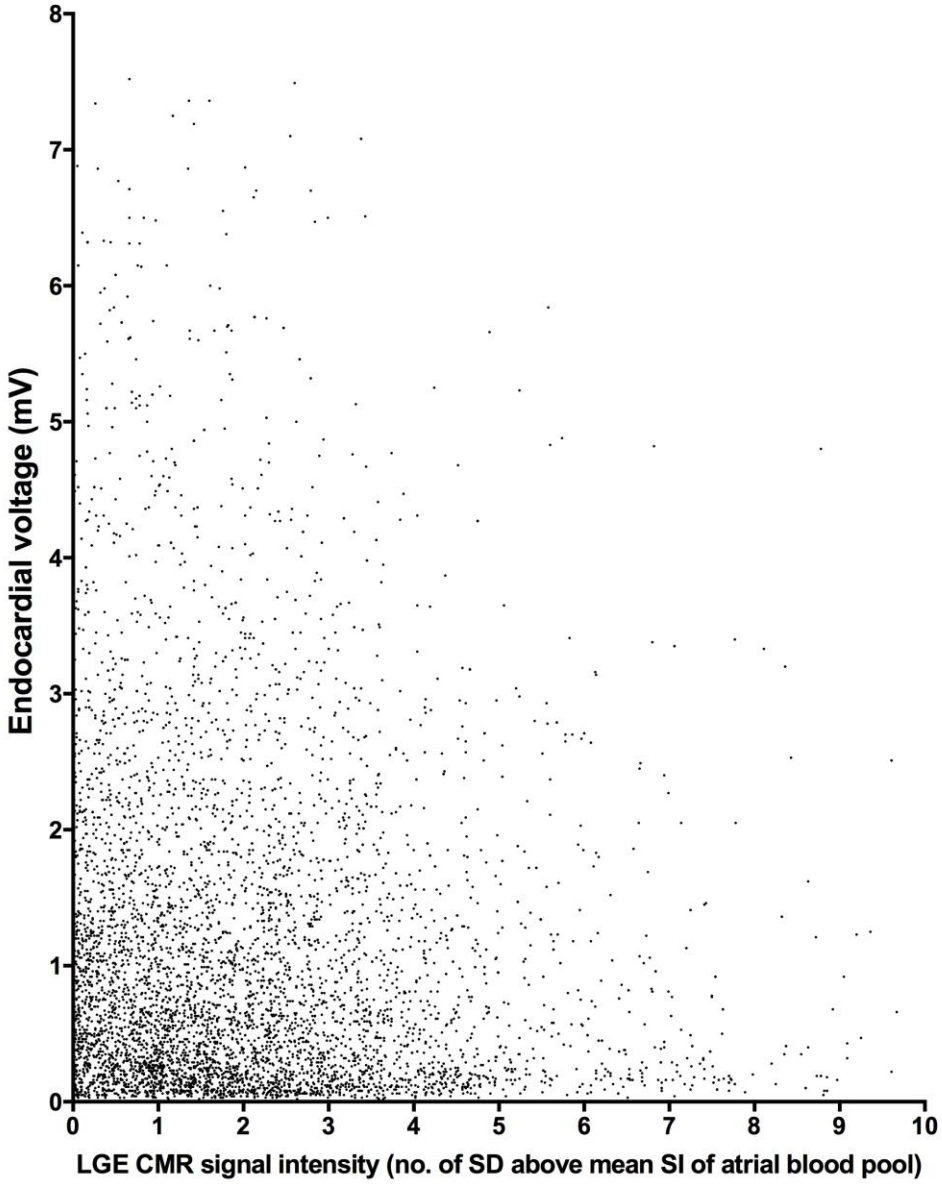

Figure 7-6: Scatter plot to show the endocardial voltage and LGE CMR SI (expressed as the number of SD above the mean SI of the atrial blood pool) for all 6767 data points. R^2=0.018.

Previous studies have transformed these data by splitting the CMR SI into bins[166] or by simply dividing the CMR data into either 'normal' or 'scar'.[165]

The former approach is shown in Figure 7-7, demonstrating a statistically significant negative trend in mean bipolar ($p<0.0001$) voltage as CMR signal intensity increases. Receiver operating characteristic (ROC) analyses to determine voltage thresholds to separate contiguous pairs are shown in Figure 7-8.

The latter approach is shown in Figure 7-9, using the chronic LGE threshold of 3.3 SD derived in the previous chapter to distinguish between 'normal' and 'scar'. This demonstrates that SI below 3.3 SD are associated with a significantly higher voltage than SI above 3.3 SD (1.27 ± 1.3 mV vs 0.94 ± 1.1 mV, $p<0.0001$). A ROC analysis to determine the voltage threshold to separate the two populations is shown in Figure 7-10. The percentage of the total LA surface area with SI greater than this threshold was the same for patients with paroxysmal AF and AT recurrences (17.9 ± 11% vs 17.4 ± 11%; $p=0.92$)

The results of performing the analysis the other way round, to assess the ability of a voltage threshold (0.3 mV as defined in the previous chapter) to determine LGE SI are shown in Figure 7-11. A ROC analysis to determine the LGE SI threshold to separate the two populations is shown in Figure 7-12.

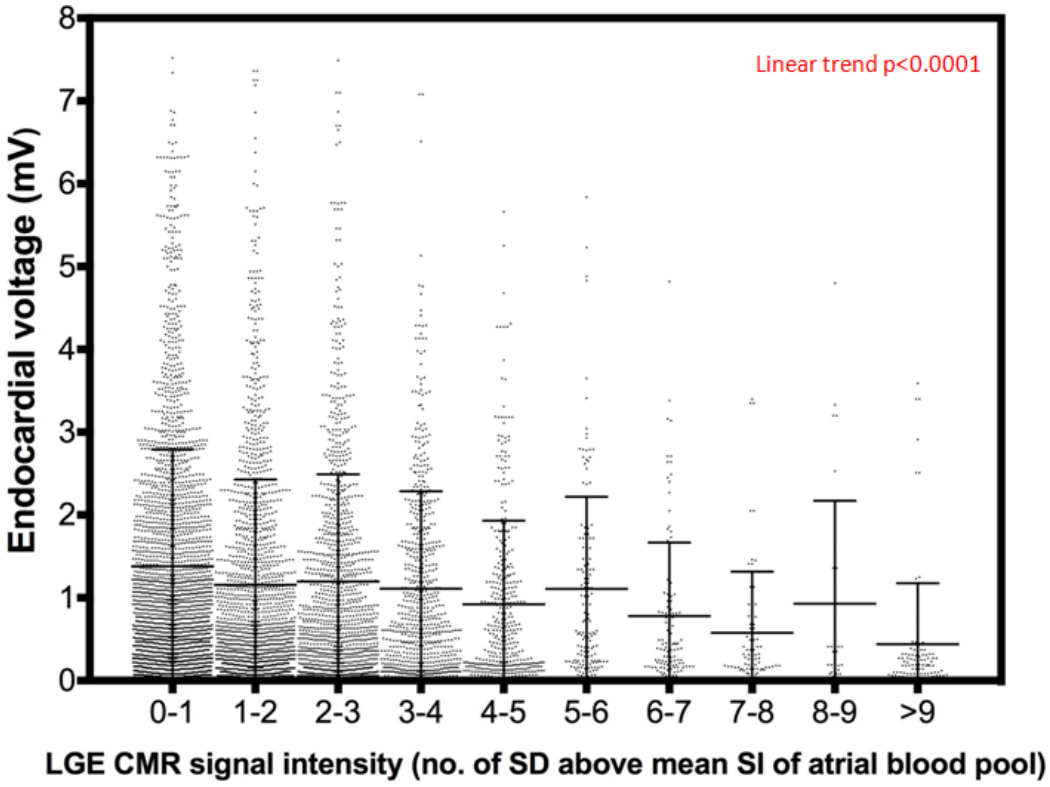

Figure 7-7: The data from Figure 7-6 have been transformed by splitting the LGE CMR SI into bins and is presented as a dot-plot of endocardial voltage against LGE CMR SI (expressed as the number of SD above the mean SI of the atrial blood pool) for all 6767 data points. Error bars indicate mean ± SD.

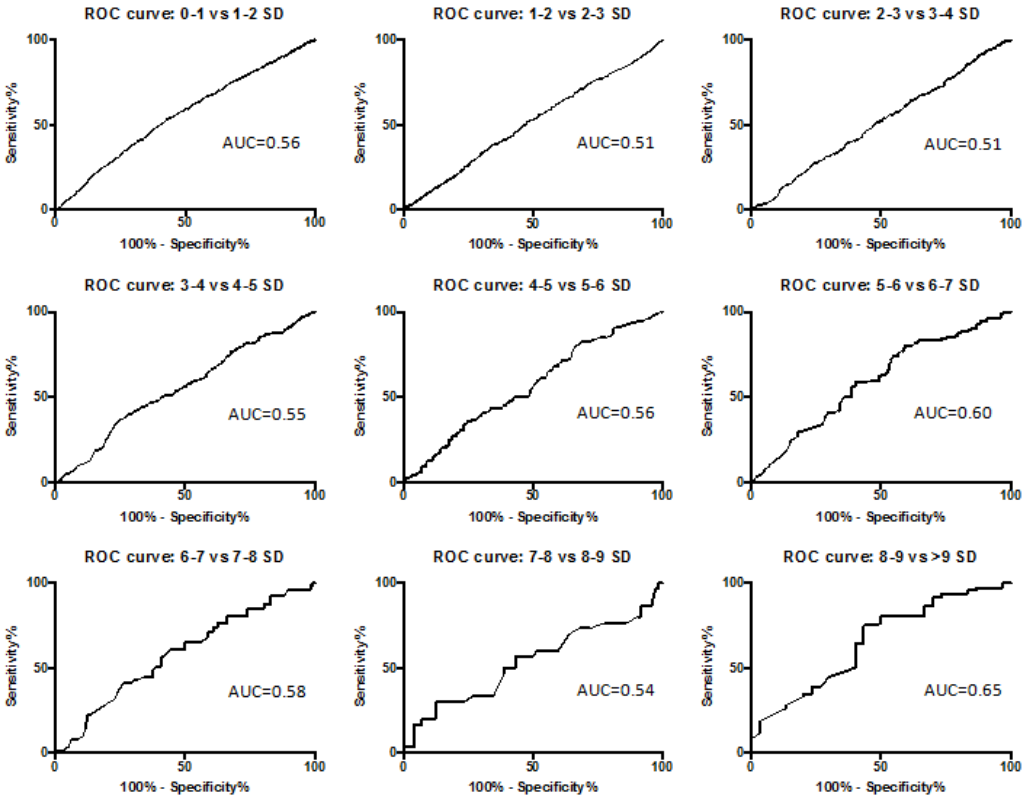

Figure 7-8: Receiver operating characteristic (ROC) analyses to show the predictive ability of different SI pairs to determine endocardial voltage. AUC=area under curve.

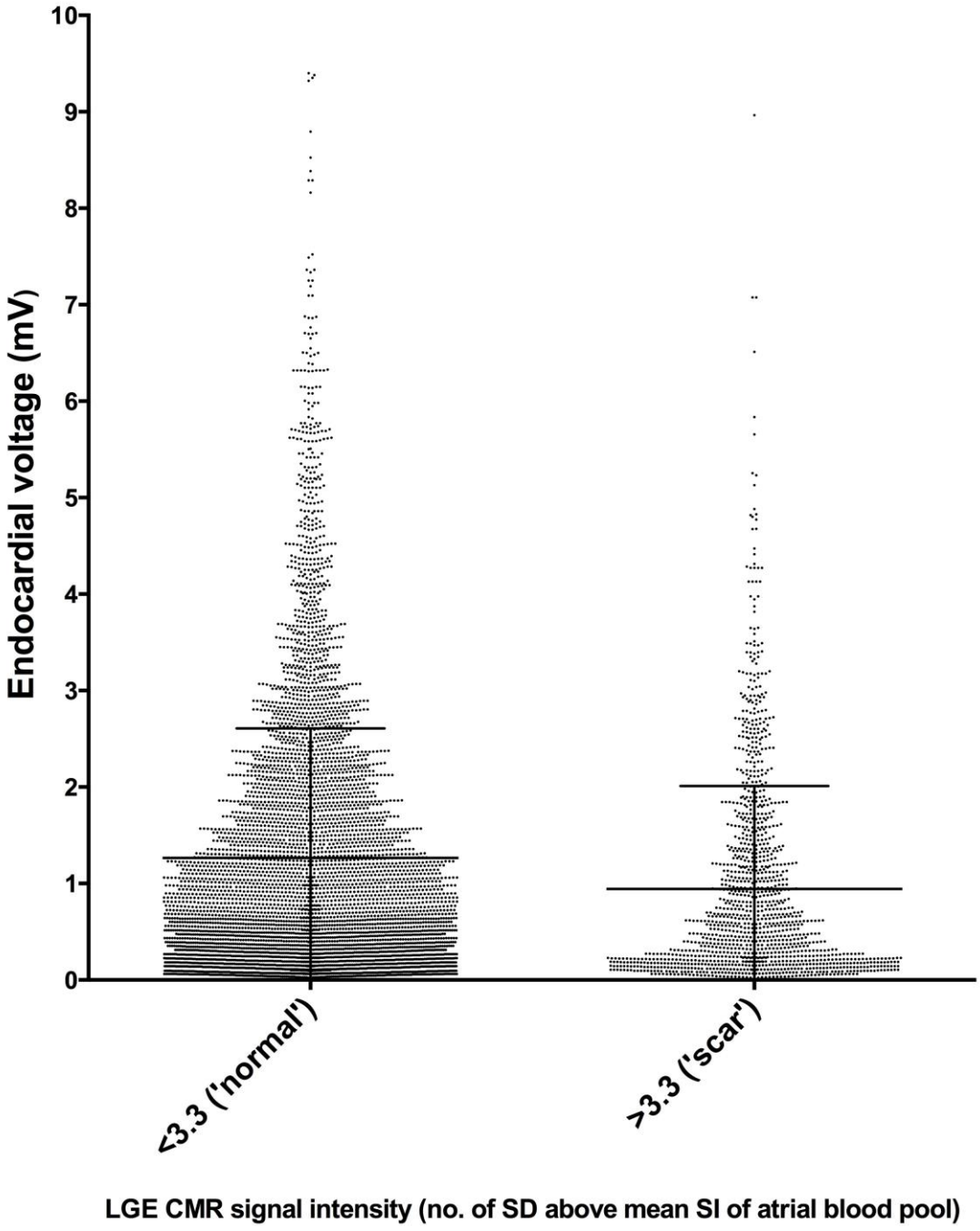

Figure 7-9: The data from Figure 7-6 have been transformed by splitting the LGE CMR SI (expressed as the number of SD above the mean SI of the atrial blood pool) into two categories (<3.3 SD 'normal' and >3.3 SD 'scar'). Endocardial voltages are displayed as a dot-plot. Error bars indicated mean ± SD.

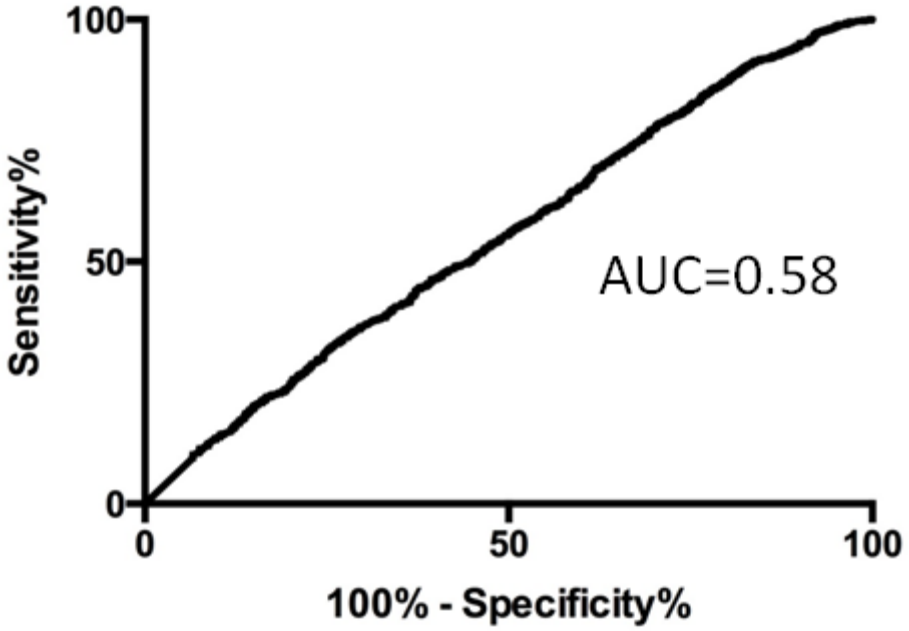

Figure 7-10: Receiver operating characteristic (ROC) analysis to show the predictive ability of an SI threshold of 3.3 SD to determine endocardial voltage. AUC=area under curve.

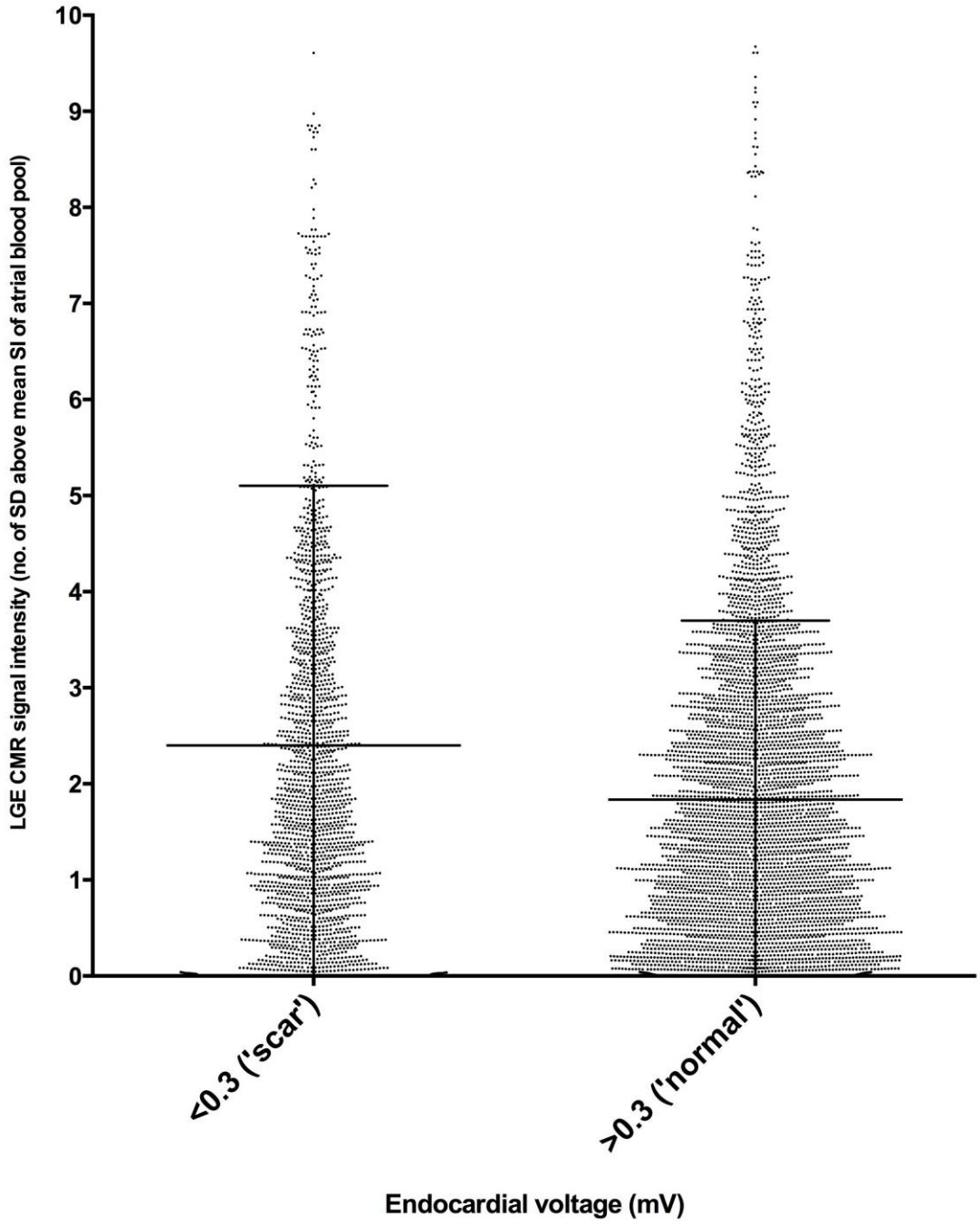

Figure 7-11: The data from Figure 7-6 have been transformed by splitting the endocardial voltage into two categories (<0.3 mV 'scar' and >0.3 'normal'). LGE CMR SI (expressed as the number of SD above the mean SI of the atrial blood pool) are displayed as a dot-plot. Error bars indicated mean ± SD.

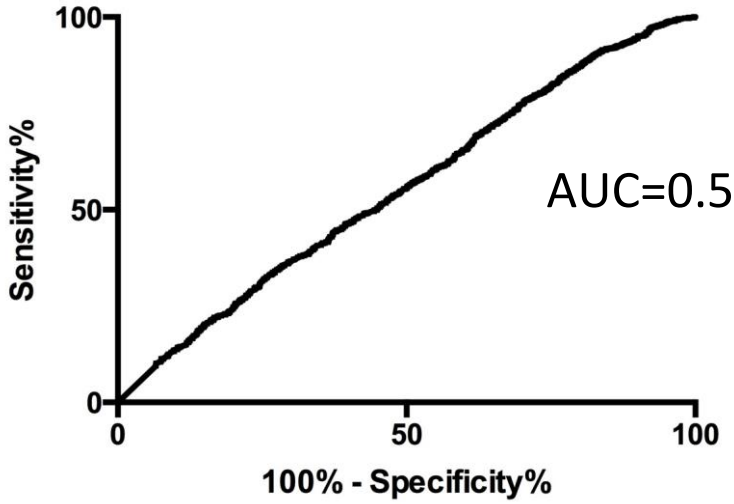

Figure 7-12: Receiver operating characteristic (ROC) analysis to show the predictive ability of a voltage threshold of 0.3 mV to determine LGE SI. AUC=area under curve.

7.3.3 CMR analysis of gaps in ablation lesions

All patients had previously undergone PVI. There was right upper PV reconnection in eight patients, right lower PV reconnection in 12 patients, left upper PV reconnection in ten patients and left lower PV reconnection in ten patients. When assessed as pairs, there was right PV reconnection in 13 patients and left PV reconnection in 12 patients. Six patients had previously undergone LA roof line ablation, but only four of these remained blocked. Five patients had previously undergone mitral line ablation, but only three of these remained blocked.

The values for LGE_{min} and LGE_{mean} for reconnected/unblocked and isolated/blocked lesions are summarized in Table 3. There were no statistically

significant differences. The data for individual patients are shown in Figure 7-13, Figure 7-14, Figure 7-15 and Figure 7-16.

		LGE_{min}	**p value**	**LGE_{mean}**	**p value**
Right PVs	**Reconnected**	0.79 ± 1.11	0.13	3.25 ± 1.88	0.19
	Isolated	0.11 ± 0.15		2.20 ± 1.07	
Left PVs	**Reconnected**	0.23 ± 0.41	0.67	1.83 ± 0.75	0.43
	Isolated	0.15 ± 0.25		2.19 ± 1.22	
Roof line	**Unblocked**	1.20 ± 2.05	0.73	2.44 ± 2.73	0.60
	Blocked	0.74 ± 1.38		1.68 ± 1.25	
Mitral line	**Unblocked**	1.26 ± 2.00	0.42	2.44 ± 1.67	0.13
	Blocked	1.50 ± 0.52		4.02 ± 0.22	

Table 3: Summary LGE_{min} and LGE_{mean} values for reconnected/unblocked and isolated/blocked lesions.

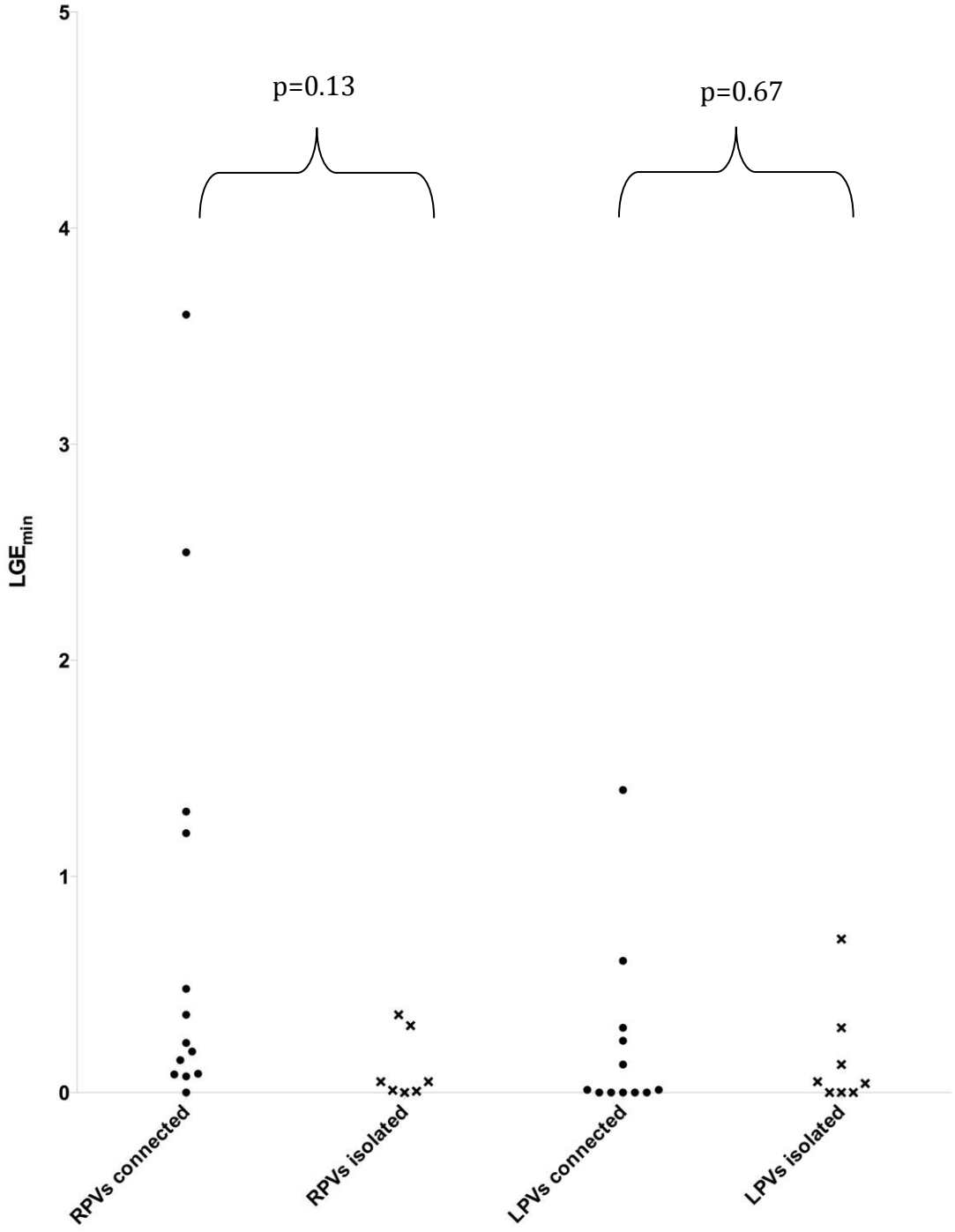

Figure 7-13: Individual LGE_{min} values for reconnected (•) and isolated veins (x). RPVs = right pulmonary veins; LPVs = left pulmonary veins.

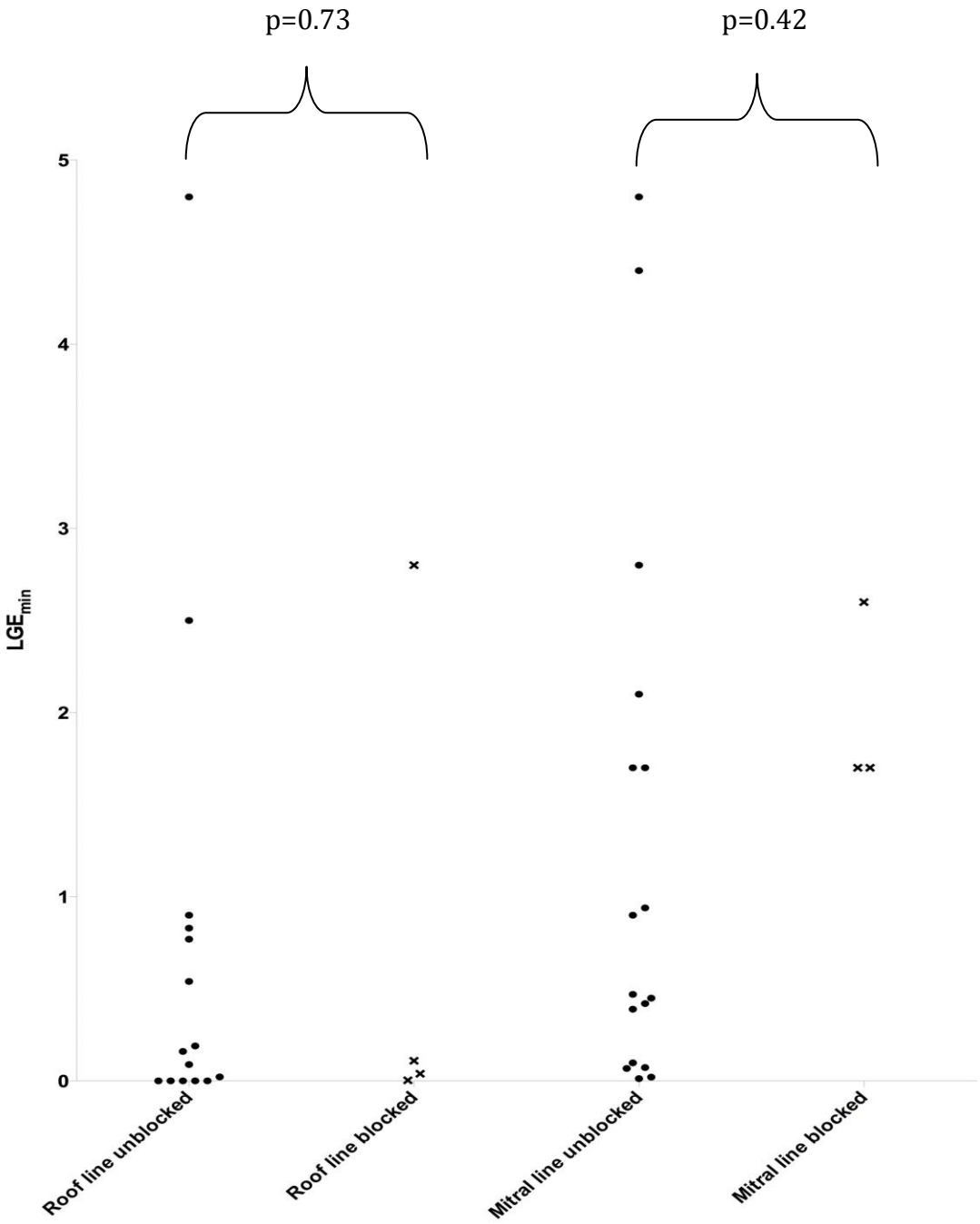

Figure 7-14: Individual LGE_{min} values for unblocked (•) and blocked ablation lines (x).

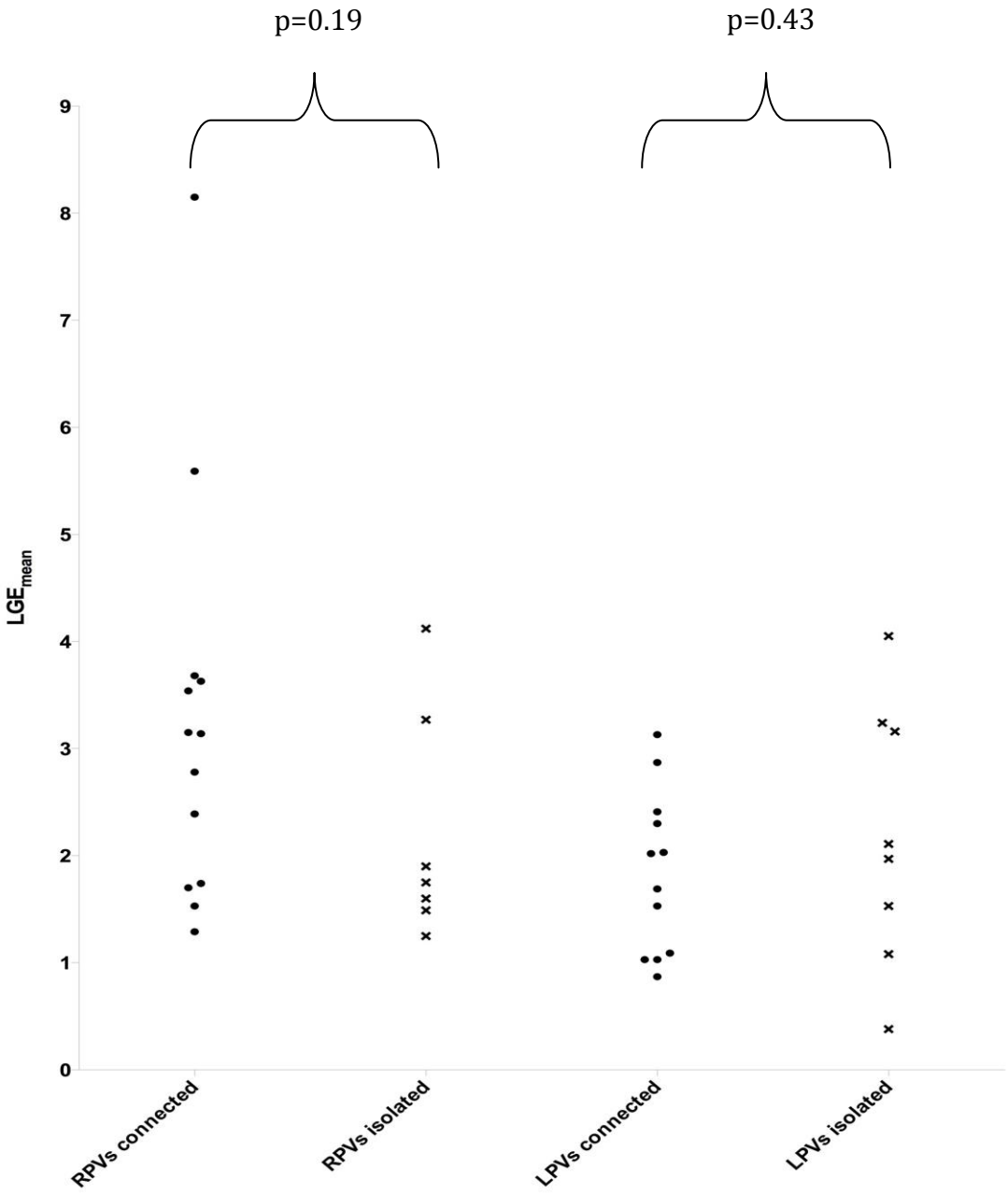

Figure 7-15: Individual LGE_{mean} values for reconnected (•) and isolated veins (x). RPVs = right pulmonary veins; LPVs = left pulmonary veins.

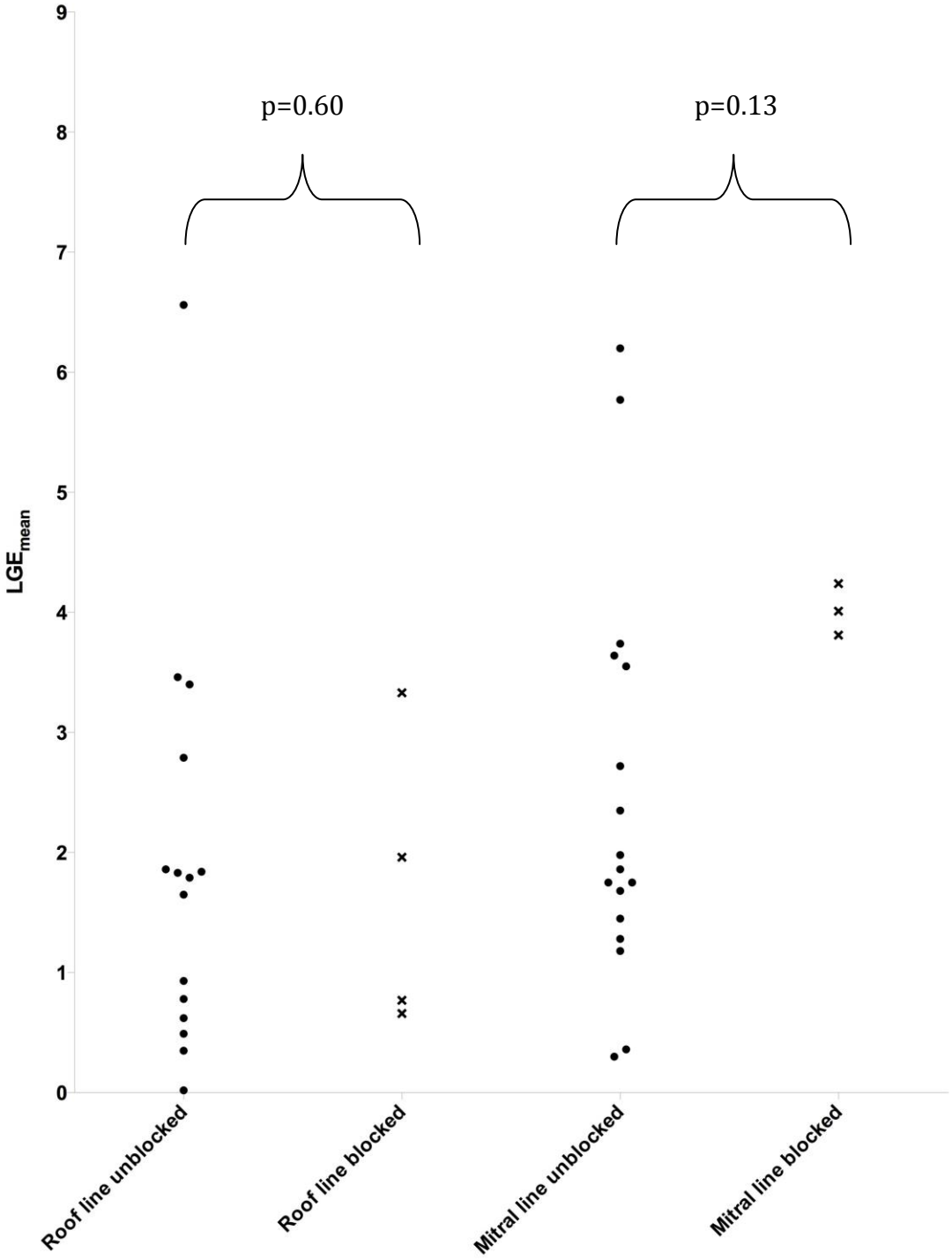

Figure 7-16: Individual LGE_{mean} values for unblocked (•) and blocked ablation lines (x).

7.4 Discussion

This study was designed: 1) to investigate the relationship between LGE CMR SI and LA endocardial voltage in patients undergoing repeat catheter ablation for LA arrhythmias; 2) to define an objective user-independent method for assessing the ability of LGE CMR to predict electrical isolation or reconnection of LA ablation lesions.

The principal findings can be summarised as follows: 1) whilst it is possible to demonstrate a negative correlation between mean endocardial voltage and CMR SI, the raw data shows that the point-by-point relationship is weak; 2) low endocardial voltage can occur at sites of low and high CMR SI, suggesting that CMR SI thresholds are poor predictors of endocardial voltage; 3) low CMR SI (LGE_{min}) occur at the site of both electrically isolated and connected ablation lesions, indicating that there is no clinically useful threshold to determine electrical integrity of LA ablation lesions.

7.4.1 Correlation between LGE CMR and LA endocardial voltage

In a retrospective analysis of 24 patients presenting to a single centre for repeat catheter ablation of AF, 13 patients had voltage maps with >100 points and interpretable LGE CMR scans.[82] The authors demonstrated a qualitative correlation between regions of LGE and low voltage in all patients and a quantitative relationship (R^2=0.57) by subdividing the LA into 18 regions and scoring the extent of LGE and low voltage on a scale from 0-3.

A study of ten patients, by different authors, demonstrated initial experience with co-registration of LGE CMR SI with endocardial voltage mapping.[165] In this

study, authors used manual segmentation to distinguish between areas of visual non-enhancement and enhancement in the LA wall to create a binary ('scar' vs 'normal') 3D LGE CMR reconstruction. They then determined whether each voltage point (mean number of points 90 ± 24, total of 893 points) fell within an area of co-registered 'scar' or not. They demonstrated that the mean voltage within areas of CMR 'scar' was lower than the mean voltage within 'normal' areas on CMR. However, whilst the mean voltages were statistically different, there was almost complete overlap of the two populations (as seen in the present study, Figure 7-9), indicating that defining LGE CMR on the basis of visual assessment is neither sensitive nor specific for predicting endocardial voltage.

More recently, a study of 11 patients undergoing repeat LA catheter ablation suggested a statistical difference between the mean bipolar endocardial voltages corresponding with LGE CMR SI thresholds of 3 to 5 SD above the mean SI of the atrial blood pool.[166] No statistical difference was seen above 5 SD, and the authors concluded that SI above this might represent fully scarred atrial myocardium. However, this would not explain the lack of statistical significance at 0 to 3 SD. More importantly, as demonstrated in Figure 7-7 and Figure 7-8, whilst there may be a trend towards lower mean voltage with increased CMR SI between 3 and 5 SD, the significant overlap between the populations means that determining a clinically useful threshold from these data is not possible.

7.4.2 Atrial endocardial voltage thresholds

As described in the previous chapter, in current clinical practice atrial scar is most commonly identified by a bipolar voltage of ≤0.05 mV.[25] When this threshold was applied in this study (in patients with previous ablation), only 1.8% of the points were below this threshold. This further suggests that using a threshold of ≤0.05 mV to define atrial scar could significantly underestimate the extent of previous ablation injury. Whilst applying a threshold of ≤0.3 mV demonstrated a better visual correlation with CMR in some patients, this was not true for most patients (Figure 7-5). The absence of low voltage points in areas of LGE on the CMR reconstructions raises the possibility that CMR cannot distinguish between complete and incomplete scar and that the two techniques may be complementary, rather than interchangeable.

7.4.3 LGE CMR prediction of electrical reconnection and isolation

In the first of the aforementioned studies, the authors reported that "all patients with incomplete ablation sets marked by identifiable gap lesions had recovery of electrical activity on repeat electrophysiological study," suggesting that LGE CMR was able to predict electrical reconnection in all 13 patients.[82]

However, in the second study, the authors found no appreciable relationship between sites of PV reconnection and 'gaps' on the LGE CMR images. They found completely circumferential enhancement on LGE CMR in only two out of 37 PVs and PV reconnection sites were frequently seen in regions of scar.

The results of the present study agree with the latter. As low SI on LGE CMR would be the most likely sites of reconnection and low SI were seen in all lesions (whether electrically isolated or not), this would suggest that LGE CMR

cannot currently predict electrical integrity with a clinically useful sensitivity or specificity. However, this finding is unsurprising, as it is known that PV isolation can occur with an incompletely circumferential ablation lesion and, equally, electrical reconnection may be due to small strands of intact atrial myocytes, well beyond the resolution of any non-invasive imaging technique or even invasive endocardial voltage mapping.[171, 172] In this study, only six patients had previously undergone LA roof line ablation, and only four of these remained blocked. Five patients had previously undergone mitral line ablation, and only three of these remained blocked. The small sample sizes indicate that these results should be interpreted with caution.

7.4.4 Limitations

There are several reasons why a linear relationship between LGE CMR SI and endocardial voltage might not be expected. These can be divided into factors: 1) related to the LGE acquisition itself; 2) related to the recording of endocardial voltage; 3) related to the comparison of the two datasets.

1) Unlike computed tomography, with conventional LGE imaging sequences, SI is expressed on an arbitrary scale that differs from one imaging study to another and is not necessarily suitable for quantification between patients. Image contrast is generated by the difference in SI between normal and abnormal myocardium and is dependent upon surface coil proximity, sequence parameters (particularly the TI), body mass index, haematocrit, renal function, field strength and pharmacokinetic handling of the contrast agent. Furthermore, there is currently no consensus on the optimum timing of atrial LGE CMR after contrast administration, or on the choice and dose of contrast agent, which also

affect SI. As the time from contrast administration to image acquisition increases, the SI of the atrial blood pool progressively reduces, whilst that of scarred atrial myocardium increases, altering the ratio between the two intensities dramatically. In this study, these parameters were chosen based on previously published studies of atrial CMR and clinical experience.

2) Whilst invasive atrial endocardial voltage mapping is the current clinical gold standard for characterising the atrial and ventricular substrate, recordings will depend on tissue contact (contact force assessment was not available for this study), catheter tip size, atrial wall thickness and far-field electrograms. In this study, these limitations were mitigated by collecting a large number of voltage points by an experienced operator using a point-by-point technique. The accuracy of future experiments could be improved by spring-based contact assessment techniques, such as SmartTouch (Biosense Webster).

3) Point-by-point comparison of the LGE CMR SI and endocardial voltage requires the image registration of two differently-acquired LA shells, which will always include a degree of error. Iterative closest point registration was used in addition to the more simplistic landmark registration to reduce this error. Despite this, the different geometries of the CMR and endocardial voltage shells could have contributed to the weak point-by-point relationship.

7.5 Conclusions

Whilst previous studies have suggested a relationship between LGE CMR SI and atrial endocardial voltage,[82, 165, 166] this study, in the largest and most uniform cohort of patients to date, demonstrates that the point-by-point correlation between the two parameters is very weak and that low endocardial voltage can

occur at sites of low and high CMR SI. Furthermore, using an objective method of assessing gaps in ablation lesions, LGE CMR is unable to predict electrical conduction. Endocardial voltage mapping and LGE CMR should be seen as complementary techniques for defining atrial substrate prior to repeat catheter ablation. These procedures have electrical, rather than anatomical, endpoints and both techniques should be seen as useful qualitative, rather than quantitative tools in assessing patients prior to repeat catheter ablation for LA arrhythmias.

In the next chapter, the techniques used in this and the previous chapter are used to develop an integrative approach between CMR and interventional cardiac electrophysiology.

8 Real-time magnetic resonance-guided atrial electroanatomical mapping and ablation using active catheter tracking

8.1 Introduction

Over the last two decades, advances in the understanding of arrhythmia mechanism and catheter design have resulted in a high degree of success for the cure of regular narrow complex tachycardias.[173] Extension of the principles and techniques of conventional electrophysiology (EP) to more complex arrhythmias such as AF, atypical LA flutters and scar-related ventricular tachycardia have led to significant advances in the management of these problems, but with more modest clinical success.[52-55, 62] This is largely related to the technical difficulties of catheter navigation and manipulation within the heart using x-ray fluoroscopy alone, together with the electrophysiological complexity of both the arrhythmia and its anatomical substrate.

Whilst catheter navigation has been greatly facilitated by the development of non-fluoroscopic EAM systems, geometries constructed by conventional EAM suffer inherent limitations, which, if overcome, might translate into improved catheter navigation and lesion delivery. There are several advantages of MR-EP over x-ray fluoroscopy and conventional EAM systems. It provides rapid, high resolution, 3D visualisation of the true anatomy and endocardial surface of the cardiac chambers with unrivalled soft tissue contrast, the potential to visualise ablation lesions and acute complications with high spatial resolution, and raises

the possibility of eliminating patient and physician exposure to ionising radiation.

Whilst previous studies have demonstrated the feasibility of MR-EP using both passively[152, 153, 174-178] and actively[151, 178-181] tracked MR-compatible catheters, translation into human studies has been limited[152, 153, 177, 178] and none of these studies has demonstrated all of the components of an MR-EP system to rival conventional EAM and ablation. The aim of this pre-clinical study was to demonstrate the feasibility of an actively-tracked, fully MR-guided system with activation mapping before and after irrigated RF ablation, as a prelude to a planned human study.

8.2 Methods

8.2.1 MR-compatible catheter and active tracking

An irrigated 9F deflectable MR-EP mapping and ablation catheter (Vision MR, Imricor Medical Systems, Burnsville, MN) was designed for this study (Figure 8-1). The catheter was equipped with two miniature MR receive coils, which allowed detection of position and orientation of the catheter tip section, and a fibre-optic temperature sensor. Transformer cables were used for signal transmission in the catheter shaft to avoid unintentional MR-induced device heating.[182] The catheter was connected to a catheter interface module, comprising pre-amplifiers for the MR tracking signal and RF safety circuitry, which in turn was connected to a coil connector of a 1.5 Tesla MR scanner (Achieva, Philips Healthcare, Best, Netherlands).

Figure 8-1: Irrigated 9F deflectable MR-EP mapping and ablation catheter (Vision MR, Imricor Medical Systems, Burnsville, MN).

Active tracking MR sequences were used to measure one-dimensional projections of the MR signal received by the miniature receive coils.[145] Subsequent projections acquired on orthogonal axes permitted the localisation of the coils in three dimensions, which were displayed on the image guidance platform (iSuite, Philips Research, Hamburg, Germany) as catheter models superimposed on MR image data at a rate of 10 Hz.

8.2.2 MR-EP suite

The MR-EP suite integrated a standard clinical 1.5 Tesla MR scanner, a patient monitoring system suitable for MR use (Expression, Invivo, Gainsville, FL), an EP recording system specifically designed for MR use (Horizon, Imricor Medical

Systems, Burnsville, MN), a standard clinical RF generator (IBI 1500, St. Jude Medical, St. Paul, MN) and a real-time image guidance platform (iSuite, Philips Research, Hamburg, Germany) (Figure 8-2). ECG transmission was established from the patient monitoring system to both the EP recording system and the MR scanner. This allowed for patient monitoring, activation mapping, and MR-triggering using a single set of ECG electrodes.

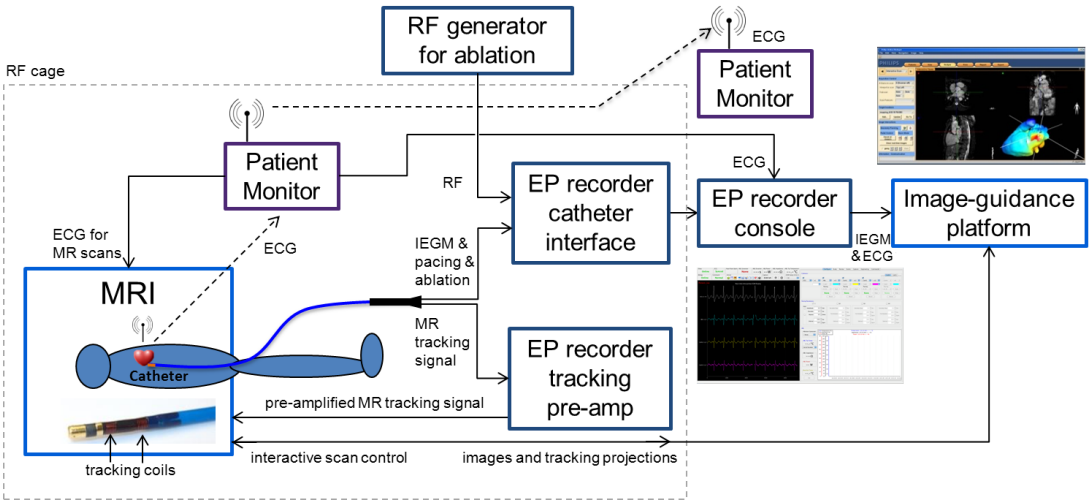

Figure 8-2: Diagram of the MR-EP suite, which comprises a standard clinical 1.5 Tesla MR scanner, a patient monitoring system suitable for MR use, an EP recording system specifically designed for MR use, a standard clinical RF generator and a real-time image guidance platform. IEGM=intracardiac electrogram.

8.2.3 iSuite image guidance platform

The iSuite image guidance platform included a computer located in the MR control room with a custom software application, a software patch for the MR scanner, and an MR-conditional foot pedal located next to the scanner. The

iSuite computer was connected to the MR scanner and the screen output of the computer was repeated on a monitor next to the scanner. A foot pedal was connected to the computer via a cable equipped with filters to remove RF noise and maintain MR image quality. All functions of the iSuite could be controlled from the computer, with simultaneous control of the imaging mode (real-time imaging or active catheter tracking) via the foot pedal. The iSuite provided visualisation of 3D datasets (by multi-planar reformatting of 2D slices in user-defined orientations or by surface models created by segmentation of anatomical structures) together with real-time MR image slices and the position of the tip section of the Imricor Vision Ablation Catheter.

8.2.4 Animal model and protocol

In five female Danish Landrace pigs, under general anaesthesia, as described in section 5.1.1 (page 77), two 9F sheaths were placed percutaneously in the right femoral vein, followed by a bolus intravenous injection of 100 IU/kg heparin.

The five pigs underwent pre-ablation T2W and 3D b-SSFP CMR as described in section 5.4 (page 83), followed by activation mapping and ablation according to the protocol described below. The animals then immediately underwent post-ablation T2W CMR and post-ablation activation mapping, before they were euthanised with an intravenous bolus of phenobarbital (80 mg/kg).

It was not possible to perform RF ablation in a sixth animal due to a technical fault with the RF generator and this animal was, therefore, excluded from the study.

8.2.5 Electroanatomical mapping and ablation

The entire procedure was performed in the MR scanner without fluoroscopy. First, active catheter tracking was used to place one Vision MR catheter in the CS and to advance a second Vision MR catheter to the RA.

The RA from the 3D b-SSFP acquisition was manually segmented using freely available 3D medical image segmentation software (itk-SNAP Version 2.2.0) and the shell imported into iSuite to act as a roadmap for mapping and ablation. As the RA catheter was moved, the actively tracked catheter position was projected on to this shell and the multi-planar reformat of the 3D b-SSFP (axial, sagittal and coronal views) was automatically updated to show the relevant views (Figure 8-3).

Activation data was acquired during CS pacing. For each sampling point, the time delay from the pacing artifact to the local RA electrogram was measured on the EP recording system and automatically transmitted to the image guidance platform to produce a colour-coded activation map on the RA shell.

Point-by-point RF ablation (35 W, 48^{o}C, 60 s per lesion, 17 ml/min irrigation) was then performed from the SVC to the IVC along the posterior wall of the RA and the location of each ablation point recorded on the RA shell. The foot pedal was used to allow rapid switching from active catheter tracking (for catheter navigation) to real-time imaging (to confirm the tracked catheter position before each RF delivery).

Following completion of the intercaval ablation lesion and post-ablation MR, the activation map was repeated according to the same protocol.

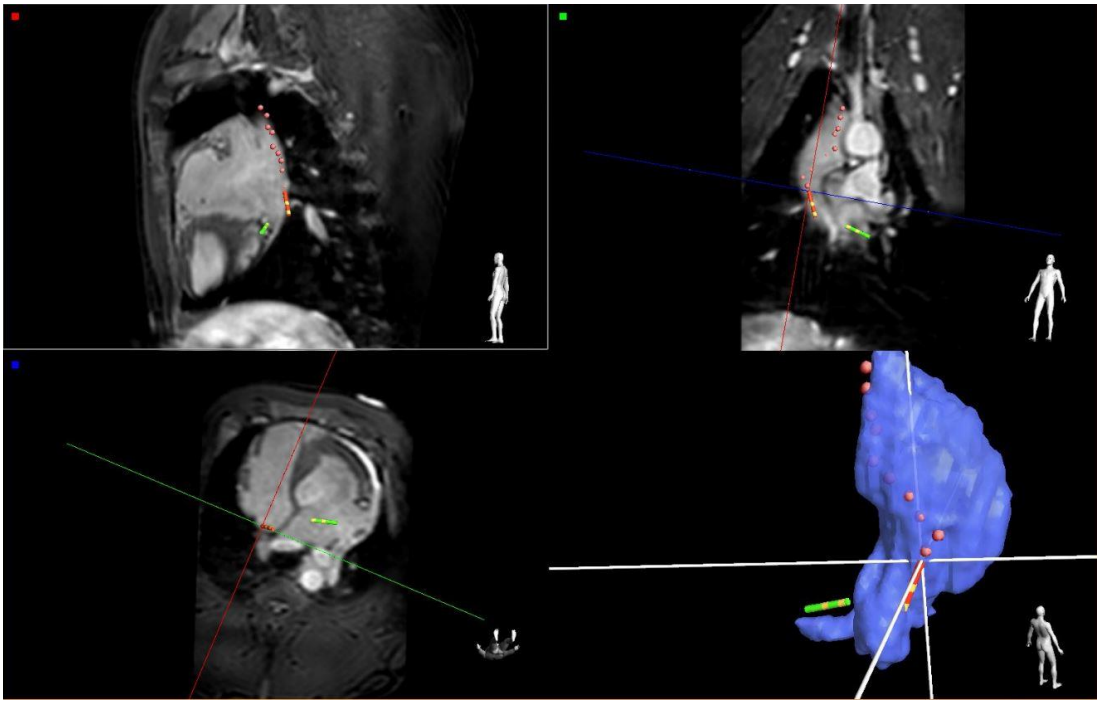

Figure 8-3: A screenshot from the iSuite image guidance platform. As the catheters (green and yellow=coronary sinus catheter; red and yellow=RA catheter) were moved, the actively tracked catheter positions were projected on to the segmented RA shell (bottom right) and the multi-planar reformat of the 3D b-SSFP was automatically updated to show the relevant views (top left – sagittal; top right – coronal; bottom left – axial). Red circles indicate the site of ablation points.

8.2.6 Macroscopic and microscopic examination

After the animals were euthanised, the hearts were explanted for macroscopic and microscopic examination as described in section 5.3 (page 79).

8.2.7 Preliminary studies and troubleshooting

Over a three year period prior to the experiments described in this chapter, a series of animal experiments (20 pigs) were performed to test and troubleshoot the individual components of the MR-EP system described in this chapter, initially using a prototype catheter. These experiments involved multiple iterations of the catheter design, iSuite image guidance platform, Horizon EP recording system and workflow efficiency. Ex-vivo safety testing of the various components were performed by the individual manufacturers and are not reported in this chapter.

8.3 Results

8.3.1 Catheter navigation and function

Using active catheter tracking, the two Vision MR catheters were easily positioned in the CS and RA in all animals, without the need for fluoroscopy (Figure 8-3). Thereafter, high-fidelity electrograms could be recorded by both catheters with minimal MR interference (Figure 8-4), and atrial capture during RA and CS pacing was seen in all animals (Figure 8-4). As the RA mapping catheter was moved around the chamber during active tracking, its position was updated on the 3D RA shell and the three-view 3D b-SSFP multi-planar reformat automatically updated according to the catheter location.

Irrigated RF ablation was successfully performed in all five animals, although two of the five SVC-IVC lines were macroscopically incomplete. The tracked catheter position was verified by real-time imaging prior to each ablation delivery (Figure 8-5).

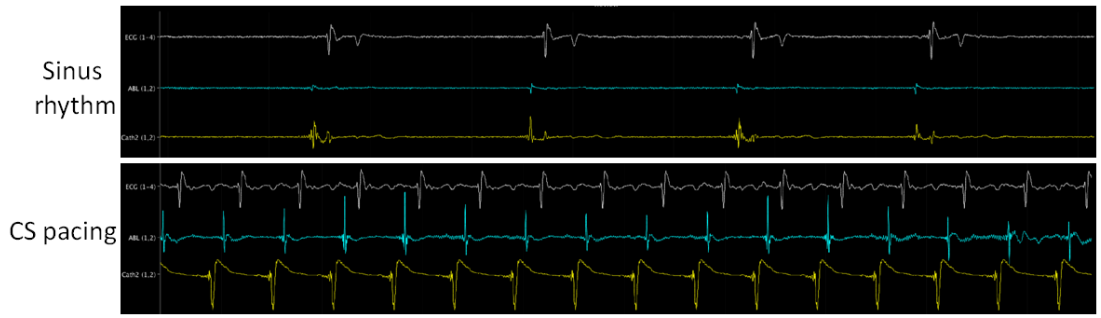

Figure 8-4: Surface ECG (white) and intracardiac electrograms from the RA (blue) and CS (yellow) catheters. The top trace is during sinus rhythm, whilst the bottom trace is during CS pacing at 100 beats per minute.

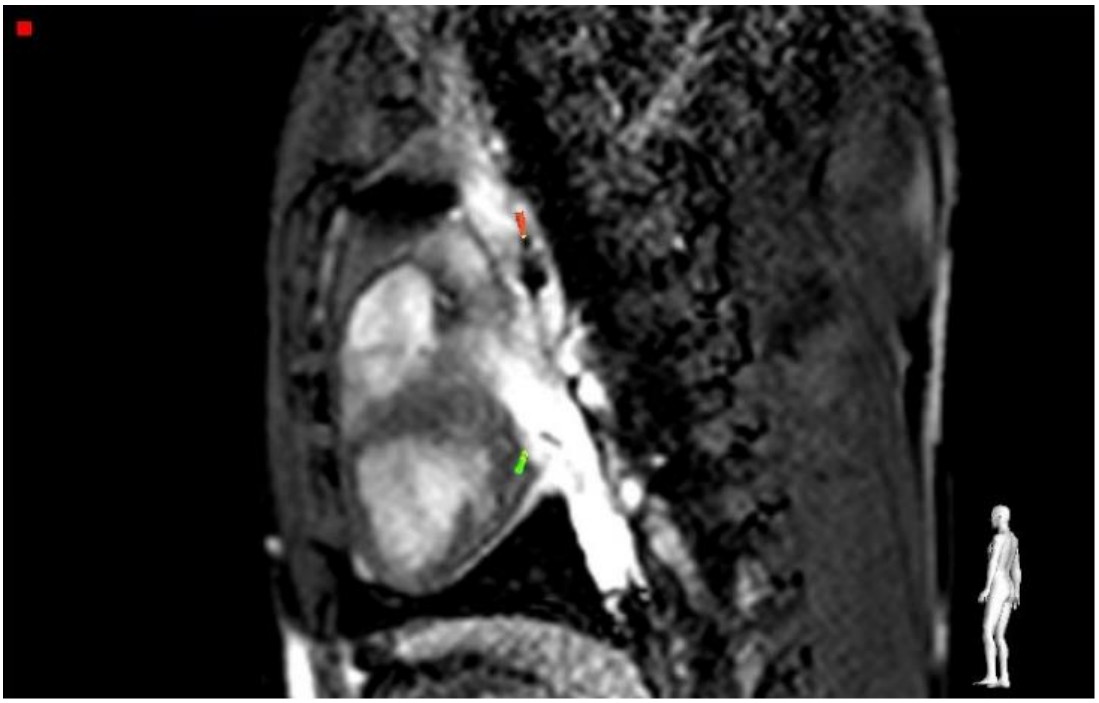

Figure 8-5: Real-time sagittal MR image confirming the red tracked catheter tip position as a signal void.

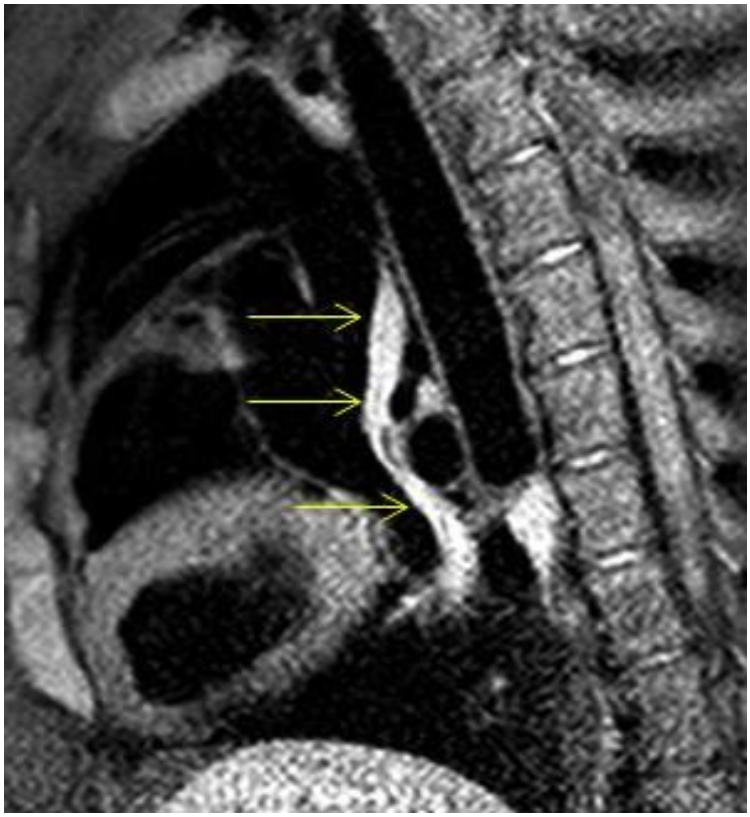

Figure 8-6: Sagittal T2W MR image following intercaval ablation demonstrating enhancement along the ablation line (arrows).

8.3.2 Pre- and post-ablation T2-weighted MR

All animals underwent pre- and post-ablation T2W MR. No appreciable pre-ablation T2W enhancement was seen in any of the animals, but was seen between the SVC and IVC in all animals post-ablation (Figure 8-6).

8.3.3 Electroanatomical mapping

The RA on the 3D b-SSFP MR acquisition was successfully segmented in all animals. This was then imported into the iSuite image guidance platform to act as the shell for EAM. Using active tracking, activation maps (mean number of points 34 ± 5; mean duration 20 ± 8 minutes) during CS pacing were created in

all animals, both before and after ablation. In one of the animals there was a change in the pattern of activation of the RA following ablation (Figure 8-7), with an activation detour around the linear ablation lesion, as seen in Chapter 6. However, in the other animals it was not possible to demonstrate an activation detour (Figure 8-8).

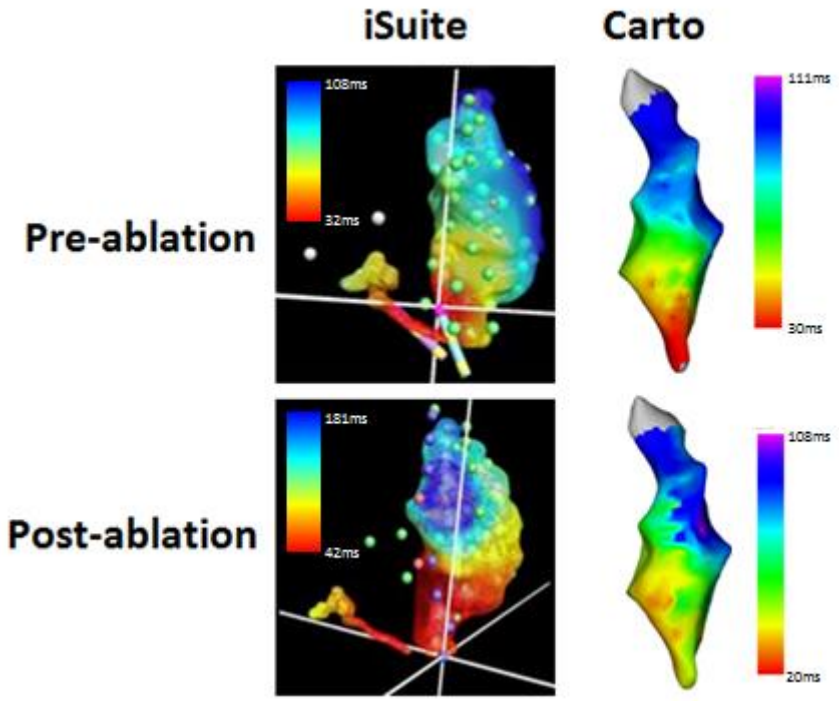

Figure 8-7: Left column – iSuite pre-ablation (top row) and post-ablation (bottom row) activation maps during coronary pacing, demonstrating an activation detour following intercaval ablation. Green points indicate mapping points; red points indicate ablation points. Right column - example Carto activation maps from Figure 6-4 are shown for comparison.

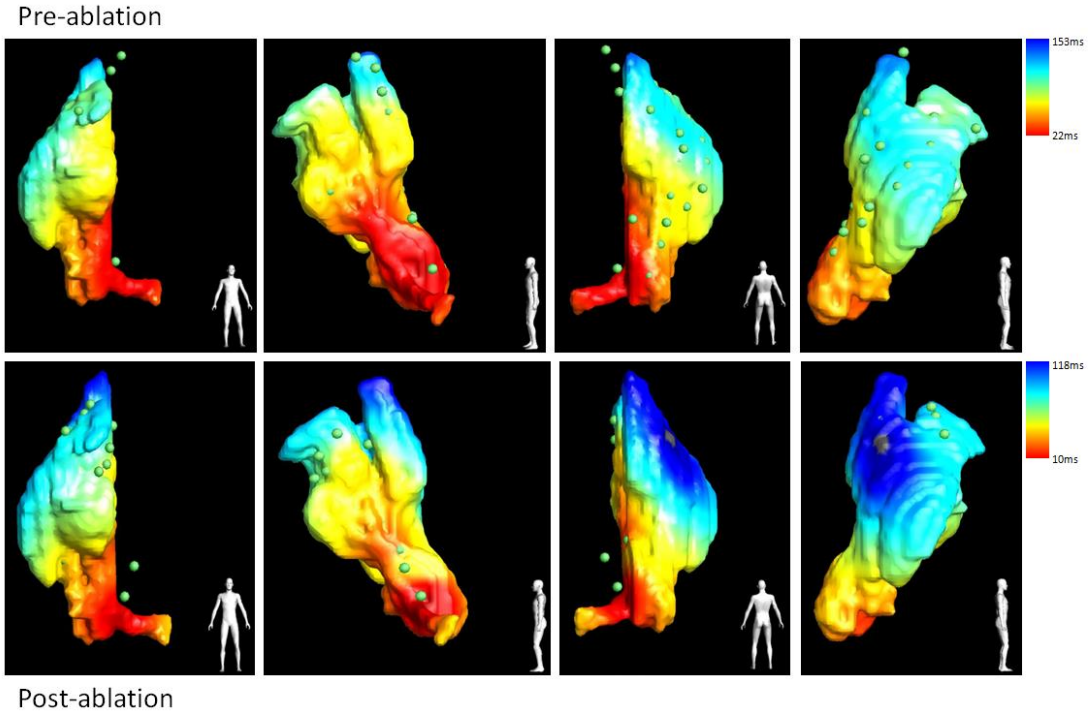

Figure 8-8: Pre-ablation (top row) and post-ablation (bottom row) activation maps of the RA during CS pacing in (from left to right) anteroposterior, left lateral, posteroanterior and right lateral views. Green points indicate mapping points.

8.3.4 Macroscopic and microscopic pathology

Macroscopic photographs of a linear ablation lesion immediately after heart explantation, together with the corresponding iSuite 3D RA shell showing the intended location of ablation, are shown in Figure 8-9. A quantitative comparison of the ablation points on iSuite with the pathological specimens was not performed. Macroscopic photographs of all five ablation lines, after fixation in formaldehyde, are shown in Figure 8-10.

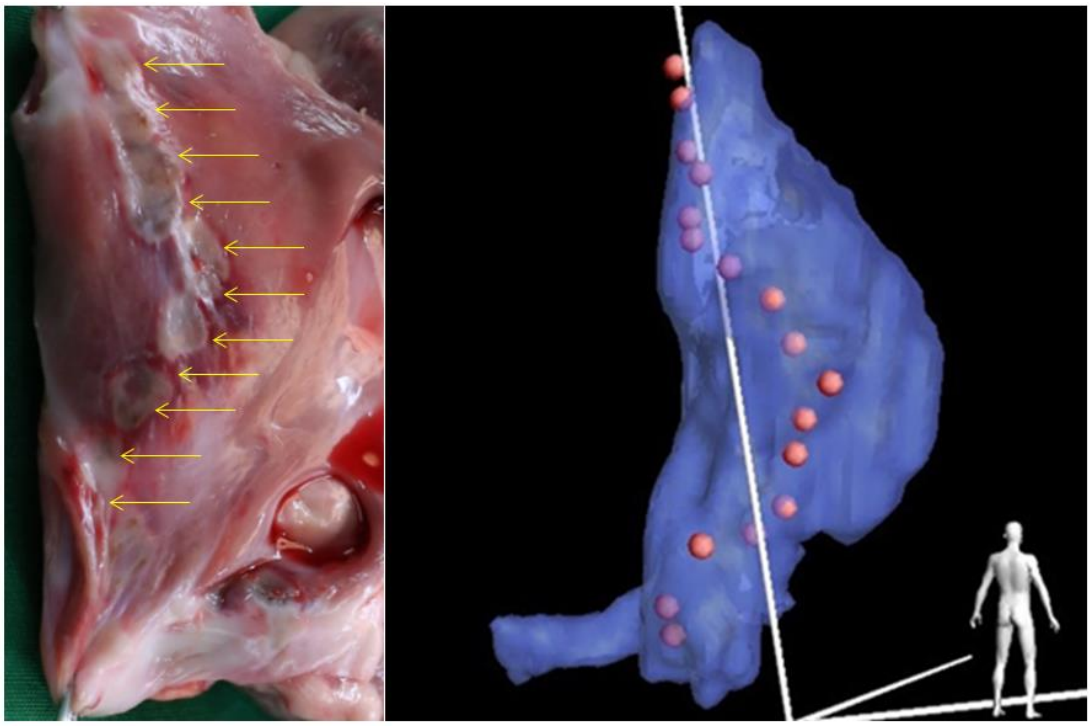

Figure 8-9: Left – macroscopic view of the opened RA, with the SVC at the top of the image and the IVC at the bottom of the image. The ablation line is seen on the posterior wall of the RA (arrows). Right – 3D anatomical shell from iSuite in a corresponding view showing the position of ablation lesions (red circles).

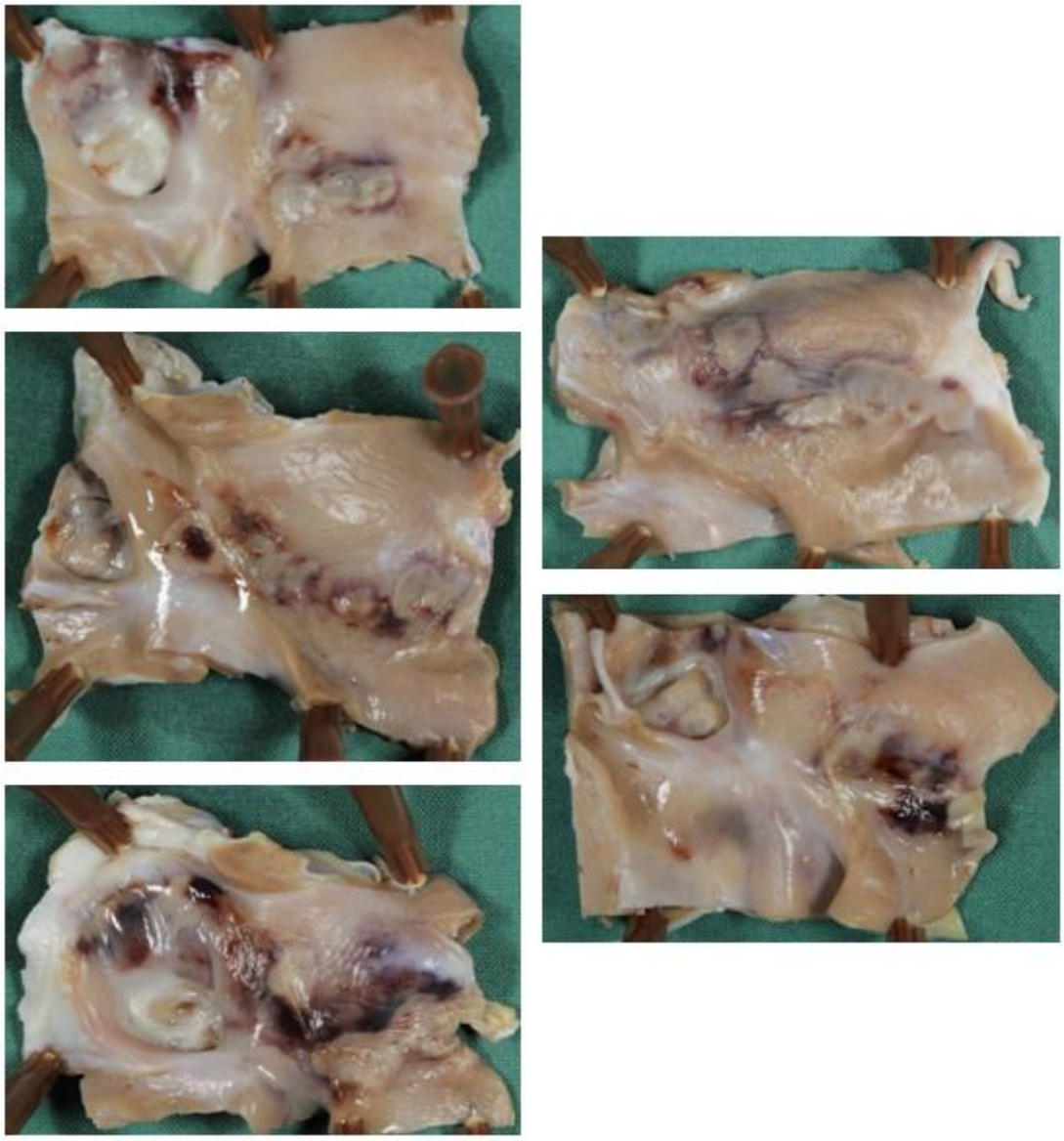

Figure 8-10: Macroscopic photographs of the ablation lines after fixation in formaldehyde.

A macroscopic cross section through the ablation line (showing the typical features of RF injury – a central zone of pallor and a surrounding hemorrhagic border zone) and microscopic sections (stained with hematoxylin and eosin) are shown in Figure 8-11. Microscopic examination demonstrated findings consistent with RF ablation: transmural coagulative necrosis, haemorrhage,

interstitial oedema, disruption of myofiber structure and increased cytoplasmic eosinophilia.

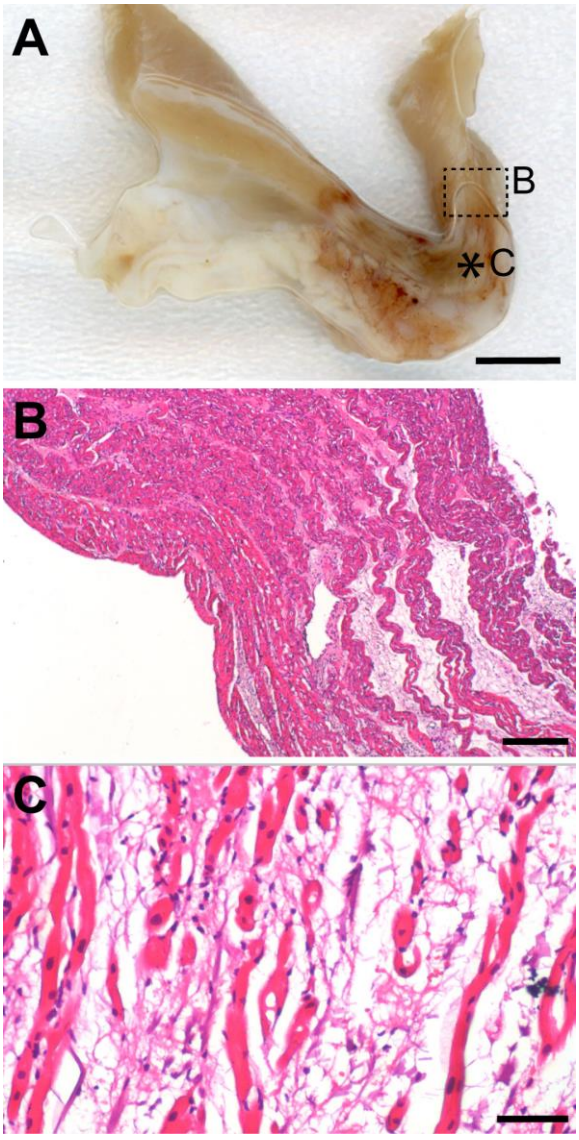

Figure 8-11: A - tissue slice cut perpendicular to the ablation line shows transmural injury. Scale bar 5 mm. B - border zone between ablated and spared atrial wall (marked with dashed box in A). Hematoxylin-eosin stain. Scale bar 250 µm. C - higher magnification of ablated tissue (marked with * in A) shows coagulative necrosis with disruption of myofiber structure, increased cytoplasmic eosinophilia and interstitial oedema. Scale bar 50 µm.

8.3.5 Safety

All five animals survived until the end of the procedure and there was no evidence of cardiac perforation, pericardial effusion or cardiac tamponade in any of the animals. Three of the animals developed AF during the procedure – this self-terminated in one animal and required intravenous flecainide (50mg) in the other two. There were no ventricular arrhythmias.

8.4 Discussion

This study was designed to show the feasibility and safety of a fully MR-guided EP system that would be suitable for use in human studies. All of the steps necessary for RA ablation were demonstrated: real-time catheter navigation, pacing, irrigated linear RF ablation and pre- and post-ablation imaging and activation mapping. However, this was a preliminary study with several limitations.

8.4.1 Technical challenges of MR-EP

Previous studies investigating the potential of MR-EP have focused on the feasibility of performing EP studies and limited RF ablation in an MR environment.[151-153, 174-181] However, the many technical challenges of performing MR-EP procedures explains why, despite the first description of MR-EP in 2000,[138] its uptake in human use has been limited to either EP studies alone (without ablation)[153] or to an isolated case report of cavotricuspid isthmus ablation.[177]

One of the principle limitations to clinical use of MR in interventional EP remains the availability of clinical-grade MR-compatible catheters. Currently

available MR-compatible catheters rely on either passive or active tracking for visualisation. Passive tracking (used in the two aforementioned human studies[153, 177]) uses magnetic susceptibility artifacts or signal voids created by the catheter tip, whilst active tracking (used in this study) requires the creation of a signal that is actively detected by a catheter tip RF coil, in order to identify its location. However, the coil needs to be connected to the scanner with a conductive wire and rapidly changing magnetic and electrical fields can result in substantial local heating, which would be unsafe for clinical use. The custom-designed transformer-based transmission lines used in the catheter in this study have been previously shown to undergo negligible RF- and pacing-induced resistive heating in safety testing.[182]

Furthermore, additional wires equipped with inductive and resonant elements allow the recording of high-fidelity intracardiac electrograms. No MR imaging was performed during recording of intracardiac electrograms in this study. However, MR-induced artefacts on electrograms can be suppressed efficiently by filtering.[178, 180] Pacing was also successfully performed via these wires with a standard clinical stimulator.

8.4.2 MR-guided electroanatomical mapping

Only two of the previous MR-EP studies (both from the same group) have demonstrated MR-guided EAM,[180, 181] which would be required if MR-EP is to replace conventional x-ray fluoroscopy and EAM-guided complex ablation. However, these studies only demonstrated voltage mapping of the LV[180] and of a limited portion of the LA.[181] This study, for the first time, demonstrated activation mapping of the entire RA using active tracking and automatic transfer

to the image guidance system to form a colour-coded shell, in a similar manner to conventional EAM systems.

Active catheter tracking allowed accurate and fast EAM, including manoeuvring the catheter to each target location and recording the intracardiac electrogram and 3D position. Approximately 30 mapping points were recorded in 20 minutes. In comparison, catheter manipulation using real-time MR imaging of a passively visualised device has been reported to require 2-5 minutes per mapping point.[174] Based on this experience, active tracking is considered to be a prerequisite for MR-guided EAM. Furthermore, active tracking allows an intuitive 3D overview of already mapped locations in relation to catheter position and cardiac anatomy, similar to conventional EAM systems.

8.4.3 Limitations

1) It was not possible to perform RF ablation in a sixth animal due to a technical fault with the RF generator and this animal was, therefore, excluded from the study.

2) It was only possible to demonstrate an activation detour following ablation in one of the animals, whereas this was seen in all animals in Chapter 6. This is likely to reflect the significantly lower point density of the iSuite activation maps (mean number of points 34 ± 5) compared with the Carto maps (mean number of points 545 ± 400), together with gaps in the SVC-IVC ablation lesions and the difficulties of demonstrating an activation change in the small tubular porcine RA.

3) A quantitative comparison of the location of ablation points on iSuite with the pathological specimens was not performed. This was due to the deformation

of the RA during pathological examination and the variation in the macroscopic features of the ablation lesions.

4) The aim of this study was to assess the feasibility of MR-guided ablation and EAM, and whilst T2W images were acquired before and after ablation, lesion assessment by MR was not the focus of this study. With the present MR-EP system, it was possible to visualise lesion formation immediately after, but not during, lesion formation. This contrasts with other emerging RF-catheter technologies such as optical coherence tomography[183] and ultrasound,[184] which have the ability to visualise lesion formation in real-time.

8.5 Conclusions

MR-guided EAM and ablation using active catheter tracking is safe and feasible in an animal model and the MR-EP setup provides an efficient workflow. Catheters show good localisation accuracy and intra-cardiac signal quality in vivo and allow for pacing and ablation using standard RF equipment. Combined with intraprocedural lesion imaging, MR-EP has the potential to significantly improve the way current ablation procedures are performed.

9 Conclusion

The overall aim of this thesis was to validate CMR of the atrial wall and to demonstrate its utility in MR-EP, using both pre-clinical animal and clinical human studies. There were three main objectives:

1) To provide a histological validation of CMR and EAM of acute and chronic ablation injury in an animal model of atrial ablation.

2) To compare atrial CMR findings with endocardial voltage mapping in patients undergoing repeat catheter ablation for LA arrhythmias and assess the ability of atrial CMR to predict gaps in ablation lesions.

3) To demonstrate the feasibility of an actively-tracked, fully MR-guided system with activation mapping before and after irrigated RF ablation, as a prelude to a future human study.

9.1 Original contributions

1) Whilst LGE CMR of acute and chronic ventricular myocardial injury has been validated pathologically, this has never been demonstrated in the atrium. This is despite several recent studies suggesting a role for atrial LGE CMR in assessing patient suitability and response to catheter ablation of AF.[51, 77-80, 82-85, 87] Chapter 6 presents the first histopathological validation of CMR to define acute and chronic atrial ablation injury, including CMR SI thresholds that best match histological lesion volumes. However, the wide range of individual SI thresholds across the animals suggests that these values should be applied with caution.

2) Invasive atrial endocardial voltage mapping, the current clinical gold standard for characterising the atrial substrate, has not been pathologically validated or systematically compared with CMR findings. Voltage thresholds in common clinical use have been extrapolated from ventricular studies comparing EAM with post-myocardial infarction scar[155, 156] and not ablation-induced injury. Chapter 7 presents endocardial voltage thresholds to define acute and chronic atrial ablation injury, which challenge values currently used in clinical practice.

3) Previous small studies have suggested a qualitative[82] and quantitative[165, 166] relationship between areas of LGE and areas of low endocardial voltage in patients undergoing repeat catheter ablation. However, there is controversy regarding the reproducibility and diagnostic ability of atrial LGE CMR.[167] Chapter 7 demonstrates in the largest and most uniform cohort of patients to date that the point-by-point correlation between the two parameters is very weak, and that low endocardial voltage can occur at sites of low and high LGE CMR SI. Whilst it is certainly possible to demonstrate areas of high LGE CMR SI in the same location as areas of low endocardial voltage (and vice versa), the sensitivity and specificity are poor.

4) There is also conflicting evidence regarding the ability of LGE CMR to predict the electrical integrity of chronic ablation lesions. One study demonstrated that LGE CMR was able to predict electrical reconnection by identifying gaps in ablation lesions,[82] whilst in another the opposite was found.[165] However, these studies used subjective thresholding to distinguish between normal and abnormal atrial tissue, and, therefore, the presence or absence of gaps. A lower

threshold would have resulted in more 'scar', whereas a higher threshold would have resulted in more 'gaps'. Using an objective method of assessing gaps in ablation lesions, Chapter 7 shows that LGE CMR is unable to reliably predict electrical conduction.

5) Whilst previous studies have demonstrated the feasibility of MR-EP using both passively[152, 153, 174-178] and actively[151, 178-181] tracked MR-compatible catheters, translation into human studies has been limited[152, 153, 177, 178] and none of these studies has demonstrated all of the components of an MR-EP system to rival conventional EAM and ablation. Chapter 8 demonstrates the feasibility of performing all of the steps necessary for RA ablation using an actively-tracked fully MR-guided system with activation mapping before and after irrigated RF ablation.

9.2 Implications and limitations

Despite the promise of early studies on atrial CMR, its clinical use has remained limited, primarily due to technical difficulties in image acquisition and consequent concerns regarding interpretation and reproducibility of the findings. Chapter 6 demonstrates that high LGE CMR SI does represent fibrous scar in the atrium eight weeks after ablation, suggesting that the technique can be used to define chronic atrial scar, at least qualitatively. Application of the LGE CMR SI thresholds presented in this chapter might allow a quantitative non-invasive assessment of the underlying atrial substrate before repeat catheter ablation for atrial arrhythmias. However, the wide range of individual SI thresholds across the animals suggests that these values should be applied

cautiously and that larger numbers would be needed to define these more accurately.

The results in Chapter 7 suggest that these findings may not readily translate to human LA ablation. This is likely to reflect the difficulties of imaging anatomically complex LA ablation (involving circumferential, linear and point ablation), compared with the single linear lesion performed in the RA animal model, or may suggest that low voltages occur at sites that do not enhance with LGE CMR and vice versa.

These findings have to be borne in mind when considering the potential of MR-EP. Whilst Chapter 8 demonstrates that MR-guided ablation and EAM is safe and feasible in an animal model, a more accurate quantitative assessment of atrial wall injury (particularly lesion transmurality) is necessary if MR-guided ablation is to achieve its principle advantage over conventional x-ray fluoroscopy.

9.3 Future directions

The findings and techniques developed in this thesis will be used for a human study of catheter ablation of typical right atrial flutter under MR guidance, performed in a hybrid XMR facility. This study will assess the safety and efficacy of using the MR-EP system described in Chapter 8. Fifteen patients undergoing first-time clinically-indicated ablation for typical atrial flutter will be recruited to the study.

Under general anaesthetic, the patient will be connected to the MR-EP system as described in Chapter 8 and two 9F sheaths will be inserted into the right

femoral vein. Pre-ablation b-SSFP CMR will then be performed. Active catheter tracking will be used to place one Vision MR catheter in the CS and to advance a second Vision MR catheter to the RA. The RA from the b-SSFP acquisition will be manually segmented and the shell imported into iSuite to act as a roadmap for mapping and ablation. An activation map of the RA during CS pacing will be created using the RA catheter.

The RA catheter will then be positioned at the ventricular end of the cavotricuspid isthmus and RF ablation will be performed point-by-point along the isthmus. Active catheter tracking will be used to position the catheter, with real-time imaging used for confirmation before each RF delivery. The procedural endpoint will be the demonstration of bidirectional conduction block across the cavotricuspid isthmus.

A post-ablation activation map of the RA will then be created during CS pacing. Post-ablation T2W and LGE CMR will then be performed, before the sheaths are removed and the patient recovered from general anaesthesia. Patients will be followed-up after three months with a repeat CMR study, a 24-hour ECG recording and a clinical review.

However, the real potential of MR-EP is in the treatment of more complex arrhythmias such as AF, atypical LA flutters and scar-related ventricular tachycardia. In order to realise this potential, several future developments and studies will be required. First, and foremost, the acute CMR findings that predict long-term, durable ablation lesions need to be defined. Whilst previous studies have investigated atrial CMR within one hour[157] and 24 hours[51] of AF ablation, these predictive findings need to be assessed during the procedure, so that

further ablation lesions can be applied as necessary. This would best be demonstrated through further longitudinal animal studies. Sequence development, target-specific contrast agents and improvements in CMR resolution are likely over the next few years and may help to make MR-EP a mainstream clinical technique.

Acknowledgements

During this PhD, I have been extremely fortunate to work alongside many talented individuals across a wide range of disciplines. First and foremost, I would like to thank my supervisors, Dr Mark O'Neill and Professor Reza Razavi for their guidance, encouragement, patience and wisdom. The transition from clinical medicine to the open-ended task of a research degree is difficult, and I owe them both a debt of gratitude for their support.

This work would not have been possible without a Clinical Research Training Fellowship from the British Heart Foundation and the skilled assistance of my colleagues at King's College London: Dr Nick Linton, Dr Steven Williams, Dr Christian Sohns, Stephen Sinclair, Annette Dahl, Dr Matthew Wright, Dr Michael Cooklin, Dr Aldo Rinaldi, Dr Kawal Rhode, Dr Rashed Karim, Dr Amedeo Chiribiri, Professor Jaswinder Gill, Dr Sarah Peel, Dr Christoph Kolbitsch and Professor Tobias Schaeffter.

The animal work in this thesis was performed at Aarhus University Hospital Skejby, and I am extremely grateful for expert help from Anne Krogh Grøndal, Lars Ølgaard Bloch, Niels Peter Andersen, Høgni Dam, Dr Steen Fjord Pedersen, Professor Won Yong Kim, Bjarne Larsen and Dr Henrik Kjærulf Jensen.

Last, and by no means least, I would like to thank my wife, Hannah, for steering me through the difficult times, and whose threats of divorce kept this thesis on track.

Awards, publications and presentations

Awards

Early Career Award (Translational), Society for Cardiovascular Magnetic Resonance, San Francisco, 2013

Best Poster Presentation, European Cardiac Arrhythmia Society, Paris, 2013

Young Investigator Award (Basic Science), Heart Rhythm Congress, Birmingham, 2012

Publications

Harrison JL, Jensen HK, Peel SA, Chiribiri A, Grondal AK, Bloch LO, Pedersen SF, Bentzon JF, Kolbitsch C, Karim R, Williams SE, Linton NW, Rhode KS, Gill J, Cooklin M, Rinaldi CA, Wright M, Kim WY, Schaeffter T, Razavi RS, O'Neill MD. Cardiac magnetic resonance and electroanatomical mapping of acute and chronic atrial ablation injury: a histological validation study. European Heart Journal, 2014.

Oral presentations

Role of MRI and electroanatomic mapping in the evaluation of AF substrate. Invited talk at European Cardiac Arrhythmia Society, Paris, 2013.

Harrison J, Linton N, Peel S, Chiribiri A, Grøndal A, Bloch L, Karim R, Williams S, Rhode K, Fjord S, Wright M, Kim W, Bentzon J, Jensen H, Schaeffter, Razavi R, O'Neill M. Magnetic Resonance Imaging of acute and chronic atrial ablation injury – a histological validation study. Society for Cardiovascular Magnetic Resonance, San Francisco, 2013.

Harrison J, Bloch L, Grøndal A, Bentzon J, Linton N, Chiribiri A, Kolbitsch C, Peel S, Fjord S, Williams S, Karim R, Gill J, Cooklin M, Rinaldi A, Rhode K, Wright M, Kim W, Jensen H, Schaeffter, Razavi R, O'Neill M. Magnetic Resonance Imaging of acute atrial ablation injury – a histological validation study. Heart Rhythm Congress, Birmingham, 2012.

Harrison J, Linton N, Williams S, Karim R, Gill J, Cooklin M, Rinaldi A, Rhode K, Wright M, Schaeffter T, Razavi R, O'Neill M. Late gadolinium enhancement Magnetic Resonance Imaging prediction of gaps in atrial ablation lesions. Heart Rhythm Congress, Birmingham, 2012.

Harrison J, Linton N, Grøndal A, Bloch L, Fjord S, Bentzon J, Chiribiri A, Kolbitsch C, Karim R, Williams S, Nagahara D, Rhode K, Kim W, Jensen H, Gill J, Cooklin M,

Rinaldi A, Wright M, Schaeffter T, Razavi R, O'Neill M. Acute atrial ablation injury is better visualised by late gadolinium enhancement than T2-weighted Magnetic Resonance Imaging. Cardiostim, Nice, 2012.

Harrison J, Linton N, Karim R, Williams S, Nagahara D, Gill J, Cooklin M, Rinaldi A, Wright M, Rhode K, Schaeffter T, Razavi R, O'Neill M. Late gadolinium enhancement Magnetic Resonance Imaging prediction of gaps in atrial ablation lesions. Cardiostim, Nice, 2012.

Pre-ablation MRI: tool or toy? Invited talk at European Cardiac Arrhythmia Society, Munich, 2012.

Karim R, Gao G, Harrison J, Arujuna A, Wright M, Linton N, Cooklin M, Leo G, Lambert H, Schaeffter T, O'Neill M, Rhode K. Magnetic Resonance Imaging analysis of tissue-contact force following catheter ablation for paroxysmal atrial fibrillation. Heart Rhythm Society, San Francisco, 2011.

Poster presentations

Harrison J, Linton N, Peel S, Chiribiri A, Grøndal A, Bloch L, Pedersen S, Bentzon J, Kolbitsch C, Karim R, Williams S, Rhode K, Gill J, Cooklin M, Rinaldi A, Wright M, Kim W, Jensen H, Schaeffter T, Razavi R, O'Neill M. Magnetic resonance

imaging of acute and chronic atrial ablation injury – a histological and electroanatomical validation study. Heart Rhythm Society, Denver, 2013.

Harrison J, Sohns C, Linton N, Karim R, Williams S, Rhode K, Gill J, Cooklin M, Rinaldi A, Wright M, Schaeffter T, Razavi R, O'Neill M. Prediction of left atrial endocardial voltage using late gadolinium enhancement Cardiac Magnetic Resonance (LGE CMR). Heart Rhythm Society, Denver, 2013.

Harrison J, Sohns C, Linton N, Karim R, Williams S, Rhode K, Gill J, Cooklin M, Rinaldi A, Wright M, Schaeffter T, Razavi R, O'Neill M. Predicting gaps in atrial ablation lesions using late gadolinium enhancement Cardiac Magnetic Resonance (LGE CMR). Heart Rhythm Society, Denver, 2013.

Harrison J, Weiss S, Krueger S, Koken P, O'Neill M, Schaeffter T, Razavi R. Real-time MR-guided Radiofrequency Atrial Ablation: Visualization of lesion formation and activation mapping. Heart Rhythm Society, Denver, 2013.

Harrison J, Linton N, Peel S, Chiribiri A, Grøndal A, Bloch L, Pedersen S, Bentzon J, Kolbitsch C, Karim R, Williams S, Rhode K, Gill J, Cooklin M, Rinaldi A, Wright M, Kim W, Jensen H, Schaeffter T, Razavi R, O'Neill M. Magnetic resonance imaging of acute and chronic atrial ablation injury – a histological and electroanatomical validation study. European Cardiac Arrhythmia Society, Paris, 2013.

Harrison J, Linton N, Williams S, Karim R, Rhode K, Wright M, Schaeffter T, Razavi R, O'Neill M. Prediction of gaps in atrial ablation lesion sets by late gadolinium enhancement Magnetic Resonance Imaging. Society for Cardiovascular Magnetic Resonance, San Francisco, 2013.

Harrison J, Linton N, Williams S, Karim R, Rhode K, Wright M, Schaeffter T, Razavi R, O'Neill M. A comparison of late gadolinium enhancement Magnetic Resonance Imaging and left atrial endocardial voltage. Society for Cardiovascular Magnetic Resonance, San Francisco, 2013.

Harrison J, Linton N, Peel S, Chiribiri A, Grøndal A, Bloch L, Pedersen S, Bentzon J, Kolbitsch C, Karim R, Williams S, Rhode K, Gill J, Cooklin M, Rinaldi A, Wright M, Kim W, Jensen H, Schaeffter, Razavi R, O'Neill M. Magnetic resonance imaging of acute and chronic atrial ablation injury – a histological and electroanatomical validation study. Boston AF Symposium, Boston, 2013.

Harrison J, Linton N, Williams S, Karim R, Gill J, Cooklin M, Rinaldi A, Rhode K, Wright M, Schaeffter T, Razavi R, O'Neill M. A systematic comparison of left atrial endocardial voltage and late gadolinium enhancement Magnetic Resonance Imaging (LGE MRI). Heart Rhythm Congress, Birmingham, 2012.

Harrison J, Linton N, Karim R, Williams S, Nagahara D, Gill J, Cooklin M, Rinaldi A, Wright M, Rhode K, Schaeffter T, Razavi R, O'Neill M. A systematic

comparison of left atrial endocardial voltage and late gadolinium enhancement Magnetic Resonance Imaging (LGE MRI). Cardiostim, Nice, 2012.

Harrison J, Linton N, Grøndal A, Bloch L, Fjord S, Bentzon J, Chiribiri A, Kolbitsch C, Karim R, Williams S, Nagahara D, Rhode K, Kim W, Jensen H, Gill J, Cooklin M, Rinaldi A, Wright M, Schaeffter T, Razavi R, O'Neill M. Acute atrial ablation injury is better visualised by late gadolinium enhancement than T2-weighted Magnetic Resonance Imaging. Heart Rhythm Society, Boston, 2012.

Harrison J, Linton N, Karim R, Williams S, Nagahara D, Gill J, Cooklin M, Rinaldi A, Wright M, Rhode K, Schaeffter T, Razavi R, O'Neill M. A systematic comparison of left atrial endocardial voltage and late gadolinium enhancement Magnetic Resonance Imaging (LGE MRI). Heart Rhythm Society, Boston, 2012.

Harrison J, Linton N, Karim R, Williams S, Nagahara D, Gill J, Cooklin M, Rinaldi A, Wright M, Rhode K, Schaeffter T, Razavi R, O'Neill M. Late gadolinium enhancement Magnetic Resonance Imaging prediction of gaps in atrial ablation lesions. Heart Rhythm Society, Boston, 2012.

Harrison J, Weiss S, Krueger S, Lips O, David B, Wirtz D, Koken P, Holthuizen R, Smink J, Gill J, O'Neill M, Schaeffter T, Razavi R. Preclinical evaluation of a Magnetic Resonance-EP (MR-EP) suite including dedicated MR-EP catheters. Heart Rhythm Society, San Francisco, 2011.

References

1. Schamroth L. *The disorders of cardiac rhythm*. Oxford,: Blackwell Scientific; 1971.

2. Saoudi N, Cosio F, Waldo A, Chen SA, Iesaka Y, Lesh M, Saksena S, Salerno J, Schoels W. A classification of atrial flutter and regular atrial tachycardia according to electrophysiological mechanisms and anatomical bases; a statement from a joint expert group from the working group of arrhythmias of the european society of cardiology and the north american society of pacing and electrophysiology. *European heart journal*. 2001;22:1162-1182

3. Jais P, Matsuo S, Knecht S, Weerasooriya R, Hocini M, Sacher F, Wright M, Nault I, Lellouche N, Klein G, Clementy J, Haissaguerre M. A deductive mapping strategy for atrial tachycardia following atrial fibrillation ablation: Importance of localized reentry. *Journal of cardiovascular electrophysiology*. 2009;20:480-491

4. Porter MJ, Morton JB, Denman R, Lin AC, Tierney S, Santucci PA, Cai JJ, Madsen N, Wilber DJ. Influence of age and gender on the mechanism of supraventricular tachycardia. *Heart rhythm : the official journal of the Heart Rhythm Society*. 2004;1:393-396

5. Rosso R, Kistler PM. Focal atrial tachycardia. *Heart*. 2010;96:181-185

6. McGuire MA, Johnson DC, Nunn GR, Yung T, Uther JB, Ross DL. Surgical therapy for atrial tachycardia in adults. *Journal of the American College of Cardiology*. 1989;14:1777-1782

7. Tang CW, Scheinman MM, Van Hare GF, Epstein LM, Fitzpatrick AP, Lee RJ, Lesh MD. Use of p wave configuration during atrial tachycardia to predict site of origin. *Journal of the American College of Cardiology*. 1995;26:1315-1324

8. Kistler PM, Roberts-Thomson KC, Haqqani HM, Fynn SP, Singarayar S, Vohra JK, Morton JB, Sparks PB, Kalman JM. P-wave morphology in focal atrial tachycardia: Development of an algorithm to predict the anatomic site of origin. *Journal of the American College of Cardiology*. 2006;48:1010-1017

9. Blomstrom-Lundqvist C, Scheinman MM, Aliot EM, Alpert JS, Calkins H, Camm AJ, Campbell WB, Haines DE, Kuck KH, Lerman BB, Miller DD, Shaeffer CW, Stevenson WG, Tomaselli GF, Antman EM, Smith SC, Jr., Alpert JS, Faxon DP, Fuster V, Gibbons RJ, Gregoratos G, Hiratzka LF, Hunt SA, Jacobs AK, Russell RO, Jr., Priori SG, Blanc JJ, Budaj A, Burgos EF, Cowie M, Deckers JW, Garcia MA, Klein WW, Lekakis J, Lindahl B, Mazzotta G, Morais JC, Oto A, Smiseth O, Trappe HJ, European Society of Cardiology Committee N-HRS. Acc/aha/esc guidelines for the management of patients with supraventricular arrhythmias--executive summary. A report of the american college of cardiology/american heart association task force on practice guidelines and the european society of cardiology committee for practice guidelines (writing committee to develop guidelines for the management of patients with supraventricular arrhythmias) developed in collaboration with naspe-

heart rhythm society. *Journal of the American College of Cardiology*. 2003;42:1493-1531

10. Poty H, Saoudi N, Haissaguerre M, Daou A, Clementy J, Letac B. Radiofrequency catheter ablation of atrial tachycardias. *American heart journal*. 1996;131:481-489

11. Kalman JM, Olgin JE, Karch MR, Hamdan M, Lee RJ, Lesh MD. "Cristal tachycardias": Origin of right atrial tachycardias from the crista terminalis identified by intracardiac echocardiography. *Journal of the American College of Cardiology*. 1998;31:451-459

12. Medi C, Kalman JM, Haqqani H, Vohra JK, Morton JB, Sparks PB, Kistler PM. Tachycardia-mediated cardiomyopathy secondary to focal atrial tachycardia: Long-term outcome after catheter ablation. *Journal of the American College of Cardiology*. 2009;53:1791-1797

13. Cosio FG, Lopez-Gil M, Goicolea A, Arribas F, Barroso JL. Radiofrequency ablation of the inferior vena cava-tricuspid valve isthmus in common atrial flutter. *The American journal of cardiology*. 1993;71:705-709

14. Shah DC, Jais P, Haissaguerre M, Chouairi S, Takahashi A, Hocini M, Garrigue S, Clementy J. Three-dimensional mapping of the common atrial flutter circuit in the right atrium. *Circulation*. 1997;96:3904-3912

15. Kalman JM, Olgin JE, Saxon LA, Lee RJ, Scheinman MM, Lesh MD. Electrocardiographic and electrophysiologic characterization of atypical atrial flutter in man: Use of activation and entrainment mapping and implications for catheter ablation. *Journal of cardiovascular electrophysiology*. 1997;8:121-144

16. Brembilla-Perrot B, Huttin O, Manenti V, Benichou M, Sellal JM, Zinzius PY, Beurrier D, Schwartz J, Laporte F, de Chillou C, Andronache M, Cismaru G, Pauriah M, Selton O, Louis P, Terrier de la Chaise A. Sex-related differences in peri- and post-ablation clinical data for patients with atrial flutter. *International journal of cardiology*. 2013

17. Moubarak G, Pavin D, Laviolle B, Solnon A, Kervio G, Daubert JC, Mabo P. Incidence of atrial fibrillation during very long-term follow-up after radiofrequency ablation of typical atrial flutter. *Archives of cardiovascular diseases*. 2009;102:525-532

18. European Heart Rhythm A, European Association for Cardio-Thoracic S, Camm AJ, Kirchhof P, Lip GY, Schotten U, Savelieva I, Ernst S, Van Gelder IC, Al-Attar N, Hindricks G, Prendergast B, Heidbuchel H, Alfieri O, Angelini A, Atar D, Colonna P, De Caterina R, De Sutter J, Goette A, Gorenek B, Heldal M, Hohloser SH, Kolh P, Le Heuzey JY, Ponikowski P, Rutten FH. Guidelines for the management of atrial fibrillation: The task force for the management of atrial fibrillation of the european society of cardiology (esc). *European heart journal*. 2010;31:2369-2429

19. Feld GK, Fleck RP, Chen PS, Boyce K, Bahnson TD, Stein JB, Calisi CM, Ibarra M. Radiofrequency catheter ablation for the treatment of human type 1 atrial flutter. Identification of a critical zone in the reentrant circuit by endocardial mapping techniques. *Circulation*. 1992;86:1233-1240

20. Natale A, Newby KH, Pisano E, Leonelli F, Fanelli R, Potenza D, Beheiry S, Tomassoni G. Prospective randomized comparison of antiarrhythmic

therapy versus first-line radiofrequency ablation in patients with atrial flutter. *Journal of the American College of Cardiology*. 2000;35:1898-1904

21. Morady F. Catheter ablation of supraventricular arrhythmias: State of the art. *Journal of cardiovascular electrophysiology*. 2004;15:124-139

22. Tada H, Oral H, Sticherling C, Chough SP, Baker RL, Wasmer K, Pelosi F, Jr., Knight BP, Strickberger SA, Morady F. Double potentials along the ablation line as a guide to radiofrequency ablation of typical atrial flutter. *Journal of the American College of Cardiology*. 2001;38:750-755

23. Spector P, Reynolds MR, Calkins H, Sondhi M, Xu Y, Martin A, Williams CJ, Sledge I. Meta-analysis of ablation of atrial flutter and supraventricular tachycardia. *The American journal of cardiology*. 2009;104:671-677

24. Stevenson IH, Kistler PM, Spence SJ, Vohra JK, Sparks PB, Morton JB, Kalman JM. Scar-related right atrial macroreentrant tachycardia in patients without prior atrial surgery: Electroanatomic characterization and ablation outcome. *Heart rhythm : the official journal of the Heart Rhythm Society*. 2005;2:594-601

25. Jais P, Shah DC, Haissaguerre M, Hocini M, Peng JT, Takahashi A, Garrigue S, Le Metayer P, Clementy J. Mapping and ablation of left atrial flutters. *Circulation*. 2000;101:2928-2934

26. Heck PM, Rosso R, Kistler PM. The challenging face of focal atrial tachycardia in the post af ablation era. *Journal of cardiovascular electrophysiology*. 2011;22:832-838

27. Knecht S, Veenhuyzen G, O'Neill MD, Wright M, Nault I, Weerasooriya R, Miyazaki S, Sacher F, Hocini M, Jais P, Haissaguerre M. Atrial tachycardias encountered in the context of catheter ablation for atrial fibrillation part ii: Mapping and ablation. *Pacing and clinical electrophysiology : PACE*. 2009;32:528-538

28. Haissaguerre M, Hocini M, Sanders P, Takahashi Y, Rotter M, Sacher F, Rostock T, Hsu LF, Jonsson A, O'Neill MD, Bordachar P, Reuter S, Roudaut R, Clementy J, Jais P. Localized sources maintaining atrial fibrillation organized by prior ablation. *Circulation*. 2006;113:616-625

29. Fuster V, Ryden LE, Cannom DS, Crijns HJ, Curtis AB, Ellenbogen KA, Halperin JL, Kay GN, Le Huezey JY, Lowe JE, Olsson SB, Prystowsky EN, Tamargo JL, Wann LS, Smith SC, Jr., Priori SG, Estes NA, 3rd, Ezekowitz MD, Jackman WM, January CT, Page RL, Slotwiner DJ, Stevenson WG, Tracy CM, Jacobs AK, Anderson JL, Albert N, Buller CE, Creager MA, Ettinger SM, Guyton RA, Hochman JS, Kushner FG, Ohman EM, Tarkington LG, Yancy CW. 2011 accf/aha/hrs focused updates incorporated into the acc/aha/esc 2006 guidelines for the management of patients with atrial fibrillation: A report of the american college of cardiology foundation/american heart association task force on practice guidelines. *Circulation*. 2011;123:e269-367

30. Feinberg WM, Blackshear JL, Laupacis A, Kronmal R, Hart RG. Prevalence, age distribution, and gender of patients with atrial fibrillation. Analysis and implications. *Arch Intern Med*. 1995;155:469-473

31. Ruigomez A, Johansson S, Wallander MA, Rodriguez LA. Incidence of chronic atrial fibrillation in general practice and its treatment pattern. *J Clin Epidemiol*. 2002;55:358-363

32. Wang TJ, Massaro JM, Levy D, Vasan RS, Wolf PA, D'Agostino RB, Larson MG, Kannel WB, Benjamin EJ. A risk score for predicting stroke or death in individuals with new-onset atrial fibrillation in the community: The framingham heart study. *JAMA*. 2003;290:1049-1056

33. Corley SD, Epstein AE, DiMarco JP, Domanski MJ, Geller N, Greene HL, Josephson RA, Kellen JC, Klein RC, Krahn AD, Mickel M, Mitchell LB, Nelson JD, Rosenberg Y, Schron E, Shemanski L, Waldo AL, Wyse DG. Relationships between sinus rhythm, treatment, and survival in the atrial fibrillation follow-up investigation of rhythm management (affirm) study. *Circulation*. 2004;109:1509-1513

34. Wijffels MC, Kirchhof CJ, Dorland R, Allessie MA. Atrial fibrillation begets atrial fibrillation. A study in awake chronically instrumented goats. *Circulation*. 1995;92:1954-1968

35. Morillo CA, Klein GJ, Jones DL, Guiraudon CM. Chronic rapid atrial pacing. Structural, functional, and electrophysiological characteristics of a new model of sustained atrial fibrillation. *Circulation*. 1995;91:1588-1595

36. Allessie M, Ausma J, Schotten U. Electrical, contractile and structural remodeling during atrial fibrillation. *Cardiovasc Res*. 2002;54:230-246

37. Burstein B, Nattel S. Atrial fibrosis: Mechanisms and clinical relevance in atrial fibrillation. *Journal of the American College of Cardiology*. 2008;51:802-809

38. Kostin S, Klein G, Szalay Z, Hein S, Bauer EP, Schaper J. Structural correlate of atrial fibrillation in human patients. *Cardiovasc Res*. 2002;54:361-379

39. Boldt A, Wetzel U, Lauschke J, Weigl J, Gummert J, Hindricks G, Kottkamp H, Dhein S. Fibrosis in left atrial tissue of patients with atrial fibrillation with and without underlying mitral valve disease. *Heart*. 2004;90:400-405

40. Xu J, Cui G, Esmailian F, Plunkett M, Marelli D, Ardehali A, Odim J, Laks H, Sen L. Atrial extracellular matrix remodeling and the maintenance of atrial fibrillation. *Circulation*. 2004;109:363-368

41. Frustaci A, Chimenti C, Bellocci F, Morgante E, Russo MA, Maseri A. Histological substrate of atrial biopsies in patients with lone atrial fibrillation. *Circulation*. 1997;96:1180-1184

42. Avitall B, Bi J, Mykytsey A, Chicos A. Atrial and ventricular fibrosis induced by atrial fibrillation: Evidence to support early rhythm control. *Heart Rhythm*. 2008;5:839-845

43. Burstein B, Qi XY, Yeh YH, Calderone A, Nattel S. Atrial cardiomyocyte tachycardia alters cardiac fibroblast function: A novel consideration in atrial remodeling. *Cardiovasc Res*. 2007;76:442-452

44. Armstrong PW, Stopps TP, Ford SE, de Bold AJ. Rapid ventricular pacing in the dog: Pathophysiologic studies of heart failure. *Circulation*. 1986;74:1075-1084

45. Li D, Fareh S, Leung TK, Nattel S. Promotion of atrial fibrillation by heart failure in dogs: Atrial remodeling of a different sort. *Circulation*. 1999;100:87-95

46. Calkins H, Kuck KH, Cappato R, Brugada J, Camm AJ, Chen SA, Crijns HJ, Damiano RJ, Jr., Davies DW, DiMarco J, Edgerton J, Ellenbogen K, Ezekowitz MD, Haines DE, Haissaguerre M, Hindricks G, Iesaka Y, Jackman W, Jalife J, Jais P, Kalman J, Keane D, Kim YH, Kirchhof P, Klein G, Kottkamp H, Kumagai K, Lindsay BD, Mansour M, Marchlinski FE, McCarthy PM, Mont JL, Morady F, Nademanee K, Nakagawa H, Natale A, Nattel S, Packer DL, Pappone C, Prystowsky E, Raviele A, Reddy V, Ruskin JN, Shemin RJ, Tsao HM, Wilber D. 2012 hrs/ehra/ecas expert consensus statement on catheter and surgical ablation of atrial fibrillation: Recommendations for patient selection, procedural techniques, patient management and follow-up, definitions, endpoints, and research trial design: A report of the heart rhythm society (hrs) task force on catheter and surgical ablation of atrial fibrillation. Developed in partnership with the european heart rhythm association (ehra), a registered branch of the european society of cardiology (esc) and the european cardiac arrhythmia society (ecas); and in collaboration with the american college of cardiology (acc), american heart association (aha), the asia pacific heart rhythm society (aphrs), and the society of thoracic surgeons (sts). Endorsed by the governing bodies of the american college of cardiology foundation, the american heart association, the european cardiac arrhythmia society, the european heart rhythm association, the society of thoracic surgeons, the asia pacific heart rhythm society, and the heart

rhythm society. *Heart rhythm : the official journal of the Heart Rhythm Society*. 2012;9:632-696 e621

47. Wokhlu A, Monahan KH, Hodge DO, Asirvatham SJ, Friedman PA, Munger TM, Bradley DJ, Bluhm CM, Haroldson JM, Packer DL. Long-term quality of life after ablation of atrial fibrillation the impact of recurrence, symptom relief, and placebo effect. *Journal of the American College of Cardiology*. 2010;55:2308-2316

48. Haissaguerre M, Jais P, Shah DC, Takahashi A, Hocini M, Quiniou G, Garrigue S, Le Mouroux A, Le Metayer P, Clementy J. Spontaneous initiation of atrial fibrillation by ectopic beats originating in the pulmonary veins. *The New England journal of medicine*. 1998;339:659-666

49. Fuster V, Ryden LE, Cannom DS, Crijns HJ, Curtis AB, Ellenbogen KA, Halperin JL, Le Heuzey JY, Kay GN, Lowe JE, Olsson SB, Prystowsky EN, Tamargo JL, Wann S, Smith SC, Jr., Jacobs AK, Adams CD, Anderson JL, Antman EM, Hunt SA, Nishimura R, Ornato JP, Page RL, Riegel B, Priori SG, Blanc JJ, Budaj A, Camm AJ, Dean V, Deckers JW, Despres C, Dickstein K, Lekakis J, McGregor K, Metra M, Morais J, Osterspey A, Zamorano JL. Acc/aha/esc 2006 guidelines for the management of patients with atrial fibrillation: A report of the american college of cardiology/american heart association task force on practice guidelines and the european society of cardiology committee for practice guidelines (writing committee to revise the 2001 guidelines for the management of patients with atrial fibrillation): Developed in collaboration with the european

heart rhythm association and the heart rhythm society. *Circulation*. 2006;114:e257-354

50. Nanthakumar K, Plumb VJ, Epstein AE, Veenhuyzen GD, Link D, Kay GN. Resumption of electrical conduction in previously isolated pulmonary veins: Rationale for a different strategy? *Circulation*. 2004;109:1226-1229

51. Arujuna A, Karim R, Caulfield D, Knowles B, Rhode K, Schaeffter T, Kato B, Rinaldi CA, Cooklin M, Razavi R, O'Neill MD, Gill J. Acute pulmonary vein isolation is achieved by a combination of reversible and irreversible atrial injury after catheter ablation: Evidence from magnetic resonance imaging. *Circulation. Arrhythmia and electrophysiology*. 2012;5:691-700

52. Calkins H, Reynolds MR, Spector P, Sondhi M, Xu Y, Martin A, Williams CJ, Sledge I. Treatment of atrial fibrillation with antiarrhythmic drugs or radiofrequency ablation: Two systematic literature reviews and meta-analyses. *Circulation. Arrhythmia and electrophysiology*. 2009;2:349-361

53. Ouyang F, Tilz R, Chun J, Schmidt B, Wissner E, Zerm T, Neven K, Kokturk B, Konstantinidou M, Metzner A, Fuernkranz A, Kuck KH. Long-term results of catheter ablation in paroxysmal atrial fibrillation: Lessons from a 5-year follow-up. *Circulation*. 2010;122:2368-2377

54. Pappone C, Rosanio S, Augello G, Gallus G, Vicedomini G, Mazzone P, Gulletta S, Gugliotta F, Pappone A, Santinelli V, Tortoriello V, Sala S, Zangrillo A, Crescenzi G, Benussi S, Alfieri O. Mortality, morbidity, and quality of life after circumferential pulmonary vein ablation for atrial

fibrillation: Outcomes from a controlled nonrandomized long-term study. *Journal of the American College of Cardiology*. 2003;42:185-197

55. Bhargava M, Di Biase L, Mohanty P, Prasad S, Martin DO, Williams-Andrews M, Wazni OM, Burkhardt JD, Cummings JE, Khaykin Y, Verma A, Hao S, Beheiry S, Hongo R, Rossillo A, Raviele A, Bonso A, Themistoclakis S, Stewart K, Saliba WI, Schweikert RA, Natale A. Impact of type of atrial fibrillation and repeat catheter ablation on long-term freedom from atrial fibrillation: Results from a multicenter study. *Heart rhythm : the official journal of the Heart Rhythm Society*. 2009;6:1403-1412

56. Nattel S, Burstein B, Dobrev D. Atrial remodeling and atrial fibrillation: Mechanisms and implications. *Circulation. Arrhythmia and electrophysiology*. 2008;1:62-73

57. Gray RA, Pertsov AM, Jalife J. Spatial and temporal organization during cardiac fibrillation. *Nature*. 1998;392:75-78

58. Sahadevan J, Ryu K, Peltz L, Khrestian CM, Stewart RW, Markowitz AH, Waldo AL. Epicardial mapping of chronic atrial fibrillation in patients: Preliminary observations. *Circulation*. 2004;110:3293-3299

59. Narayan SM, Krummen DE, Clopton P, Shivkumar K, Miller JM. Direct or coincidental elimination of stable rotors or focal sources may explain successful atrial fibrillation ablation: On-treatment analysis of the confirm trial (conventional ablation for af with or without focal impulse and rotor modulation). *Journal of the American College of Cardiology*. 2013;62:138-147

60. Narayan SM, Patel J, Mulpuru S, Krummen DE. Focal impulse and rotor modulation ablation of sustaining rotors abruptly terminates persistent atrial fibrillation to sinus rhythm with elimination on follow-up: A video case study. *Heart rhythm : the official journal of the Heart Rhythm Society*. 2012;9:1436-1439

61. Narayan SM, Krummen DE, Shivkumar K, Clopton P, Rappel WJ, Miller JM. Treatment of atrial fibrillation by the ablation of localized sources: Confirm (conventional ablation for atrial fibrillation with or without focal impulse and rotor modulation) trial. *Journal of the American College of Cardiology*. 2012;60:628-636

62. Brooks AG, Stiles MK, Laborderie J, Lau DH, Kuklik P, Shipp NJ, Hsu LF, Sanders P. Outcomes of long-standing persistent atrial fibrillation ablation: A systematic review. *Heart rhythm : the official journal of the Heart Rhythm Society*. 2010;7:835-846

63. O'Neill MD, Jais P, Takahashi Y, Jonsson A, Sacher F, Hocini M, Sanders P, Rostock T, Rotter M, Pernat A, Clementy J, Haissaguerre M. The stepwise ablation approach for chronic atrial fibrillation--evidence for a cumulative effect. *Journal of interventional cardiac electrophysiology : an international journal of arrhythmias and pacing*. 2006;16:153-167

64. Judd RM, Lugo-Olivieri CH, Arai M, Kondo T, Croisille P, Lima JA, Mohan V, Becker LC, Zerhouni EA. Physiological basis of myocardial contrast enhancement in fast magnetic resonance images of 2-day-old reperfused canine infarcts. *Circulation*. 1995;92:1902-1910

65. Lima JA, Judd RM, Bazille A, Schulman SP, Atalar E, Zerhouni EA. Regional heterogeneity of human myocardial infarcts demonstrated by contrast-enhanced mri. Potential mechanisms. *Circulation*. 1995;92:1117-1125

66. Kim RJ, Wu E, Rafael A, Chen EL, Parker MA, Simonetti O, Klocke FJ, Bonow RO, Judd RM. The use of contrast-enhanced magnetic resonance imaging to identify reversible myocardial dysfunction. *N Engl J Med*. 2000;343:1445-1453

67. Kim RJ, Fieno DS, Parrish TB, Harris K, Chen EL, Simonetti O, Bundy J, Finn JP, Klocke FJ, Judd RM. Relationship of mri delayed contrast enhancement to irreversible injury, infarct age, and contractile function. *Circulation*. 1999;100:1992-2002

68. Mahrholdt H, Wagner A, Judd RM, Sechtem U, Kim RJ. Delayed enhancement cardiovascular magnetic resonance assessment of non-ischaemic cardiomyopathies. *European heart journal*. 2005;26:1461-1474

69. Ricciardi MJ, Wu E, Davidson CJ, Choi KM, Klocke FJ, Bonow RO, Judd RM, Kim RJ. Visualization of discrete microinfarction after percutaneous coronary intervention associated with mild creatine kinase-mb elevation. *Circulation*. 2001;103:2780-2783

70. Wu E, Judd RM, Vargas JD, Klocke FJ, Bonow RO, Kim RJ. Visualisation of presence, location, and transmural extent of healed q-wave and non-q-wave myocardial infarction. *Lancet*. 2001;357:21-28

71. Karamitsos TD, Francis JM, Myerson S, Selvanayagam JB, Neubauer S. The role of cardiovascular magnetic resonance imaging in heart failure. *J Am Coll Cardiol*. 2009;54:1407-1424

72. McCrohon JA, Moon JC, Prasad SK, McKenna WJ, Lorenz CH, Coats AJ, Pennell DJ. Differentiation of heart failure related to dilated cardiomyopathy and coronary artery disease using gadolinium-enhanced cardiovascular magnetic resonance. *Circulation*. 2003;108:54-59

73. Spiewak M, Malek LA, Misko J, Chojnowska L, Milosz B, Klopotowski M, Petryka J, Dabrowski M, Kepka C, Ruzyllo W. Comparison of different quantification methods of late gadolinium enhancement in patients with hypertrophic cardiomyopathy. *Eur J Radiol*. 2010;74:e149-153

74. Amado LC, Gerber BL, Gupta SN, Rettmann DW, Szarf G, Schock R, Nasir K, Kraitchman DL, Lima JA. Accurate and objective infarct sizing by contrast-enhanced magnetic resonance imaging in a canine myocardial infarction model. *Journal of the American College of Cardiology*. 2004;44:2383-2389

75. Bondarenko O, Beek AM, Hofman MB, Kuhl HP, Twisk JW, van Dockum WG, Visser CA, van Rossum AC. Standardizing the definition of hyperenhancement in the quantitative assessment of infarct size and myocardial viability using delayed contrast-enhanced cmr. *J Cardiovasc Magn Reson*. 2005;7:481-485

76. Hsu LY, Ingkanisorn WP, Kellman P, Aletras AH, Arai AE. Quantitative myocardial infarction on delayed enhancement mri. Part ii: Clinical

application of an automated feature analysis and combined thresholding infarct sizing algorithm. *J Magn Reson Imaging*. 2006;23:309-314

77. Peters DC, Wylie JV, Hauser TH, Kissinger KV, Botnar RM, Essebag V, Josephson ME, Manning WJ. Detection of pulmonary vein and left atrial scar after catheter ablation with three-dimensional navigator-gated delayed enhancement mr imaging: Initial experience. *Radiology*. 2007;243:690-695

78. McGann CJ, Kholmovski EG, Oakes RS, Blauer JJ, Daccarett M, Segerson N, Airey KJ, Akoum N, Fish E, Badger TJ, DiBella EV, Parker D, MacLeod RS, Marrouche NF. New magnetic resonance imaging-based method for defining the extent of left atrial wall injury after the ablation of atrial fibrillation. *J Am Coll Cardiol*. 2008;52:1263-1271

79. Badger TJ, Oakes RS, Daccarett M, Burgon NS, Akoum N, Fish EN, Blauer JJ, Rao SN, Adjei-Poku Y, Kholmovski EG, Vijayakumar S, Di Bella EV, MacLeod RS, Marrouche NF. Temporal left atrial lesion formation after ablation of atrial fibrillation. *Heart Rhythm*. 2009;6:161-168

80. Oakes RS, Badger TJ, Kholmovski EG, Akoum N, Burgon NS, Fish EN, Blauer JJ, Rao SN, DiBella EV, Segerson NM, Daccarett M, Windfelder J, McGann CJ, Parker D, MacLeod RS, Marrouche NF. Detection and quantification of left atrial structural remodeling with delayed-enhancement magnetic resonance imaging in patients with atrial fibrillation. *Circulation*. 2009;119:1758-1767

81. Segerson NM, Daccarett M, Badger TJ, Shabaan A, Akoum N, Fish EN, Rao S, Burgon NS, Adjei-Poku Y, Kholmovski E, Vijayakumar S, DiBella EV,

MacLeod RS, Marrouche NF. Magnetic resonance imaging-confirmed ablative debulking of the left atrial posterior wall and septum for treatment of persistent atrial fibrillation: Rationale and initial experience. *J Cardiovasc Electrophysiol*. 2010;21:126-132

82. Badger TJ, Daccarett M, Akoum NW, Adjei-Poku YA, Burgon NS, Haslam TS, Kalvaitis S, Kuppahally S, Vergara G, McMullen L, Anderson PA, Kholmovski E, MacLeod RS, Marrouche NF. Evaluation of left atrial lesions after initial and repeat atrial fibrillation ablation: Lessons learned from delayed-enhancement mri in repeat ablation procedures. *Circulation. Arrhythmia and electrophysiology*. 2010;3:249-259

83. Akoum N, Daccarett M, McGann C, Segerson N, Vergara G, Kuppahally S, Badger T, Burgon N, Haslam T, Kholmovski E, Macleod R, Marrouche N. Atrial fibrosis helps select the appropriate patient and strategy in catheter ablation of atrial fibrillation: A de-mri guided approach. *J Cardiovasc Electrophysiol*. 2011;22:16-22

84. Mahnkopf C, Badger TJ, Burgon NS, Daccarett M, Haslam TS, Badger CT, McGann CJ, Akoum N, Kholmovski E, Macleod RS, Marrouche NF. Evaluation of the left atrial substrate in patients with lone atrial fibrillation using delayed-enhanced mri: Implications for disease progression and response to catheter ablation. *Heart rhythm : the official journal of the Heart Rhythm Society*. 2010;7:1475-1481

85. Peters DC, Wylie JV, Hauser TH, Nezafat R, Han Y, Woo JJ, Taclas J, Kissinger KV, Goddu B, Josephson ME, Manning WJ. Recurrence of atrial fibrillation correlates with the extent of post-procedural late gadolinium

enhancement: A pilot study. *JACC. Cardiovascular imaging*. 2009;2:308-316

86. Reddy VY, Schmidt EJ, Holmvang G, Fung M. Arrhythmia recurrence after atrial fibrillation ablation: Can magnetic resonance imaging identify gaps in atrial ablation lines? *Journal of cardiovascular electrophysiology*. 2008;19:434-437

87. Knowles BR, Caulfield D, Cooklin M, Rinaldi CA, Gill J, Bostock J, Razavi R, Schaeffter T, Rhode KS. 3-d visualization of acute rf ablation lesions using mri for the simultaneous determination of the patterns of necrosis and edema. *IEEE transactions on bio-medical engineering*. 2010;57:1467-1475

88. Verma A, Wazni OM, Marrouche NF, Martin DO, Kilicaslan F, Minor S, Schweikert RA, Saliba W, Cummings J, Burkhardt JD, Bhargava M, Belden WA, Abdul-Karim A, Natale A. Pre-existent left atrial scarring in patients undergoing pulmonary vein antrum isolation: An independent predictor of procedural failure. *Journal of the American College of Cardiology*. 2005;45:285-292

89. Abhayaratna WP, Seward JB, Appleton CP, Douglas PS, Oh JK, Tajik AJ, Tsang TS. Left atrial size: Physiologic determinants and clinical applications. *Journal of the American College of Cardiology*. 2006;47:2357-2363

90. Gage BF, Waterman AD, Shannon W, Boechler M, Rich MW, Radford MJ. Validation of clinical classification schemes for predicting stroke: Results

from the national registry of atrial fibrillation. *JAMA*. 2001;285:2864-2870

91. Daccarett M, Badger TJ, Akoum N, Burgon NS, Mahnkopf C, Vergara G, Kholmovski E, McGann CJ, Parker D, Brachmann J, Macleod RS, Marrouche NF. Association of left atrial fibrosis detected by delayed-enhancement magnetic resonance imaging and the risk of stroke in patients with atrial fibrillation. *Journal of the American College of Cardiology*. 2011;57:831-838

92. Wittkampf FH, Vonken EJ, Derksen R, Loh P, Velthuis B, Wever EF, Boersma LV, Rensing BJ, Cramer MJ. Pulmonary vein ostium geometry: Analysis by magnetic resonance angiography. *Circulation*. 2003;107:21-23

93. Hauser TH, Yeon SB, McClennen S, Katsimaglis G, Kissinger KV, Josephson ME, Rofsky NM, Manning WJ. A method for the determination of proximal pulmonary vein size using contrast-enhanced magnetic resonance angiography. *Journal of cardiovascular magnetic resonance : official journal of the Society for Cardiovascular Magnetic Resonance*. 2004;6:927-936

94. Hauser TH, Yeon SB, McClennen S, Katsimaglis G, Kissinger KV, Josephson ME, Rofsky NM, Manning WJ. Subclinical pulmonary vein narrowing after ablation for atrial fibrillation. *Heart*. 2005;91:672-673

95. Mansour M, Holmvang G, Sosnovik D, Migrino R, Abbara S, Ruskin J, Keane D. Assessment of pulmonary vein anatomic variability by magnetic resonance imaging: Implications for catheter ablation

techniques for atrial fibrillation. *Journal of cardiovascular electrophysiology*. 2004;15:387-393

96. Mlcochova H, Tintera J, Porod V, Peichl P, Cihak R, Kautzner J. Magnetic resonance angiography of pulmonary veins: Implications for catheter ablation of atrial fibrillation. *Pacing and clinical electrophysiology : PACE*. 2005;28:1073-1080

97. Syed MA, Peters DC, Rashid H, Arai AE. Pulmonary vein imaging: Comparison of 3d magnetic resonance angiography with 2d cine mri for characterizing anatomy and size. *Journal of cardiovascular magnetic resonance : official journal of the Society for Cardiovascular Magnetic Resonance*. 2005;7:355-360

98. Tamborero D, Mont L, Nava S, de Caralt TM, Molina I, Scalise A, Perea RJ, Bartholomay E, Berruezo A, Matiello M, Brugada J. Incidence of pulmonary vein stenosis in patients submitted to atrial fibrillation ablation: A comparison of the selective segmental ostial ablation vs the circumferential pulmonary veins ablation. *Journal of interventional cardiac electrophysiology : an international journal of arrhythmias and pacing*. 2005;14:21-25

99. Tsao HM, Wu MH, Huang BH, Lee SH, Lee KT, Tai CT, Lin YK, Hsieh MH, Kuo JY, Lei MH, Chen SA. Morphologic remodeling of pulmonary veins and left atrium after catheter ablation of atrial fibrillation: Insight from long-term follow-up of three-dimensional magnetic resonance imaging. *Journal of cardiovascular electrophysiology*. 2005;16:7-12

100. Vonken EP, Velthuis BK, Wittkampf FH, Rensing BJ, Derksen R, Cramer MJ. Contrast-enhanced mra and 3d visualization of pulmonary venous anatomy to assist radiofrequency catheter ablation. *Journal of cardiovascular magnetic resonance : official journal of the Society for Cardiovascular Magnetic Resonance*. 2003;5:545-551

101. Lickfett L, Dickfeld T, Kato R, Tandri H, Vasamreddy CR, Berger R, Bluemke D, Luderitz B, Halperin H, Calkins H. Changes of pulmonary vein orifice size and location throughout the cardiac cycle: Dynamic analysis using magnetic resonance cine imaging. *Journal of cardiovascular electrophysiology*. 2005;16:582-588

102. Earls JP, Rofsky NM, DeCorato DR, Krinsky GA, Weinreb JC. Breath-hold single-dose gadolinium-enhanced three-dimensional mr aortography: Usefulness of a timing examination and mr power injector. *Radiology*. 1996;201:705-710

103. Dittrich HC, Pearce LA, Asinger RW, McBride R, Webel R, Zabalgoitia M, Pennock GD, Safford RE, Rothbart RM, Halperin JL, Hart RG. Left atrial diameter in nonvalvular atrial fibrillation: An echocardiographic study. Stroke prevention in atrial fibrillation investigators. *American heart journal*. 1999;137:494-499

104. Sanfilippo AJ, Abascal VM, Sheehan M, Oertel LB, Harrigan P, Hughes RA, Weyman AE. Atrial enlargement as a consequence of atrial fibrillation. A prospective echocardiographic study. *Circulation*. 1990;82:792-797

105. Jarvinen VM, Kupari MM, Hekali PE, Poutanen VP. Right atrial mr imaging studies of cadaveric atrial casts and comparison with right and

left atrial volumes and function in healthy subjects. *Radiology*. 1994;191:137-142

106. Hof IE, Velthuis BK, Van Driel VJ, Wittkampf FH, Hauer RN, Loh P. Left atrial volume and function assessment by magnetic resonance imaging. *Journal of cardiovascular electrophysiology*. 2010;21:1247-1250

107. Lang RM, Bierig M, Devereux RB, Flachskampf FA, Foster E, Pellikka PA, Picard MH, Roman MJ, Seward J, Shanewise JS, Solomon SD, Spencer KT, Sutton MS, Stewart WJ, Chamber Quantification Writing G, American Society of Echocardiography's G, Standards C, European Association of E. Recommendations for chamber quantification: A report from the american society of echocardiography's guidelines and standards committee and the chamber quantification writing group, developed in conjunction with the european association of echocardiography, a branch of the european society of cardiology. *Journal of the American Society of Echocardiography : official publication of the American Society of Echocardiography*. 2005;18:1440-1463

108. Pujadas S, Reddy GP, Weber O, Lee JJ, Higgins CB. Mr imaging assessment of cardiac function. *Journal of magnetic resonance imaging : JMRI*. 2004;19:789-799

109. Dulce MC, Mostbeck GH, Friese KK, Caputo GR, Higgins CB. Quantification of the left ventricular volumes and function with cine mr imaging: Comparison of geometric models with three-dimensional data. *Radiology*. 1993;188:371-376

110. Sievers B, Brandts B, Franken U, Trappe HJ. Single and biplane truefisp cardiovascular magnetic resonance for rapid evaluation of left ventricular volumes and ejection fraction. *Journal of cardiovascular magnetic resonance : official journal of the Society for Cardiovascular Magnetic Resonance*. 2004;6:593-600

111. Kato R, Lickfett L, Meininger G, Dickfeld T, Wu R, Juang G, Angkeow P, LaCorte J, Bluemke D, Berger R, Halperin HR, Calkins H. Pulmonary vein anatomy in patients undergoing catheter ablation of atrial fibrillation: Lessons learned by use of magnetic resonance imaging. *Circulation*. 2003;107:2004-2010

112. Ishimoto N, Ito M, Kinoshita M. Signal-averaged p-wave abnormalities and atrial size in patients with and without idiopathic paroxysmal atrial fibrillation. *American heart journal*. 2000;139:684-689

113. Anselmino M, Blandino A, Beninati S, Rovera C, Boffano C, Belletti M, Caponi D, Scaglione M, Cesarani F, Gaita F. Morphologic analysis of left atrial anatomy by magnetic resonance angiography in patients with atrial fibrillation: A large single center experience. *Journal of cardiovascular electrophysiology*. 2011;22:1-7

114. Therkelsen SK, Groenning BA, Svendsen JH, Jensen GB. Atrial and ventricular volume and function in persistent and permanent atrial fibrillation, a magnetic resonance imaging study. *Journal of cardiovascular magnetic resonance : official journal of the Society for Cardiovascular Magnetic Resonance*. 2005;7:465-473

115. Therkelsen SK, Groenning BA, Svendsen JH, Jensen GB. Atrial and ventricular volume and function evaluated by magnetic resonance imaging in patients with persistent atrial fibrillation before and after cardioversion. *The American journal of cardiology*. 2006;97:1213-1219

116. Montefusco A, Biasco L, Blandino A, Cristoforetti Y, Scaglione M, Caponi D, Di Donna P, Boffano C, Cesarani F, Coin D, Perversi J, Gaita F. Left atrial volume at mri is the main determinant of outcome after pulmonary vein isolation plus linear lesion ablation for paroxysmal-persistent atrial fibrillation. *Journal of cardiovascular medicine*. 2010;11:593-598

117. von Bary C, Dornia C, Eissnert C, Nedios S, Roser M, Hamer OW, Gerds-Li JH, Paetsch I, Jahnke C, Gebker R, Weber S, Fleck E, Kriatselis C. Predictive value of left atrial volume measured by non-invasive cardiac imaging in the treatment of paroxysmal atrial fibrillation. *Journal of interventional cardiac electrophysiology : an international journal of arrhythmias and pacing*. 2012;34:181-188

118. Hof IE, Velthuis BK, Chaldoupi SM, Wittkampf FH, van Driel VJ, van der Heijden JF, Cramer MJ, Meine M, Hauer RN, Loh P. Pulmonary vein antrum isolation leads to a significant decrease of left atrial size. *Europace : European pacing, arrhythmias, and cardiac electrophysiology : journal of the working groups on cardiac pacing, arrhythmias, and cardiac cellular electrophysiology of the European Society of Cardiology*. 2011;13:371-375

119. Nori D, Raff G, Gupta V, Gentry R, Boura J, Haines DE. Cardiac magnetic resonance imaging assessment of regional and global left atrial function

before and after catheter ablation for atrial fibrillation. *Journal of interventional cardiac electrophysiology : an international journal of arrhythmias and pacing*. 2009;26:109-117

120. Wylie JV, Jr., Peters DC, Essebag V, Manning WJ, Josephson ME, Hauser TH. Left atrial function and scar after catheter ablation of atrial fibrillation. *Heart rhythm : the official journal of the Heart Rhythm Society*. 2008;5:656-662

121. Muellerleile K, Groth M, Steven D, Hoffmann BA, Saring D, Radunski UK, Lund GK, Adam G, Rostock T, Willems S. Cardiovascular magnetic resonance demonstrates reversible atrial dysfunction after catheter ablation of persistent atrial fibrillation. *Journal of cardiovascular electrophysiology*. 2013;24:762-767

122. Dill T, Neumann T, Ekinci O, Breidenbach C, John A, Erdogan A, Bachmann G, Hamm CW, Pitschner HF. Pulmonary vein diameter reduction after radiofrequency catheter ablation for paroxysmal atrial fibrillation evaluated by contrast-enhanced three-dimensional magnetic resonance imaging. *Circulation*. 2003;107:845-850

123. Lin WS, Prakash VS, Tai CT, Hsieh MH, Tsai CF, Yu WC, Lin YK, Ding YA, Chang MS, Chen SA. Pulmonary vein morphology in patients with paroxysmal atrial fibrillation initiated by ectopic beats originating from the pulmonary veins: Implications for catheter ablation. *Circulation*. 2000;101:1274-1281

124. Francois CJ, Tuite D, Deshpande V, Jerecic R, Weale P, Carr JC. Pulmonary vein imaging with unenhanced three-dimensional balanced steady-state

free precession mr angiography: Initial clinical evaluation. *Radiology*. 2009;250:932-939

125. Bowman AW, Kovacs SJ. Prediction and assessment of the time-varying effective pulmonary vein area via cardiac mri and doppler echocardiography. *American journal of physiology. Heart and circulatory physiology*. 2005;288:H280-286

126. Groth M, Bannas P, Regier M, Buhk JH, Mullerleile K, Adam G, Henes FO. Precision of pulmonary vein diameter measurements assessed by ce-mra and steady-state-free precession imaging. *European radiology*. 2013;23:1546-1552

127. Robbins IM, Colvin EV, Doyle TP, Kemp WE, Loyd JE, McMahon WS, Kay GN. Pulmonary vein stenosis after catheter ablation of atrial fibrillation. *Circulation*. 1998;98:1769-1775

128. Dong J, Vasamreddy CR, Jayam V, Dalal D, Dickfeld T, Eldadah Z, Meininger G, Halperin HR, Berger R, Bluemke DA, Calkins H. Incidence and predictors of pulmonary vein stenosis following catheter ablation of atrial fibrillation using the anatomic pulmonary vein ablation approach: Results from paired magnetic resonance imaging. *Journal of cardiovascular electrophysiology*. 2005;16:845-852

129. Arentz T, Jander N, von Rosenthal J, Blum T, Furmaier R, Gornandt L, Josef Neumann F, Kalusche D. Incidence of pulmonary vein stenosis 2 years after radiofrequency catheter ablation of refractory atrial fibrillation. *European heart journal*. 2003;24:963-969

130. Narumiya T, Sakamaki T, Sato Y, Kanmatsuse K. Relationship between left atrial appendage function and left atrial thrombus in patients with nonvalvular chronic atrial fibrillation and atrial flutter. *Circulation journal : official journal of the Japanese Circulation Society*. 2003;67:68-72

131. Ohyama H, Hosomi N, Takahashi T, Mizushige K, Osaka K, Kohno M, Koziol JA. Comparison of magnetic resonance imaging and transesophageal echocardiography in detection of thrombus in the left atrial appendage. *Stroke; a journal of cerebral circulation*. 2003;34:2436-2439

132. Rathi VK, Reddy ST, Anreddy S, Belden W, Yamrozik JA, Williams RB, Doyle M, Thompson DV, Biederman RW. Contrast-enhanced cmr is equally effective as tee in the evaluation of left atrial appendage thrombus in patients with atrial fibrillation undergoing pulmonary vein isolation procedure. *Heart rhythm : the official journal of the Heart Rhythm Society*. 2013;10:1021-1027

133. Mohrs OK, Nowak B, Petersen SE, Welsner M, Rubel C, Magedanz A, Kauczor HU, Voigtlaender T. Thrombus detection in the left atrial appendage using contrast-enhanced mri: A pilot study. *AJR. American journal of roentgenology*. 2006;186:198-205

134. Beinart R, Heist EK, Newell JB, Holmvang G, Ruskin JN, Mansour M. Left atrial appendage dimensions predict the risk of stroke/tia in patients with atrial fibrillation. *Journal of cardiovascular electrophysiology*. 2011;22:10-15

135. Fyrenius A, Wigstrom L, Ebbers T, Karlsson M, Engvall J, Bolger AF. Three dimensional flow in the human left atrium. *Heart*. 2001;86:448-455

136. Verma A, Kilicaslan F, Pisano E, Marrouche NF, Fanelli R, Brachmann J, Geunther J, Potenza D, Martin DO, Cummings J, Burkhardt JD, Saliba W, Schweikert RA, Natale A. Response of atrial fibrillation to pulmonary vein antrum isolation is directly related to resumption and delay of pulmonary vein conduction. *Circulation*. 2005;112:627-635

137. Ouyang F, Antz M, Ernst S, Hachiya H, Mavrakis H, Deger FT, Schaumann A, Chun J, Falk P, Hennig D, Liu X, Bansch D, Kuck KH. Recovered pulmonary vein conduction as a dominant factor for recurrent atrial tachyarrhythmias after complete circular isolation of the pulmonary veins: Lessons from double lasso technique. *Circulation*. 2005;111:127-135

138. Lardo AC, McVeigh ER, Jumrussirikul P, Berger RD, Calkins H, Lima J, Halperin HR. Visualization and temporal/spatial characterization of cardiac radiofrequency ablation lesions using magnetic resonance imaging. *Circulation*. 2000;102:698-705

139. Dickfeld T, Kato R, Zviman M, Nazarian S, Dong J, Ashikaga H, Lardo AC, Berger RD, Calkins H, Halperin H. Characterization of acute and subacute radiofrequency ablation lesions with nonenhanced magnetic resonance imaging. *Heart rhythm : the official journal of the Heart Rhythm Society*. 2007;4:208-214

140. Dickfeld T, Kato R, Zviman M, Lai S, Meininger G, Lardo AC, Roguin A, Blumke D, Berger R, Calkins H, Halperin H. Characterization of radiofrequency ablation lesions with gadolinium-enhanced cardiovascular magnetic resonance imaging. *Journal of the American College of Cardiology*. 2006;47:370-378

141. Schmidt EJ, Reddy VK, Ruskin JN. Nonenhanced magnetic resonance imaging for characterization of acute and subacute radiofrequency ablation lesions. *Heart rhythm : the official journal of the Heart Rhythm Society*. 2007;4:215-217

142. Elgort DR, Duerk JL. A review of technical advances in interventional magnetic resonance imaging. *Academic radiology*. 2005;12:1089-1099

143. Niendorf T, Sodickson DK. Parallel imaging in cardiovascular mri: Methods and applications. *NMR in biomedicine*. 2006;19:325-341

144. Bock M, Muller S, Zuehlsdorff S, Speier P, Fink C, Hallscheidt P, Umathum R, Semmler W. Active catheter tracking using parallel mri and real-time image reconstruction. *Magnetic resonance in medicine : official journal of the Society of Magnetic Resonance in Medicine / Society of Magnetic Resonance in Medicine*. 2006;55:1454-1459

145. Dumoulin CL, Souza SP, Darrow RD. Real-time position monitoring of invasive devices using magnetic resonance. *Magnetic resonance in medicine : official journal of the Society of Magnetic Resonance in Medicine / Society of Magnetic Resonance in Medicine*. 1993;29:411-415

146. Elgort DR, Wong EY, Hillenbrand CM, Wacker FK, Lewin JS, Duerk JL. Real-time catheter tracking and adaptive imaging. *Journal of magnetic resonance imaging : JMRI*. 2003;18:621-626

147. Nitz WR, Oppelt A, Renz W, Manke C, Lenhart M, Link J. On the heating of linear conductive structures as guide wires and catheters in interventional mri. *Journal of magnetic resonance imaging : JMRI*. 2001;13:105-114

148. Konings MK, Bartels LW, Smits HF, Bakker CJ. Heating around intravascular guidewires by resonating rf waves. *Journal of magnetic resonance imaging : JMRI*. 2000;12:79-85

149. Weiss S, Wirtz D, David B, Krueger S, Lips O, Caulfield D, Pedersen SF, Bostock J, Razavi R, Schaeffter T. In vivo evaluation and proof of radiofrequency safety of a novel diagnostic mr-electrophysiology catheter. *Magnetic resonance in medicine : official journal of the Society of Magnetic Resonance in Medicine / Society of Magnetic Resonance in Medicine*. 2011;65:770-777

150. Ranjan R, Kholmovski EG, Blauer J, Vijayakumar S, Volland NA, Salama ME, Parker DL, Macleod R, Marrouche NF. Identification and acute targeting of gaps in atrial ablation lesion sets using a real time mri system. *Circulation. Arrhythmia and electrophysiology*. 2012

151. Vergara GR, Vijayakumar S, Kholmovski EG, Blauer JJ, Guttman MA, Gloschat C, Payne G, Vij K, Akoum NW, Daccarett M, McGann CJ, Macleod RS, Marrouche NF. Real-time magnetic resonance imaging-guided radiofrequency atrial ablation and visualization of lesion formation at 3

tesla. *Heart rhythm : the official journal of the Heart Rhythm Society*. 2011;8:295-303

152. Nordbeck P, Hiller KH, Fidler F, Warmuth M, Burkard N, Nahrendorf M, Jakob PM, Quick HH, Ertl G, Bauer WR, Ritter O. Feasibility of contrast-enhanced and nonenhanced mri for intraprocedural and postprocedural lesion visualization in interventional electrophysiology: Animal studies and early delineation of isthmus ablation lesions in patients with typical atrial flutter. *Circulation. Cardiovascular imaging*. 2011;4:282-294

153. Sommer P, Grothoff M, Eitel C, Gaspar T, Piorkowski C, Gutberlet M, Hindricks G. Feasibility of real-time magnetic resonance imaging-guided electrophysiology studies in humans. *Europace : European pacing, arrhythmias, and cardiac electrophysiology : journal of the working groups on cardiac pacing, arrhythmias, and cardiac cellular electrophysiology of the European Society of Cardiology*. 2013;15:101-108

154. Hunter RJ, Jones DA, Boubertakh R, Malcolme-Lawes LC, Kanagaratnam P, Juli CF, Davies DW, Peters NS, Baker V, Earley MJ, Sporton S, Davies LC, Westwood M, Petersen SE, Schilling RJ. Diagnostic accuracy of cardiac magnetic resonance imaging in the detection and characterization of left atrial catheter ablation lesions: A multicenter experience. *Journal of cardiovascular electrophysiology*. 2012

155. Callans DJ, Ren JF, Michele J, Marchlinski FE, Dillon SM. Electroanatomic left ventricular mapping in the porcine model of healed anterior myocardial infarction. Correlation with intracardiac echocardiography and pathological analysis. *Circulation*. 1999;100:1744-1750

156. Sivagangabalan G, Pouliopoulos J, Huang K, Lu J, Barry MA, Thiagalingam A, Ross DL, Thomas SP, Kovoor P. Comparison of electroanatomic contact and noncontact mapping of ventricular scar in a postinfarct ovine model with intramural needle electrode recording and histological validation. *Circulation. Arrhythmia and electrophysiology*. 2008;1:363-369

157. McGann C, Kholmovski E, Blauer J, Vijayakumar S, Haslam T, Cates J, DiBella E, Burgon N, Wilson B, Alexander A, Prastawa M, Daccarett M, Vergara G, Akoum N, Parker D, MacLeod R, Marrouche N. Dark regions of no-reflow on late gadolinium enhancement magnetic resonance imaging result in scar formation after atrial fibrillation ablation. *Journal of the American College of Cardiology*. 2011;58:177-185

158. Flett AS, Hasleton J, Cook C, Hausenloy D, Quarta G, Ariti C, Muthurangu V, Moon JC. Evaluation of techniques for the quantification of myocardial scar of differing etiology using cardiac magnetic resonance. *JACC. Cardiovascular imaging*. 2011;4:150-156

159. Marchlinski FE, Callans DJ, Gottlieb CD, Zado E. Linear ablation lesions for control of unmappable ventricular tachycardia in patients with ischemic and nonischemic cardiomyopathy. *Circulation*. 2000;101:1288-1296

160. Huang SK, Bharati S, Graham AR, Lev M, Marcus FI, Odell RC. Closed chest catheter desiccation of the atrioventricular junction using radiofrequency energy--a new method of catheter ablation. *Journal of the American College of Cardiology*. 1987;9:349-358

161. Gepstein L, Hayam G, Shpun S, Cohen D, Ben-Haim SA. Atrial linear ablations in pigs. Chronic effects on atrial electrophysiology and pathology. *Circulation*. 1999;100:419-426

162. Prasad SM, Maniar HS, Schuessler RB, Damiano RJ, Jr. Chronic transmural atrial ablation by using bipolar radiofrequency energy on the beating heart. *The Journal of thoracic and cardiovascular surgery*. 2002;124:708-713

163. Prasad SM, Maniar HS, Diodato MD, Schuessler RB, Damiano RJ, Jr. Physiological consequences of bipolar radiofrequency energy on the atria and pulmonary veins: A chronic animal study. *The Annals of thoracic surgery*. 2003;76:836-841; discussion 841-832

164. Flett AS, Hayward MP, Ashworth MT, Hansen MS, Taylor AM, Elliott PM, McGregor C, Moon JC. Equilibrium contrast cardiovascular magnetic resonance for the measurement of diffuse myocardial fibrosis: Preliminary validation in humans. *Circulation*. 2010;122:138-144

165. Spragg DD, Khurram I, Zimmerman SL, Yarmohammadi H, Barcelon B, Needleman M, Edwards D, Marine JE, Calkins H, Nazarian S. Initial experience with magnetic resonance imaging of atrial scar and co-registration with electroanatomic voltage mapping during atrial fibrillation: Success and limitations. *Heart rhythm : the official journal of the Heart Rhythm Society*. 2012;9:2003-2009

166. Malcolme-Lawes LC, Juli C, Karim R, Bai W, Quest R, Lim PB, Jamil-Copley S, Kojodjojo P, Ariff B, Davies DW, Rueckert D, Francis DP, Hunter R, Jones D, Boubertakh R, Petersen SE, Schilling R, Kanagaratnam P, Peters

NS. Automated analysis of atrial late gadolinium enhancement imaging that correlates with endocardial voltage and clinical outcomes: A 2-center study. *Heart rhythm : the official journal of the Heart Rhythm Society*. 2013

167. Hunter RJ, Jones DA, Boubertakh R, Malcolme-Lawes LC, Kanagaratnam P, Juli CF, Davies DW, Peters NS, Baker V, Earley MJ, Sporton S, Davies LC, Westwood M, Petersen SE, Schilling RJ. Diagnostic accuracy of cardiac magnetic resonance imaging in the detection and characterization of left atrial catheter ablation lesions: A multicenter experience. *Journal of cardiovascular electrophysiology*. 2013;24:396-403

168. Santangeli P, Di Biase L, Horton R, Burkhardt JD, Sanchez J, Al-Ahmad A, Hongo R, Beheiry S, Bai R, Mohanty P, Lewis WR, Natale A. Ablation of atrial fibrillation under therapeutic warfarin reduces periprocedural complications: Evidence from a meta-analysis. *Circulation. Arrhythmia and electrophysiology*. 2012;5:302-311

169. Jais P, Hocini M, Hsu LF, Sanders P, Scavee C, Weerasooriya R, Macle L, Raybaud F, Garrigue S, Shah DC, Le Metayer P, Clementy J, Haissaguerre M. Technique and results of linear ablation at the mitral isthmus. *Circulation*. 2004;110:2996-3002

170. Hocini M, Jais P, Sanders P, Takahashi Y, Rotter M, Rostock T, Hsu LF, Sacher F, Reuter S, Clementy J, Haissaguerre M. Techniques, evaluation, and consequences of linear block at the left atrial roof in paroxysmal atrial fibrillation: A prospective randomized study. *Circulation*. 2005;112:3688-3696

171. Cheema A, Dong J, Dalal D, Marine JE, Henrikson CA, Spragg D, Cheng A, Nazarian S, Bilchick K, Sinha S, Scherr D, Almasry I, Halperin H, Berger R, Calkins H. Incidence and time course of early recovery of pulmonary vein conduction after catheter ablation of atrial fibrillation. *Journal of cardiovascular electrophysiology*. 2007;18:387-391

172. Cappato R, Negroni S, Pecora D, Bentivegna S, Lupo PP, Carolei A, Esposito C, Furlanello F, De Ambroggi L. Prospective assessment of late conduction recurrence across radiofrequency lesions producing electrical disconnection at the pulmonary vein ostium in patients with atrial fibrillation. *Circulation*. 2003;108:1599-1604

173. Calkins H, Yong P, Miller JM, Olshansky B, Carlson M, Saul JP, Huang SK, Liem LB, Klein LS, Moser SA, Bloch DA, Gillette P, Prystowsky E. Catheter ablation of accessory pathways, atrioventricular nodal reentrant tachycardia, and the atrioventricular junction: Final results of a prospective, multicenter clinical trial. The atakr multicenter investigators group. *Circulation*. 1999;99:262-270

174. Nordbeck P, Bauer WR, Fidler F, Warmuth M, Hiller KH, Nahrendorf M, Maxfield M, Wurtz S, Geistert W, Broscheit J, Jakob PM, Ritter O. Feasibility of real-time mri with a novel carbon catheter for interventional electrophysiology. *Circulation. Arrhythmia and electrophysiology*. 2009;2:258-267

175. Hoffmann BA, Koops A, Rostock T, Mullerleile K, Steven D, Karst R, Steinke MU, Drewitz I, Lund G, Koops S, Adam G, Willems S. Interactive real-time mapping and catheter ablation of the cavotricuspid isthmus

guided by magnetic resonance imaging in a porcine model. *European heart journal*. 2010;31:450-456

176. Ganesan AN, Selvanayagam JB, Mahajan R, Grover S, Nayyar S, Brooks AG, Finnie J, Sunnarborg D, Lloyd T, Chakrabarty A, Abed HS, Sanders P. Mapping and ablation of the pulmonary veins and cavo-tricuspid isthmus with a magnetic resonance imaging-compatible externally irrigated ablation catheter and integrated electrophysiology system. *Circulation. Arrhythmia and electrophysiology*. 2012;5:1136-1142

177. Piorkowski C, Grothoff M, Gaspar T, Eitel C, Sommer P, Huo Y, John S, Gutberlet M, Hindricks G. Cavotricuspid isthmus ablation guided by real-time magnetic resonance imaging. *Circulation. Arrhythmia and electrophysiology*. 2013;6:e7-10

178. Nazarian S, Kolandaivelu A, Zviman MM, Meininger GR, Kato R, Susil RC, Roguin A, Dickfeld TL, Ashikaga H, Calkins H, Berger RD, Bluemke DA, Lardo AC, Halperin HR. Feasibility of real-time magnetic resonance imaging for catheter guidance in electrophysiology studies. *Circulation*. 2008;118:223-229

179. Ranjan R, Kholmovski EG, Blauer J, Vijayakumar S, Volland NA, Salama ME, Parker DL, MacLeod R, Marrouche NF. Identification and acute targeting of gaps in atrial ablation lesion sets using a real-time magnetic resonance imaging system. *Circulation. Arrhythmia and electrophysiology*. 2012;5:1130-1135

180. Dukkipati SR, Mallozzi R, Schmidt EJ, Holmvang G, d'Avila A, Guhde R, Darrow RD, Slavin G, Fung M, Malchano Z, Kampa G, Dando JD,

McPherson C, Foo TK, Ruskin JN, Dumoulin CL, Reddy VY. Electroanatomic mapping of the left ventricle in a porcine model of chronic myocardial infarction with magnetic resonance-based catheter tracking. *Circulation*. 2008;118:853-862

181. Schmidt EJ, Mallozzi RP, Thiagalingam A, Holmvang G, d'Avila A, Guhde R, Darrow R, Slavin GS, Fung MM, Dando J, Foley L, Dumoulin CL, Reddy VY. Electroanatomic mapping and radiofrequency ablation of porcine left atria and atrioventricular nodes using magnetic resonance catheter tracking. *Circulation. Arrhythmia and electrophysiology*. 2009;2:695-704

182. Weiss S, Vernickel P, Schaeffter T, Schulz V, Gleich B. Transmission line for improved rf safety of interventional devices. *Magnetic resonance in medicine : official journal of the Society of Magnetic Resonance in Medicine / Society of Magnetic Resonance in Medicine*. 2005;54:182-189

183. Fleming CP, Wang H, Quan KJ, Rollins AM. Real-time monitoring of cardiac radio-frequency ablation lesion formation using an optical coherence tomography forward-imaging catheter. *Journal of biomedical optics*. 2010;15:030516

184. Wright M, Harks E, Deladi S, Suijver F, Barley M, van Dusschoten A, Fokkenrood S, Zuo F, Sacher F, Hocini M, Haissaguerre M, Jais P. Real-time lesion assessment using a novel combined ultrasound and radiofrequency ablation catheter. *Heart rhythm : the official journal of the Heart Rhythm Society*. 2011;8:304-312